PALACKÝ UNIVERSITY OLOMOUC

Faculty of Science

Department of Physical Chemistry

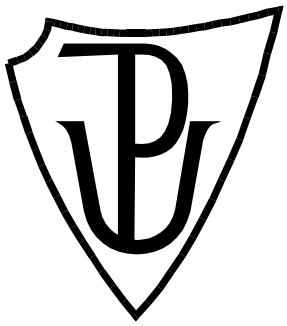

Behavior of Membrane Anchored Cytochromes P450

Doctoral Thesis

Author:	Mgr. Veronika Navrátilová
Supervisor:	prof. RNDr. Michal Otyepka, Ph.D
Consultant:	doc. RNDr. Karel Berka, Ph.D.

Study programme:	Chemistry
Study field:	Physical chemistry
Study form:	Daily
Date of submission:	29. 3. 2018

Olomouc 2018

Bibliografická identifikace:

Jméno a příjmení autora	Mgr. Veronika Navrátilová
Název práce	Chování membránově kotvených cytochromů P450
Typ práce	Disertační
Pracoviště	Katedra fyzikální chemie
Vedoucí práce	prof. RNDr. Michal Otyepka, Ph.D
Konzultant	doc. RNDr. Karel Berka, Ph.D.
Rok obhajoby práce	2018
Klíčová slova	cytochrome P450, channel, tunnel, molecular dynamics, MOLE
Počet stran	52
Počet příloh	4 publikace
Jazyk	Anglický

Abstrakt

Cytochromy P450 (CYP) jsou enzymy podílející se na metabolismu většiny cizorodých látek v lidském těle, ať už se jedná např. o léčiva, či polutanty vyskytující se v životním prostředí. Savčí CYP metabolizující cizorodé látky jsou membránově kotveny v endoplasmatickém retikulu. Transport látek z hydrofobního prostředí membrány do hluboce zanořené kavity aktivního místa je zprostředkován sítí kanálů, které zajišťují jak příjem substrátů, tak výstup metabolitů. Všechny tyto procesy je možno sledovat pomocí nástrojů výpočetní chemie např. metodami molekulární dynamiky (MD) či specializovanými bioinformatickými nástroji pro identifikaci a analýzu kanálů (např. MOLE). Oba tyto přístupy lze navíc vzájemně propojit, čímž lze získat nástroj umožňující popis energetiky celého procesu průchodu molekuly z membrány do aktivního místa CYP a také výstup jejich metabolitů kanály, a navíc identifikovat kanál, který je pro průchod dané látky nejvhodnější. Přístupy použité v rámci této disertační práce mohou pomoci při objasnění struktury a dynamiky membránově kotvených cytochromů P450 a kombinací MD a nástroje MOLE lze také získat další informace potřebné k vysvětlení potenciálního mechanismu vazby ligandu do aktivního místa CYP a určení vhodné výstupní cesty metabolitů. Takto získané informace a výpočetní postupy lze použít např. při návrhu nových léčiv s ohledem na jejich metabolismus, popřípadě při racionálním návrhu nových enzymů s námi požadovanými vlastnostmi přístupových či výstupních kanálů.

Bibliographical identification:

Author's first name and surname	Mgr. Veronika Navrátilová
Title	Behavior of Membrane Anchored Cytochromes P450
Type of thesis	Doctoral
Department	Department of Physical Chemistry
Supervisor	prof. RNDr. Michal Otyepka, Ph.D
Consultant	doc. RNDr. Karel Berka, Ph.D.
The year of presentation	2018
Keywords	cytochrome P450, channel, tunnel, molecular dynamics, MOLE
Number of pages	52
Number of appendices	4 publications
Language	English

Abstract

The cytochromes P450 (CYP) are enzymes involved in the metabolism of most xenobiotics in the human body such as drugs or some environmental pollutants. Mammalian CYPs metabolizing xenobiotics are membrane-attached to the endoplasmic reticulum. The transport of molecules from the membrane hydrophobic core towards CYP's deeply buried active site cavity is provided by the network of transportation channels managing substrate ingress and metabolite egress. These processes can be studied by the computational chemistry methods such as molecular dynamics (MD) or specialized bioinformatics tools which allow identification and characterization of channels leading to the active site (e.g. MOLE). Both approaches can be combined and together allow the detailed description of the substrate uptake from the membrane to the CYP active site and metabolite egress to cytosol. Moreover, combination of software tools also allows to obtain the energetics of the whole process of compound permeation through the network of channels to identify the most favorable path. In this thesis, these approaches were successfully used for elucidation of the structure and dynamics of the membrane-attached cytochromes P450 and the combination of the MD and MOLE helped us to explain the potential binding mechanism of the ligands to the CYP active site and to evaluate metabolite's egress paths. The data and processes presented in this thesis may be therefore used e.g. in the *in silico* drug design including drug metabolism and for rational design of new enzymes with desirable properties of their access/egress channels.

Declaration of the author

I declare that I have worked out this thesis by myself using the cited sources. Neither the thesis nor any of its part was previously used for obtaining any academic degree.

Olomouc 2018

Veronika Navrátilová

“Not everything that can be counted counts, and not everything that counts can be counted.”

„Ne vše, co se dá spočítat, se počítá; ne vše, co se počítá, se dá spočítat.“

Albert Einstein

Acknowledgement

I am deeply grateful to my supervisor prof. Michal Otyepka for guidance and support. I would like to also thank my consultant Assoc. Prof. Karel Berka for his endless help, good pieces of advice, patience and friendship. I sincerely thank all students, postdocs and the members of the Department of physical chemistry for friendly, sometimes crazy but always inspiring atmosphere.

Last but not least, I would like to express my deep gratitude to my family and friends for support, love and understanding during all my PhD study.

The author of the thesis gratefully acknowledges student projects IGA_Prf_2014023, IGA_Prf_2016_028, IGA_Prf_2017_028, IGA_Prf_2018_032.

Outline

Abstract

The cytochromes P450 (CYP) are enzymes involved in the metabolism of most xenobiotics in the human body such as drugs or some environmental pollutants. Mammalian CYPs metabolizing xenobiotics are membrane-attached to the endoplasmic reticulum. The transport of molecules from the membrane hydrophobic core towards CYP's deeply buried active site cavity is provided by the network of transportation channels managing substrate ingress and metabolite egress. These processes can be studied by the computational chemistry methods such as molecular dynamics (MD) or specialized bioinformatics tools which allow identification and characterization of channels leading to the active site (e.g. MOLE). Both approaches can be combined and together allow the detailed description of the substrate uptake from the membrane to the CYP active site and metabolite egress to cytosol. Moreover, combination of software tools also allows to obtain the energetics of the whole process of compound permeation through the network of channels to identify the most favorable path. In this thesis, these approaches were successfully used for elucidation of the structure and dynamics of the membrane-attached cytochromes P450 and the combination of the MD and MOLE helped us to explain the potential binding mechanism of the ligands to the CYP active site and to evaluate metabolite's egress paths. The data and processes presented in this thesis may be therefore used e.g. in the *in silico* drug design including drug metabolism and for rational design of new enzymes with desirable properties of their access/egress channels.

Abstrakt

Cytochromy P450 (CYP) jsou enzymy podílející se na metabolismu většiny cizorodých látek v lidském těle, ať už se jedná např. o léčiva, či polutanty vyskytující se v životním prostředí. Savčí CYP metabolizující cizorodé látky jsou membránově kotveny v endoplasmatickém retikulu. Transport látek z hydrofobního prostředí membrány do hluboce zanořené kavity aktivního místa je zprostředkován sítí kanálů, které zajišťují jak příjem substrátů, tak výstup metabolitů. Všechny tyto procesy je možno sledovat pomocí nástrojů výpočetní chemie např. metodami molekulární dynamiky (MD) či specializovanými bioinformatickými nástroji pro identifikaci a analýzu kanálů (např. MOLE). Oba tyto přístupy lze navíc vzájemně propojit, čímž lze získat nástroj umožňující popis energetiky celého procesu průchodu molekuly z membrány do aktivního místa CYP a také výstup jejich metabolitů kanály, a navíc identifikovat kanál, který je pro průchod dané látky nejvhodnější. Přístupy použité v rámci této disertační práce mohou pomoci při objasnění struktury a dynamiky membránově kotvených cytochromů P450 a kombinací MD a nástroje MOLE lze také získat další informace potřebné k vysvětlení potenciálního mechanismu vazby ligandu do aktivního místa CYP a určení vhodné výstupní cesty metabolitů. Takto získané informace a výpočetní postupy lze použít např. při návrhu nových léčiv s ohledem na jejich metabolismus, popřípadě při racionálním návrhu nových enzymů s námi požadovanými vlastnostmi přístupových či výstupních kanálů.

1. INTRODUCTION

Cytochromes P450 (CYP) are heme-thiolate enzymes involved in metabolism of more than 75% of drugs [1]. The "cytochrome P450" name originates in their unique spectral properties observed in the microsomal fraction of the rabbit liver [2]. The P in cytochrome P450 means "Pigment" and numeral "450" represents the absorption peak maximum at 450 nm for the reduced form of carbon monoxide bound CYP so called Soret's band [3] because CYP was firstly observed as an unknown pigment in the microsomal fraction and after that was identified as P450 hemoprotein [4]. CYP have been called ubiquitous because they were observed in almost all living organisms from the prokaryotic single-celled *Archea* up to bacteria, plants and animals [4]. Thus, CYP are versatile biocatalysts involved in majority of metabolic processes.

The function of the CYP can be also called detoxification due to its ability to metabolize the xenobiotics. The origin of the word "xenobiotics" is based on two Greek words *ξένος (xenos)* "foreigner" and *βίος* (bios) "life" as these compounds are generally new to the organism. CYP catalyze wide range of biochemical reactions [3,5] in the most of living organisms and belong to the group of oxidoreductases – EC1 at enzyme classification system [6]. The ability to metabolize such a large set of the various compounds is given by the specific characteristics of CYP such as their promiscuity and regioselectivity. These properties relate to CYP conformational changes of the amino acid residues, especially near the active site cavity, which are either inherent to the CYP structure or it may be altered by interaction with: i) substrate, ii) inhibitor, iii) redox partner or iv) membrane.

CYP do not only metabolize xenobiotics, but also many endobiotic compounds produced within the body, are also catalyzed by CYP during their metabolic cycle. CYP typically change more hydrophobic substrates to their more hydrophilic metabolites which can be easily eliminated from the organism [7]. This mechanism is nicely connected with the pathways which the substrates or metabolites are transported into/from CYP active site. These pathways are called channels and form a network of mutually connected routes [8,9]. The proper mechanism of the transportation by channels is not trivial and is still the object of many studies.

This study is focused on elucidating of the processes connected with metabolism of the CYP. There are many factors affecting the CYP catalytic activity, starting from the role of the secondary structure and the flexibility, conformational changes caused by interaction with membrane, substrate or the redox partner. All these factors should be counted in exploration of the CYP properties and may play significant role in the CYP activity. Description of as much interactions between CYP and the membrane or ligands as possible may shed light on the mechanism of function of these important enzymes.

2. CYTOCHROMES P450

There are 57 human CYP enzymes. CYP represent major drug metabolizing enzymes which are involved in biotransformation of the most of drugs in the human body [10,11]. CYP metabolize wide range of the compounds from the small ones (e.g. ethanol) up to the larger molecules (e.g. macrolide antibiotics) [12]. Moreover, CYPs are involved in biosynthesis of endobiotic compounds which are produced directly in the human body e.g. cholesterol, vitamin D3, retinoic acid etc. [13]. CYP are typically involved in monooxygenation reactions during the catalytic cycle but they are involved in variety of chemical reactions: oxidation, epoxidation, sulfoxidation, dealkylation, dehydrogenation but mostly hydroxylation [3,14]. The metabolism is mediated by the heme cofactor with the iron atom in the center of its porphyrin ring which is positioned in the deeply buried active site cavity [15]. The catalytic reaction also needs the addition of the electrons and this function is ensured by CYP electron transfer partners. The catalytic activity of CYP is guided by their specific structure which significantly affects their properties.

2.1 Structure of CYP

Despite of their small sequential similarity the main structural fold of CYPs still remains conserved [3]. CYP represent group of proteins with typical secondary structure which is called CYP common fold [15]. CYP enzymes are mainly α-helical proteins with small portion of β-sheets. Generally, CYP are considered as a orthogonal bundle according to the specific CATH classification number 1.10.630.10 [16]. We recognize several secondary structural features which are named in alphabetical order from the N-terminal towards to the C-terminal of the protein - helices A-L and β-sheets 1-5 (Figure 1).

The general nomenclature of secondary structural features of CYP was assumed from the terminology used by Poulos et al. for the prototypic CYP – bacterial P450cam [17]. The longest α-helix is the I-helix interacting with its typically threonine residue with the heme cofactor during catalytic cycle. Another important structural motif is the so-called F/G loop in the tip located between helices F and G perpendicular to the highly conserved I-helix. The second important loop – B/C loop is closing the active site cavity and together with the F/G loop may considerably affect the access of the substrates towards the heme cofactor. The other helices form the CYP common fold in order from the N-terminal A-helix up to the C-terminal to the last L-helix. The last part called meander is actually misnomer because in real it is only about 20 amino acids in surrounding of the K' helix [18] (Figure 1).

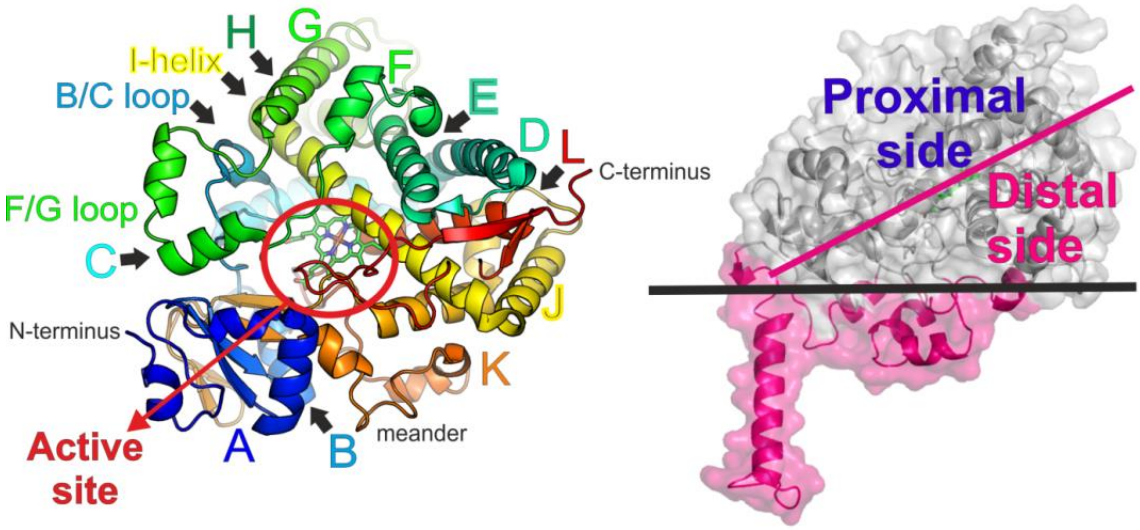

Figure 1. Left panel: Main structural features of cytochrome P450. There are the letter names for each helix from the N-terminus (A-helix) to C-terminus (L-helix). The heme cofactor lying deep inside of the structure (green sticks with blue nitrogen atoms and red Fe iron as central atom). The orange region near the K-helix is called meander. Right panel: The proximal and distal sides of the CYP catalytic domain. Figures were prepared in Pymol 1.7 software [19].

The overall CYP structure can be divided to the N-terminal transmembrane helix and the catalytic domain. The N-terminal transmembrane α-helix serves as the anchor holding CYP structure in the membrane and may be also involved in the formations of CYP's heteromers [20]. Catalytic domain has a proximal and a distal side defined in orientation against heme cofactor (Figure 1). The distal side represents the center of overall metabolic action because it nestles the active site cavity and is oriented towards the membrane environment. The proximal side is necessary for the interaction with the CYP's redox partners (cytochrome P450 reductase (CPR), cytochrome b5) [21].

For the reaction, CYP needs to consume two consecutive electrons during the catalytic cycle. The electrons are provided by CYP's redox partners such as cytochrome P450 reductase (CPR) and cytochrome b5. Whilst the CPR is large flavoprotein using FAD and FMN cofactors, the cytochrome b5 is rather smaller protein with heme cofactor [22]. Both cytochrome b5 and CPR interact with CYP by his proximal side (see Figure 2), while the substrates and products enter the active site from the distal side.

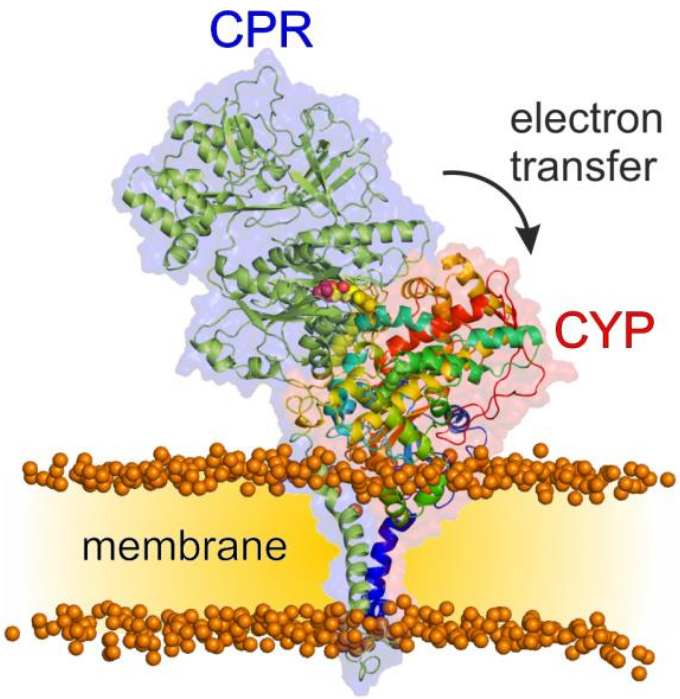

Figure 2. CYP and cytochrome P450 reductase complex. CPR is represented as green cartoon and blue transparent surface and CYP as cartoon (rainbow coloring) and red surface, membrane phosphates are showed as orange spheres. The black arrow showed the direction of electron transfer from the redox partner CPR to CYP. Figures were prepared in Pymol 1.7 software [19].

2.2 CYP Active Site Cavity

The active site cavity is typically buried deeply in the structure of the CYP (Figure 3). In the center of the active site cavity is placed the heme cofactor with the iron atom surrounded by nitrogen atoms of the porphyrin skeleton. The most often CYP's cofactor is protoporphyrin IX (heme b). The heme is connected to the CYP catalytic domain by S-Fe bond of thiolate group of the nearest cysteine of the protein backbone. The cysteine thiolate group plays a role also as an axial ligand on proximal side [11]. This region is known as highly conserved and called "cys-pocket" [23]. The microsomal CYPs share the same pattern of structural flexibility. The most rigid part is obviously heme cofactor in the active site center. The distal side is considered as a malleable and finally the proximal side is intermediately flexible [21].

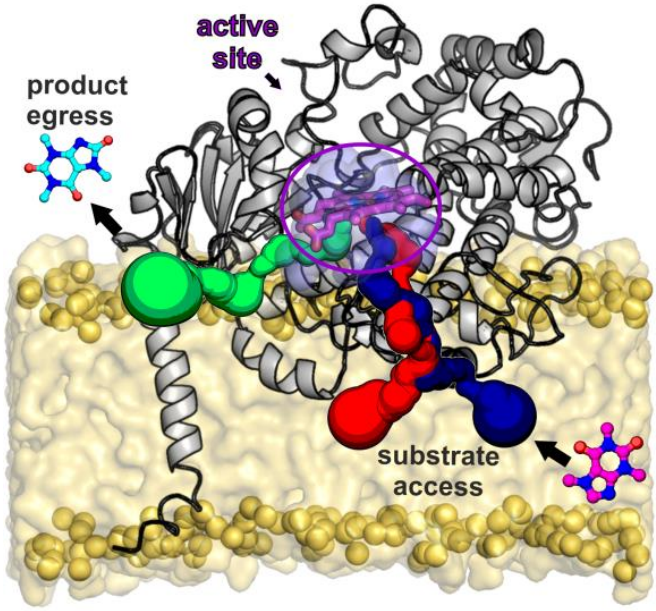

Figure 3. Active site cavity is deeply buried in the CYP structure (highlighted by purple ellipse) and it is connected to the membrane or the cytosol by the network of the access/egress channels transporting the substrates or metabolites. Figures were prepared in Pymol 1.7 software [19].

The active site of many CYP is often called malleable [24] or promiscuous [3,12,25]. These terms originate from the CYP's ability to metabolize more than one type of the substrates of various shapes and sizes. For example, human CYP3A4 is extremely promiscuous and may consume more than 600 compounds[1] ranging from small ones such as acetaminophen [26] to huge ones as erythromycin [12]. Structurally, CYP3A4 has large and highly flexible active site cavity. On the other hand, the CYP1A2 has its active site small, narrow and quite rigid [27], thus CYP1A2 is able to metabolize only small planar molecules. The promiscuity of the enzyme may be characterized by the substrate promiscuity index established by Atkins et al. [28]. The malleability and flexibility of the active site therefore represent an important characteristic. The flexibility of the CYP can be specifically localized using so called flexible regions (FR) which are related to the range of flexibility of this position. We recognize ten flexible regions in the structure of CYP labeled as FR1 - FR10 (Figure 4) [15,27].

Moreover, the substrate access relates to certain amino acids sites allowing the suitable interaction with molecule of drug or another substrate. These places are called substrate recognition sites (SRS) [29,30] and were firstly established by Gotoh [29]. The most SRS are placed in the proximity of the I-helix where also the highly conserved threonine is localized and can play important roles in CYPs catalytic activity (Figure 4) [31].

[1] data taken from: http://www.uniprot.org/uniprot/P08684

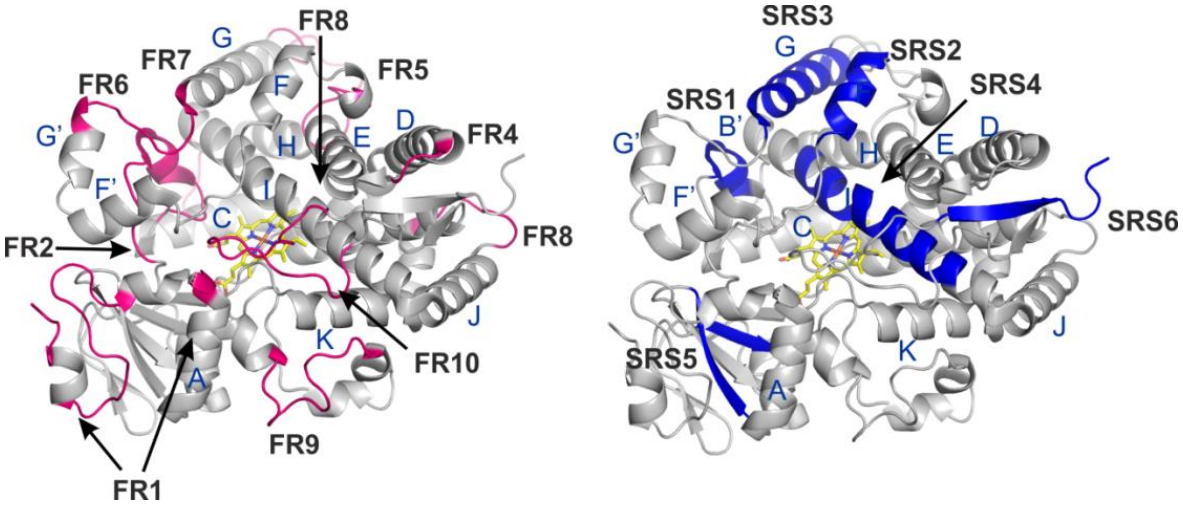

Figure 4. Left: Flexible regions (FRs) – FR1 – FR10 according to Hendrychova et al. [27]*; Right: Substrate recognition sites (SRS) - SRS1 - SRS6 according to Gotoh* [29].

The catalytic function of CYP is also connected to the movement of water molecules towards and from the active site cavity. In the unbound state, CYP active site is occupied by water molecules. After the binding of the substrate molecule, the water molecules start to move from the cavity to the outside of the CYP by specific water and solvent channels as they make more space for the binding of the substrate and allow the catalytic reaction on the heme cofactor [32–34]. It was also suggested that the opening of the water channel could be affected by the interactions with the CYP redox partners. All in all, CYP active site is interconnected with surface by the network of access/egress channels. The properties of the channels may significantly affect the input of the potential substrates or egress of the products. We will focus on the detailed description of the channels in the next section.

2.3 CYP Channels

The buried active site of the CYP is connected to surrounding environment by the network of access/egress channels (Figure 5). The channels are divided to the families and subfamilies according to the nomenclature established by Wade at co-workers [8]. The channel nomenclature is based on Arabic numerals which describe the main channel families: 1, 2, 3, 4, 5 and also specific channel names according to their function such as solvent channel and water channel.

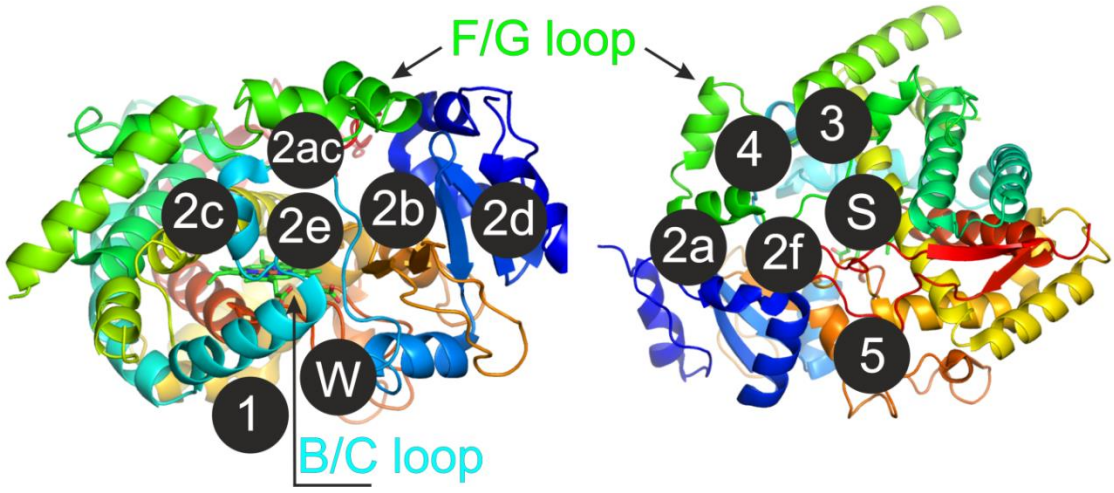

Figure 5. The schematic overview of the CYP channels. Left panel shows the view from the B/C loop side where the black circles show the channels: channel 1 and water channel both below the B/C loop, 2e, 2b, 2ac, 2c around the B/C loop and 2e go through B/C loop. Right panel: channels 3 and 4 go through the F/G loop, channel 2a and 2f are positioned near the tip of the F/G loop, solvent channel (S) lies between I-helix, F-helix and β5-sheet, channel 5 is in proximity of the meander and K-helix.

Most channels can be found on distal side, where they can serve as substrate access or metabolite egress routes. The channels of family 2 are localized in the proximity of the F/G loop and F, G helices, while their relative position against other secondary structure elements allows their subdivision into subfamilies such as 2a, 2b, 2c, 2ac, 2d, 2e and 2f. F/G loop also represents the part of catalytic domain which is in interaction with membrane. For this reason, most of the family 2 channels can be involved in the substrate access from the membrane environment. Channels 3 and 4 are passing through the F and G helices and channel 4 especially go through the F/G loop. These channels are usually oriented towards the membrane and thus may play some roles in the substrate intake. The solvent channel is proposed as an access/egress channel for the water solvating the active site. As such it is positioned towards cytosol and can serve as the channel for the egress of the products of metabolism which was observed in several works including ours [7,35] (Appendix C).

In contrast, Channels 1, 5 and water channel can be found on the proximal side of CYP. The water channel may serve as the additional pathway of water molecules. The channel 1 occasionally occurred but not very often. The suggested function of this channel is transport of gases, such as oxygen or carbon monoxide [36]. The function of channel 5 has not been described yet.

We can summarize that distal-side channels can be involved in the substrate ingress and the egress of products, while proximal-side channels might be rather used for smaller molecules – gases or water. The channels can be characterized not only by their geometric characteristics (length, radius), but also according to the physicochemical properties of amino acids lining the channel (charge, polarity, hydrophobicity, mutability, etc.). The most important part of each channel is a bottleneck which

represents the narrowest part of the channel and can control the ingress or egress of the substrates or metabolites (Figure 6).

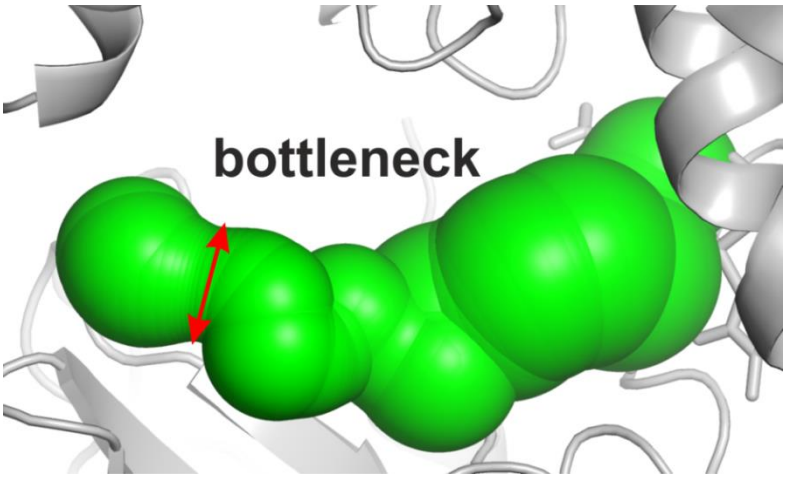

Figure 6. Visualization of channel bottleneck – the narrowest part of channel (red arrow). Channel 2b in the structure of CYP3A4 is depicted (PDB ID: 1W0F).

The movements of the ligands passing through the access channels are connected to some structural rearrangements. The specific movements of the ligand in the channel lead to the conformational changes, depending on the size and shape of the passing molecule. This phenomenon can be resembled as something like peristaltic wave observed previously, where the position of bottleneck is moving along the channel as it is influenced by the presence of ligand or water within channel [7,35]. The conformational rearrangements may also cause opening of the new channels which may affect the catalytic efficiency of the CYP. Similarly, the channel opening can be affected by the presence of the membrane[7].

2.4 CYP on Membranes

Mammalian CYPs are mostly attached to the endoplasmic reticulum membrane (ER) or on the inner mitochondrial membrane [37,38]. The anchoring is ensured by N-terminal α-helical transmembrane anchor as a hydrophobic part of the CYP which holds the catalytic domain on the membrane surface. The main parts involved in the interaction with the membrane are F/G loop, B/C loop, B'-helix, parts of F and G-helices, and so called β-finger (β4-β5 sheet). But the size of the interacting region and the number of amino acids immersed to the membrane may alter according to the membrane lipids. The CYP embedding to the membrane causes the formation of the funnel-like shape of the surrounding membrane lipids [7] (Figure 7). The character of the interaction of the CYP with membrane lipids depends on the type of the lipid involved in the membrane.

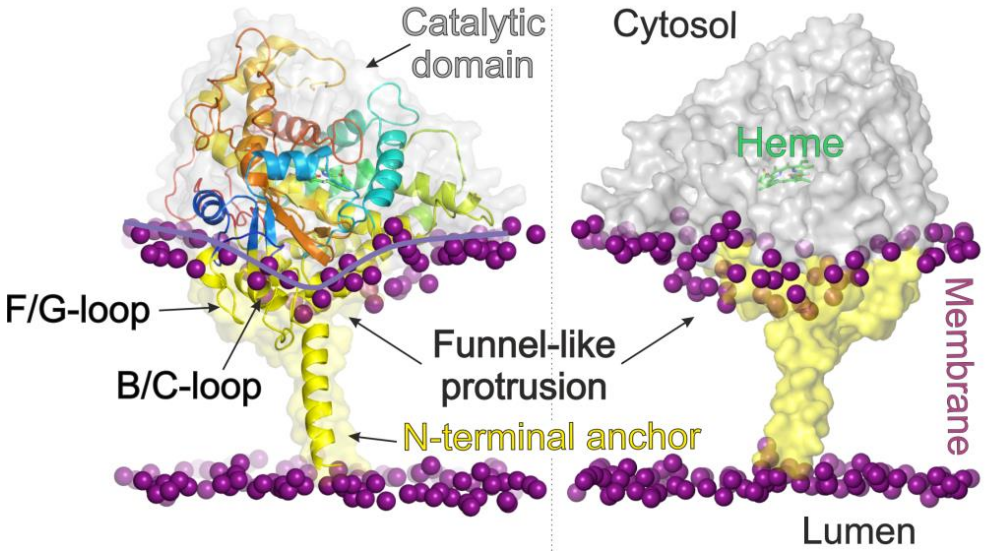

Figure 7. The parts of the catalytic domain interacting with the membrane environment - yellow. CYP is represented as cartoons and transparent surface. Membrane phosphates are showed as purple spheres. The part of the membrane in contact with the CYP catalytic domain (yellow) has funnel-like shape typical for the interaction between CYP and membrane.

The membrane immersion of the CYPs to the membrane significantly affects their behavior and potential transport of the substrates towards to the active site from the hydrophobic membrane environment. Not only the amino acid sequence of the enzyme but also the lipid composition of the membrane affects the catalytic activity of the CYP which was already observed experimentally [39].

3. COMPUTATIONAL METHODS

This part briefly summarizes utilized computational methods. The most results arose from the data obtained by molecular dynamics simulations of the CYP attached to the membrane. This approach will be briefly introduced at the beginning. After that the specialized advanced simulation technique called metadynamics will be described. On the end of this session a bioinformatics tool MOLE 2.0 used for channels computation will be briefly explained.

3.1. Molecular Dynamics

Molecular dynamics simulations (MD) allow study the dynamic behavior of atomistic system which is exposed to the predefined conditions such as temperature or pressure during the time of the simulation. MD is based on the combination of molecular mechanics with classical Newton's equations of motion that helps describe how the forces may affect the motions of atoms of the studied system.

$$m_i \cdot \frac{\partial^2 r_i}{\partial t^2} = -\frac{\partial V}{\partial r_i} \cdot U(r_1, r_2, \dots, r_N) = f_i \quad (1)$$

$U(r_1,r_2,\dots,r_N)$ represents potential energy which depends on the coordinates of the N-particles [40]; m_i represents mass of the atom, r_i its Cartesian coordinates; a_i acceleration of atom i; V is potential energy of the studied system.

The requirement of the MD simulations is the knowledge of the parameters and equations describing all required characteristics of studied system such as information about: bonds, angles, dihedrals, electrostatics and van der Waals interactions to obtain the potential energy of simulated system. The collection of parameters and equations alike is usually named as force field.

The exact description of all of characteristics of the studied system would be probably impossible (or incredibly expensive in terms of computational time). For this reason, generally, MD used the approximations e.g. the bonds are described with using the harmonic oscillator (Hook's law) which depicts the bond between two molecules as a spring. Non-bonded interactions are defined with using Lennard-Jones potential and electrostatic interactions by Coulombs law. The overview of equations for individual interactions is summarized in Table 1.

Table 1. Overview of interactions defined in MD simulations in AMBER forcefield.

Interaction	Equation	
Bonds	$V_{bond}(r_{ij}) = \frac{1}{2} r_{ij}^{b}(r_{ij} - b_{ij})^2$	(2)
Angles	$V_{angle}(\theta_{ijk}) = \frac{1}{2} k_{ijk}^{\theta}(\theta_{ijk} - \theta_{ijk}^{0})^2$	(3)
Dihedral angles	$V_{dihedral} = V_{proper} + V_{improper}$	(4)
Proper (periodic) dihedral	$V_{proper-periodic}(\varphi_{ijkl}) = k_{\varphi}(1 + \cos(n\varphi - \varphi_s))$	(5)
Improper dihedrals	$V_{improper}(\xi_{ijkl}) = \frac{1}{2} k_{\xi}(\xi_{ijkl} - \xi_0)^2$	(6)
Electrostatic interactions	$V_{ele}(r_{ij}) = \frac{1}{4\pi\varepsilon_0} \frac{q_i q_j}{\varepsilon_r r_{ij}}$	(7)
van der Waals interactions	$V_{LJ}(r_{ij}) = \frac{C_{ij}^{(12)}}{r_{ij}^{12}} - \frac{C_{ij}^{(6)}}{r_{ij}^{6}}$	(8)

The force field then represents a set of the parameters which describes the simulated system. There is the wide variety of the force fields and their usage depends on the character of studied system and its environment. In case of simulations of protein-membrane complexes one of the appropriate combinations of the protein and membrane force field is AMBER99sb [41] for protein and Slipids [42] for membrane, which we used thorough our simulations.

However, all parameters used in MD simulations represent certain level of approximation and therefore the simulation results must be taken with caution. Generally, the best procedure is the connection of the MD simulations and experimental results to validate the result obtained from computations.

3.2. Metadynamics

The metadynamics represents a special type of biased MD simulation. This method is based on the reconstruction of multidimensional free energy surface of the studied system as a function of several specified degrees of freedom called "collective variables" (CV). Metadynamics is the method which enhances sampling of the coordination space by biasing CVs by gradually adding an external potential on actual position in defined CVs (Figure 8).

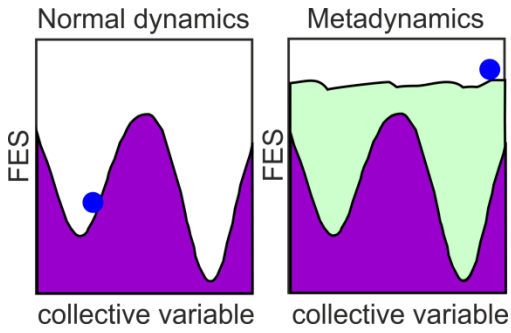

Figure 8. Normal dynamics (left) versus metadynamics (right). Metadynamics allows escapes the free energy minima by adding the sum of Gaussians which fill the free energy surface (FES) and provides the negative image of the free energy (green area).

Metadynamics is therefore history-dependent method where the set of Gaussians potentials are placed along the CV during the trajectory to destabilize energy minima and thus it allows the acceleration of the biased simulation [43]. The process of the addition of the Gaussians for each time step (t_G) can be described by equation (9):

$$V_G(S(x),t) = \sum_{t'=t_G,2t_G,3t_G,\ldots} w \exp\left(-\frac{(S(x)-s_{t'})^2}{2\delta s^2}\right) \quad (9)$$

The w is height and δs is the width of the Gaussians. CV at time t is defined as $s_t = S(x(t))$.

Finally, when the system moves freely, the metadynamics simulation is converged and the final sum of Gaussians along CV is negative to the free energy profile along that CV and therefore metadynamics can be used to describe free energy surface [44].

The abovementioned method can be used also for description of the rare events which could not be reached by classical MD techniques. Additional extension of the metadynamics method is bias-exchange metadynamics (BE-META) [35,45] which is using several replicas biasing various CVs that are switching between replicas. The bias switching between replicas are attempted at regular time intervals. The switch of CV biases are accepted according to a probability that depends on the difference in the bias potentials between replicas [46]. As such, the replica exchange can be successfully used for the increase of the convergence rate of metadynamics if free energy profiles depend on several CVs [47].

3.3. Channels Computation

There are many programs for channel computation such as Hole [48], Caver [49], Mole [50], MolAxis [51], etc. In this work, we used our tool Mole 2. Mole 2.0/2.5 [52] is the specialized program for

analysis of channels, tunnels and pores. The basic principle of the channel recognition is using the Voronoi diagram and Delauney's triangulation for the description of the protein surface and inner cavities. The channels calculation then starts at the initial coordinates called starting point and end up either on the surface or close to user-defined end point. This mechanism allows to find multiple channels which have various length. But the most favorite channel should be the shortest one, and for this reason the MOLE used also the shortest path Dijkstra algorithm which filters only the channel with the smallest distance from the starting point to end (surface) point. The basic scheme of the channel computation can be described in the seven steps (see Figure 9):

a) The computation of the Delauney triangulation (Voronoi diagram) of the atomic centers
b) The calculation of the molecular surface
c) The detection of the cavities
d) The starting point/s detection
e) The end point/s detection
f) The channels computation
g) Filtering of the found channels

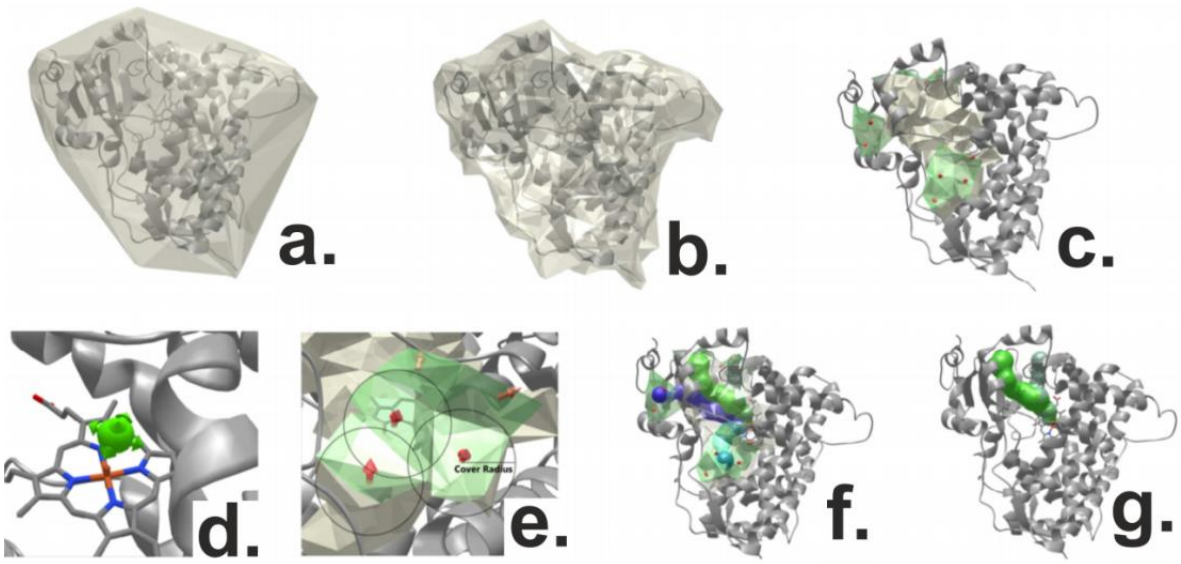

Figure 9. The methodology of the channel computation - PDB ID: 1TQN in MOLE 2.0. (Figure adopted from the Mole 2.0 documentation pages).

The calculation of the channels can be refined by using of advanced properties such as the set of parameters which can be manually configured by user. The major parameters are:

- **Interior Threshold** – determines the narrowest radius of the channel
- **Probe Radius** – radius which is used for description the protein surface
- **Surface Cover Radius** – represents the maximal density of channel end points on the protein surface
- **Origin Radius** – this radius is used for the positioning of the starting point

Moreover the physicochemical properties such as polarity [53], hydropathy [54], hydrophobicity [55], charge and mutability [56] can be computed. All physico-chemical properties are calculated from the set of all channel lining residues (without backbone parts). The charge is calculated as a simple sum of all charges involved in lining amino acids.

The output of the channel calculation by MOLE 2 is the PDB file with network of channels or PDB with separated channels and XML or JSON files containing the geometrical and physicochemical properties for each channel.

4. RESULTS AND DISCUSSION

Following sections will be focused on our contribution to CYP field. Firstly, the role of the various content of cholesterol in the membrane to the CYP3A4 was studied (Appendix A). In the second part, the effect of membrane lipid composition to the behavior of CYP3A4 will be discussed (Appendix B). Afterwards, the permeation of CYP3A4 metabolite – 1,3,7-trimethyluric acid (TMU) and energetics connected with TMU passage through the CYP channels will be described (Appendix C). Finally, last section will be dedicated to the explanation of the mechanism of the tuning of metabolism of dioxins and persistent organic pollutants by mutation of rat CYP1A1 (Appendix D).

4.1 Effect of Cholesterol on the Membrane-attached CYP3A4

As was discussed in the previous sections, CYPs are attached to the several biological membranes. Almost every membrane has different composition of lipids which is significantly reflected in its properties and behavior. CYPs are attached to the several biological membranes. The biological membranes differ by the amounts of individual neutral and charged lipids and by cholesterol content. The cholesterol concentration differs according to the membrane type and even the localization in the body. Generally, cholesterol content ranges from the lowest cholesterol concentration ~3-6 wt% (in dependency of it is the inner (matrix) or outer mitochondrial membrane [57]) in mitochondria, ~6 wt% in ER membrane and the highest cholesterol content can be found in the plasma membrane ~20%wt [58]. The cholesterol plays significant roles in the many processes such as the regulation of the mechanistic properties of membranes and also behaviour of the proteins embedded in them [59,60]. However, the completely different situation can be observed in the lipid rafts, which show the changeable inhomogeneity in membranes, while cholesterol enriches some types of lipid rafts [61]. Thus, the membrane may affect the CYP behavior as well as the CYP may alter local membrane properties. For this reason, we carried out 200 ns-long MD simulations of the CYP3A4 on membranes with various concentration of cholesterol (3, 6, 20, 50 wt%) and monitored the changes caused by presence of cholesterol in the membrane (Appendix A).

4.1.1. Rising Cholesterol Content Alters Membrane Properties

The increase of cholesterol concentration in the membrane caused the thickening of the membrane where the maximal head group-head group distance 4.6 nm was observed in membrane with 20% of cholesterol. Similar trend was observed elsewhere [59]. The area for lipid (APL) was in range from 0.59 to 0.42 (Table 1 - Appendix A). The presence of cholesterol was also manifested in the change of

the membrane density profile and it was shown as the raising density of the lipid plateau region and in the membrane head groups. However, the lipid tails part did not change its density significantly. The order parameters of each membrane mirrored of the cholesterol concentration.

4.1.2. Presence of Cholesterol May Affect the Orientation of the CYP on the Membrane

The amount of cholesterol in the membrane with attached CYP can significantly change the number of interacting residues of the catalytic domain. The major membrane-interaction parts of CYP are N-terminal helix and F/G loop. Similarly the β1 and β2-sheets, B/C loop and also the small part of the I-helix were interacting with pure DOPC membrane in consensus with data observed before [7]. However, with rising concentration of the cholesterol in the membrane, the catalytic domain sunk deeper into the membrane inside, mirrored in number of amino acids in contact with the membrane (Table S2, Appendix A – Supporting information). The highest number of the amino acids in contact with membrane was observed at 6 wt% of cholesterol in the membrane, while the smallest interacting part was in pure DOPC membrane (Figure 10).

In similar way, the different concentration of cholesterol mirrored in the value of heme tilt angle (HTA) which represents the angle between the heme plane and the membrane normal in the z-axis. We observed increasing HTA from the lowest value 52° in DOPC membrane up to the 68° in the 50 wt% of cholesterol in the membrane. It should be noticed that the experimentally obtained value of the heme tilt angle was $60 \pm 4°$ [62]. On the other hand, the presence of cholesterol in various concentrations in membrane did not cause any important changes in secondary structural elements.

4.1.3. Cholesterol Cause Differences in the Access/Egress Channels Opening/Closing Pattern

We have observed different channel pattern with change of cholesterol concentration. After the addition of the cholesterol to the membrane the channels opening pattern changed significantly in comparison with the channels observed in the pure DOPC membrane. In 3 and 6 wt% of cholesterol the solvent channel was opened but vice versa the water channel closed. Channels around the partly membrane-immersed F/G loop an F and G helices still unaffected by the 3 or 6 wt% of cholesterol in the membrane. On the other hand, the higher cholesterol content may cause the closure of the membrane immersed access channels such as closing of 2af and 2b in 20 and 50 wt% of cholesterol. The presence of greater amount of cholesterol in membrane caused narrowing in bottleneck radius of the distal side channels (Table 2 - Appendix A). Whilst, the membrane-faced channels were rather closed in the cholesterol-rich membranes, the channels on the proximal water-exposed side were suddenly opened i.e. solvent channel and 2e. Surprisingly, we also observed a new channel on the proximal side which had not been described previously. This brand-new channel is localized between K-helix and K/L-loop and we called it “channel 7” in addition to nomenclature by Wade and her group

[8]. The explanation why this channel was opened could be the little movement of the F/G loop and also K and L-helices. Briefly the changes of the access/egress channel opening/closing could be caused by the conformational changes of the amino acids lining these channels which were mirrored in the subtle changes of the secondary structural features of CYP3A4 which may also cause the opening or closing the distal or proximal region. We also recognized the amino acid R212 which may serve as the gate-keeper of the solvent channel in dependence of the rotation of the arginine residue. The R212 caused closure of solvent channel in CYP3A4 structure immersed to the membrane with 0 and 3 wt% of cholesterol, whilst in 20 wt% of cholesterol the solvent channel was opened (Figure 10).

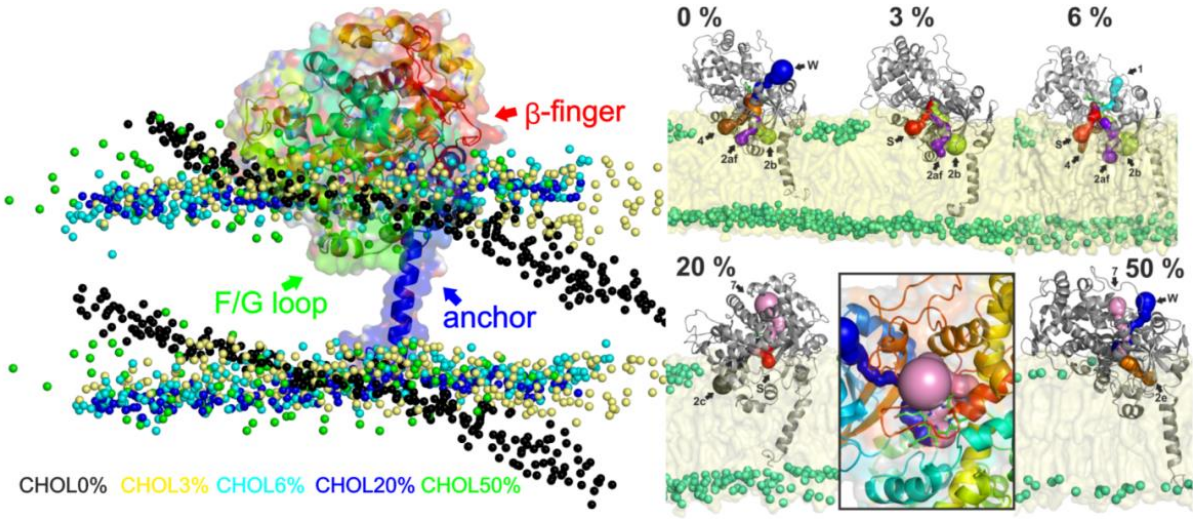

Figure 10. Left: Changes of the CYP3A4 orientation caused by different concentration of the cholesterol in the membrane. Right: Channels opening in the CYP3A4 anchored to the membranes with different cholesterol content – 0, 3, 6, 20 and 50 % wt of cholesterol. The middle panel in the bottom line shows the detail of the newly observed channel 7 (pink spheres). Figure taken from Appendix A.

So the CYPs are interacting with cholesterol variously. Whilst the CYP7A1, 27A1 and 46A1 are involved in the elimination of cholesterol and starting the cholesterol transformation to the final product bile acid [63] in contrast the CYP3A4 can play two roles. CYP3A4 can hydroxylate (4β-hydroxylation) cholesterol but moreover CYP3A4 can be also inhibited by higher cholesterol content [39]. The non-competitive inhibition was observed for example in case of the decreased activity of CYP3A4 towards the nifedipine [39]. The simplest explanation of the two roles of the cholesterol in the CYP3A4 is that the inhibitor interacts with the different amino acids – so in the different position than where the substrate cholesterol interacts as the substrate.

Finally, in this study we learnt that the relationship between CYP and cholesterol is two ways as they are affecting each other. Firstly, CYP can regulate the cholesterol biosynthesis [64] but on the other side the higher concentration of cholesterol inhibit CYP3A4 [39] as it alters behavior of membrane attached CYP due to the local changes caused in increased cholesterol content in membrane. This may

be an explanation, why CYPs are predominantly located in biological membranes with low cholesterol concentration (ER and mitochondria).

4.2 Effect of Lipid Charge to the CYP3A4

The biological membranes have different composition in dependency of their positioning. For example, the most abundant membrane lipids of ER are phosphatidylcholine (PC) and phosphatidylethanolamine (PE) and also charged lipids such as phosphatidylserine (PS) or phosphatidylinositol (PI) as well as the cardiolipin, cholesterol or sphingomyelin [65]. Every single lipid has its own properties and the different way how he interacts with its surroundings. Also, the proteins embedded in the membranes can be affected by the lipids involved in the bilayer. As was mentioned above, the character of the lipids plays a major role in the interactions with the attached protein and can significantly affect the protein orientation, number of channels openings and the catalytic activity of the enzyme.

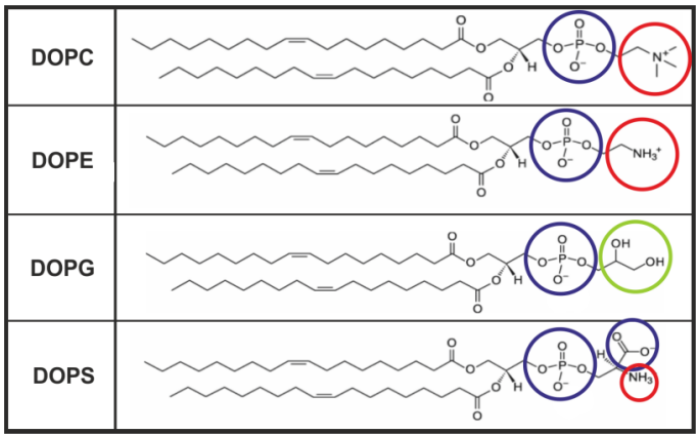

Figure 11. Lipids used for the construction of the four membrane bilayers: 1,2-dioleoyl-sn-glycero-3-phosphocholine (DOPC), 1,2-dioleoyl-sn-glycero-3-phosphoethanolamine (DOPE), 1,2-dioleoyl-sn-glycero-3-[phospho-rac-(3-lysyl(1-glycerol))] (DOPG) and 1,2-dioleoyl-sn-glycero-3-phosphoserine (DOPS). The charges are highlighted by circles in the following colors: blue – negative, red – positive, green – neutral polar. Figure adopted from Appendix B.

We studied the effect of the four various membranes on the CYP3A4 molecule. The CYP3A4 was inserted into two neutral membranes – 1,2-dioleoyl-*sn*-glycero-3-phosphocholine (DOPC) and 1,2-dioleoyl-*sn*-glycero-3-phosphoethanolamine (DOPE) and on the other hand to the two negatively charged membranes 1,2-dioleoyl-*sn*-glycero-3-[phospho-*rac*-(3-lysyl(1-glycerol))] (DOPG) and 1,2-dioleoyl-*sn*-glycero-3-phosphoserine (DOPS). The different head groups interact differently with the CYP3A4 which was mirrored in the structure, orientation and position of the catalytic domain Figure 11). All these changes altered the opening/closing of the access/egress channels which may significantly affect the catalytic activity of the CYP3A4 and also the localization in the membrane microdomains (Appendix B).

4.2.1. Differences of CYP Immersion in Various Membranes

The lipid charge significantly affected behavior of CYP3A4 on membrane. Specifically, the negatively charged membrane lipids (DOPS, DOPG) caused deeper immersion of the CYP3A4 to the individual membrane. The stable position of the CYP3A4 was reached after 1 μs of unbiased MD simulation on all membranes. The main parts of CYP3A4 in contact with membrane were the N-terminal transmembrane anchor which is holding the catalytic domain in the membrane, the tip of F/G-loop and A, F, G-helices and the small part of B/C-loop which is in agreement with previous publications [7,66–70]. The K-helix and β3-β5-sheets (β-finger) formed additional contacts with DOPS or DOPG membrane, respectively. The major changes were observed in case CYP3A4 embedded to the DOPS membrane where the C and H-helices sunk deeper to the membrane core and caused the deformation of the I-helix which formed the kink in the center of the helix.

The orientation of the CYP3A4 on the membrane was also affected by various lipids reflected in the changes of the HTA values. The HTA was increased gradually from the DOPC up to DOPG (DOPC < DOPS < DOPE < DOPG) in the range of HTA from the ~64° to 77°. The highest HTA was observed in the DOPG membrane 77 ± 5° which is in a good correlation with the high number of amino acids in contact with membrane (Figure 12). Due to the long-scale fluctuations (100+ ns slow floating motions of the enzyme on the membrane) of the HTA observed in studied systems can be suggested that the CYP-membrane should have the simulation time at least 500+ ns.

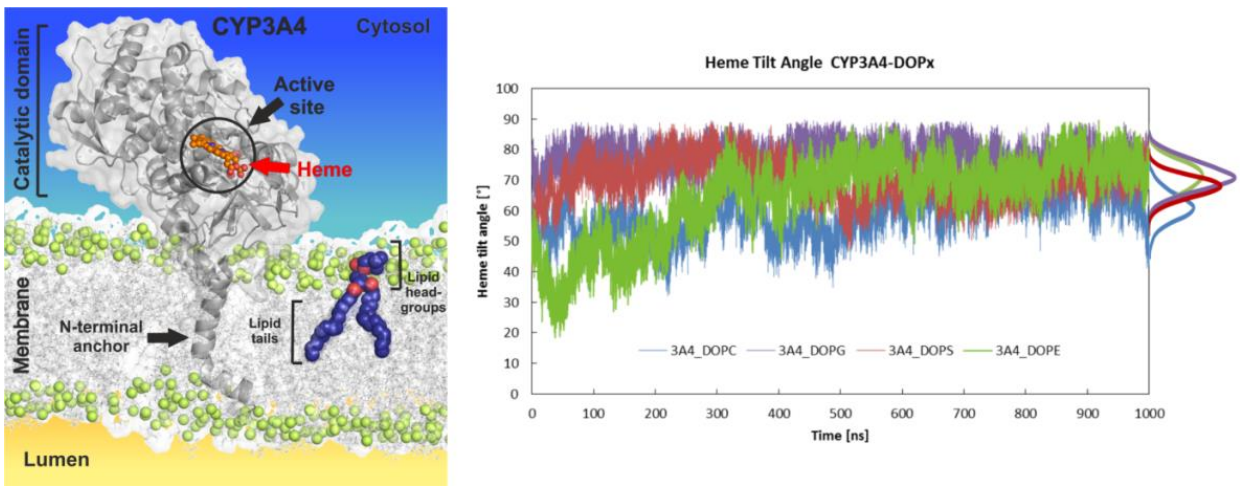

Figure 12. Left panel: Overall view of the CYP3A4 attached to the membrane. The CYP is represented as gray cartons with transparent surface. The active site is marked by black ring and the heme cofactor as orange spheres. Right panel: Heme tilt angle of the CYP3A4 on various membranes (DOPC – blue, DOPG – purple, DOPS – red, DOPE – green) during 1000 ns long MD simulation. Figures were taken from Appendix B.

4.2.2. The effect of the Charge of the Lipids to the Depth of Immersion and the Catalytic Activity of CYP3A4

The different lipid headgroups represented the different interactions with the CYP3A4 and may also affect the catalytic activity of the enzyme. The small ethanolamine headgroup of the DOPE composed of ammonium groups which may serve as the hydrogen bond proton donor. On the other hand, the DOPC choline group cannot forms more hydrogen bonds with CYP3A4 and it can interact only via electrostatic field. DOPG bears the single negative charge given by phosphate part of the lipid. DOPS has phosphate group and zwitterion from serine residue which allow electrostatic interactions too. The hydrogen bonding was most evident in case of DOPG which also caused the larger inclination of the CYP3A4 to the membrane. The other lipids showed smaller inclination towards the membrane in following order: DOPS > DOPE > DOPC.

Noteworthy, negatively charged lipids may easily interact with the positively charged amino acids on the distal side of the CYP3A4 surface. The CYP3A4 showed the deepest immersion in DOPG membrane even deeper than the DOPS. However, from the point of catalytic activity of the CYP, the lipids with the PS headgroups may cause the decrease of the catalytic activity but only if the concertation of the PS lipid is higher than 50%. The loss of the CYP3A4 activity can be connected with the aggregation of the lipid vesicles [71]. However experimental data about catalytic activity of the CYP3A4 in the pure PS membrane are not available. Moreover, the electrostatic interaction between CYP3A4 and the membranes may affect positioning of the mouth opening (deeper in negatively charged membranes). However, the position of the CYP3A4 metabolites and substrates remains in the same positions in the inner part of membrane.

It should be noted that the various membrane lipids lead to the different interactions with CYP3A4. The composition of biological membranes involved the various types of differently charged lipids which may alter the behavior of the membrane protein, but it could be also affected by the type of the protein especially in case of CYP enzymes by the individual CYP isoform. The distal (membrane-faced) and proximal (cytosol-faced) side of the CYP is unevenly distributed. In addition, more than 90% of charged residues are localized on the CYP surface. The negative amino acids are typically more abundant on the proximal side which is in consensus with the binding of CYP redox partners [15,72,73]. The distal sides of CYP are composed in majority of positively charged residues which may cause the higher amount of interactions with negatively charged membrane lipids.

The interactions of the CYP with the various membrane lipids may be also connected with the ordering of the individual membranes and with preferences of the individual CYP isoforms towards ordered or disordered lipid phases, which was observed e.g. in case of CYP1A1 and CYP1A2 [74,75]. Thus, the interaction of the CYP with membranes is mostly driven by electrostatic interactions caused

by the positive charge of the CYP distal side and the negative lipids such as components of the huge variety of lipids involved in biological membranes as well as the preference of CYP isoforms to the ordered or disordered membrane phases.

Finally, we can summarize that differently charged membrane lipids affect lot of properties such as depth of immersion, orientation, opening/closing of channels and even the catalytic activity of the CYP. The CYP3A4 interacts with negatively charged lipids much strongly because the attraction of the positively charged distal side of CYP3A4 and these lipids alter the overall interacting area between CYP and membrane. The major interactions in this case are based on the electrostatics and the hydrogen bonds forming. According to the observed data in the CYP-membrane interactions is mirrored in different CYP catalytic activity and even the preference for the localization in specifically ordered microdomains. The CYP-membrane interactions represent the complex problem which is connected to changes of the main characteristics of the CYP behavior on the membrane surface but also the activity of the CYP. There can be suggested that the membrane in not only passive medium, but the active collaborator of the membrane attached proteins.

4.3 Permeation of the 1,3,7-trimethyluric Acid through the Enzyme Channels

As we know the buried active site of the CYP is connected to the surface by the network of access/egress channels. These pathways serve as the routes or highways which allow traffic of smaller or bigger compounds according to their physico-chemical and geometrical properties given by the amino acid composition. In this study, we were focused on the permeation of the 1,3,7-trimethyluric acid (TMU; Figure 13) through the chosen channels with using the advanced molecular dynamics technique called bias-exchange metadynamics (henceforth BE-META)[47] in combination with MOLE 2.0 tool [52] (see Appendix C).

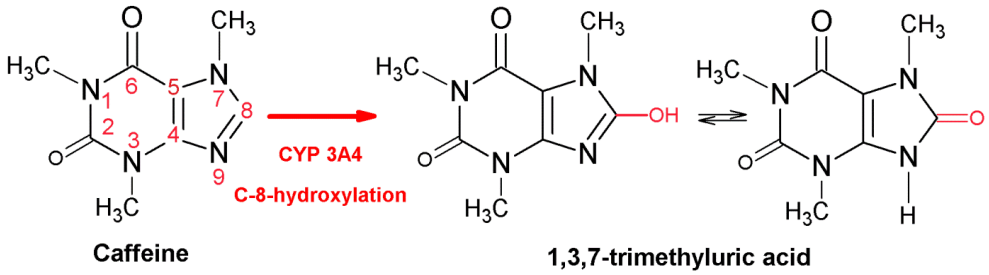

Figure 13. C8 hydroxylation/oxylation of caffeine in CYP3A4. For MD simulations we used the keto-form of 1,3,7-trimethyluric acid. Figure was adopted from Appendix C – Supporting Information.

Firstly we performed computation and analysis of access/egress channels of CYP3A4 with using the software tool MOLE 2.0 [52]. The most abundant were channels 2e, 4 and solvent channel (S). For this reason, we used these three channels in the next steps. Firstly, we docked the chosen molecule – 1,3,7-trimethyluric acid (TMU) through all selected channels. The docked positions of the TMU in the 2e, 4 and solvent were finally used as starting points for the BE-META simulations.

Surprisingly, TMU permeation through the channel 2e was not possible as BE-META showed too high penetration barrier, but the TMU spontaneously permeated through the different channel of channel family 2 – 2af. After this observation we continued with the channel 2af as the proper pathway for TMU transport. We finally performed MD simulations in total time approximately 6 μs and obtained free energy profiles of the TMU permeation through the three channels (2af, 4, S) due to using the BE-META.

4.3.1. BE-META Procedure

In this study the bias-exchange metadynamics (BE-META) [47] was used. The basis of this method is running many metadynamics [44] in parallel and each is biased by different collective variable (CV). Replicas are exchanged in regular time intervals according to the replica-exchange scheme. The exchanges serve as the mediators which enhance the convergence of the free energy estimates on each

replica and allows multidimensional free energy landscapes associated with complex process such as ligand passage through the channel to be simulated.

The choosing of proper CV in BE-META is critical for the proper description of the studied process. The channel path was defined as the set of 5-10 milestones (obtained by docking of ligand to defined channels), in which ligand – TMU was placed in a regularly spaced sequence of configurations between the enzyme cavity and mouth of each channel. In this case the CV which can depict the ligand permeation through the channel was new CV called DMSDDrug, which is a slight modification of previously used DMSD metric:

$$d^{(m)}(X) = \frac{1}{N_{ligand}N_{channel}} \sum_{i=1}^{N_{ligand}} \sum_{j=1}^{N_{channel}} (r_{ij} - r_{ij}^{(m)})^2$$

where r_{ij} and $r_{ij}^{(m)}$ are the distance between atom i and j in configuration X and the configuration of milestone m, respectively. The sums of i and j run from one to N_{ligand} atoms belonging to the ligands and $N_{channel}$ atoms belonging to the channel wall, respectively (Figure 14). The specificity of the DMSDdrug (against classical DMSD metric according to ref. [76]) is in the differentiation of the sums which describe set of atoms of the ligand and channel respectively, instead of in DMSD where the sets of atoms are the same.

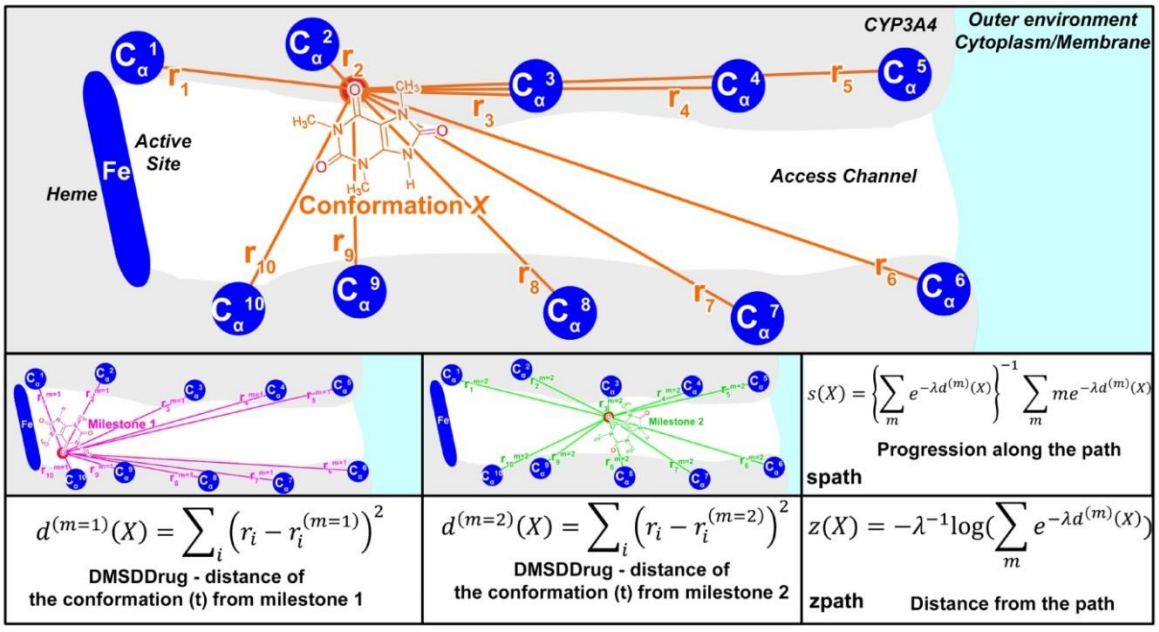

Figure 14. Scheme of 1,3,7-trimethyluric acid (TMU) permeation through one of the CYP3A4 enzyme channels. The path through the channel (spath) was defined by several milestones – reference structures equally distributed in the chosen space. The metric defining the milestones was the drug distance mean square deviation (DMSDDrug) (one of the pair of atoms used for DMSDDrug enumeration was a TMU heavy atom (red), the other was the Cα atom of the channel lining residues or heme atoms (blue), for clarity we only show contacts to one oxygen atom of the ligand). The value

of spath determines the position along the path (for conformation in time t (orange) in the figure spath ~ 1.5 – between milestones 1 and 2). The value of zpath determines the distance from the path. Figure was adopted from Appendix C.

The modification of the DMSDDrug was essential for following usage of another CV – *spath (d(m))* and on the base of the ref. [47] can be defined as follows:

$$s(X) = \frac{\sum_m m e^{-\lambda d^{(m)}(X)}}{\sum_m e^{-\lambda d^{(m)}(X)}}$$

The final set of CVs for BE-META involved eight variables such as the *spath* (CV1) and seven other characteristics. CV2 and CV3 described the number of hydrophobic/hydrophilic interactions between channel and the ligand; CV4 and CV5 were used for the orientation of the ligand (respecting the channels axis); CV6 represented the radius of gyration (*Rg*) of the channel mouth; CV7 depicted distance between drug and the heme cofactor and CV8 as the *zpath*.

4.3.2. TMU Permeation through the Three Channels

Permeation of TMU through the CYP channels was described with using BE-META and eighth CVs (CV1-CV8). The newly defined CV *spath* defined by DMSDDrug metric allowed us to distinguish between the motions of the ligand and channel respectively to comprehend high channel flexibility.

The progress of TMU along the respective channel was described as free energy profiles as a function of the *spath* CV. The minimum of energy was observed in all three cases in the active site (barrier 4-6 kcal/mol). After permeation of the TMU through the channel towards the surface the energy gradually rose up to transition state (below the protein surface) and after that point the energy decreased. The energetic barriers of the transition state in all cases was 10.2 ± 0.6 kcal/mol for solvent channel, 14.5 ± 0.9 kcal/mol for channel 4, 16.5 ± 0.9 kcal/mol for channel 2af. That results nicely showed that preferential path for the TMU permeation is solvent channel which was previously proposed as the important channel used for the product egress [7] (Figure 15). Our study was recently complemented by the study of substrate access (cholesterol) into the CYP3A4 by Hackett, which showed that the access channel from the membrane is channel 2af [77].

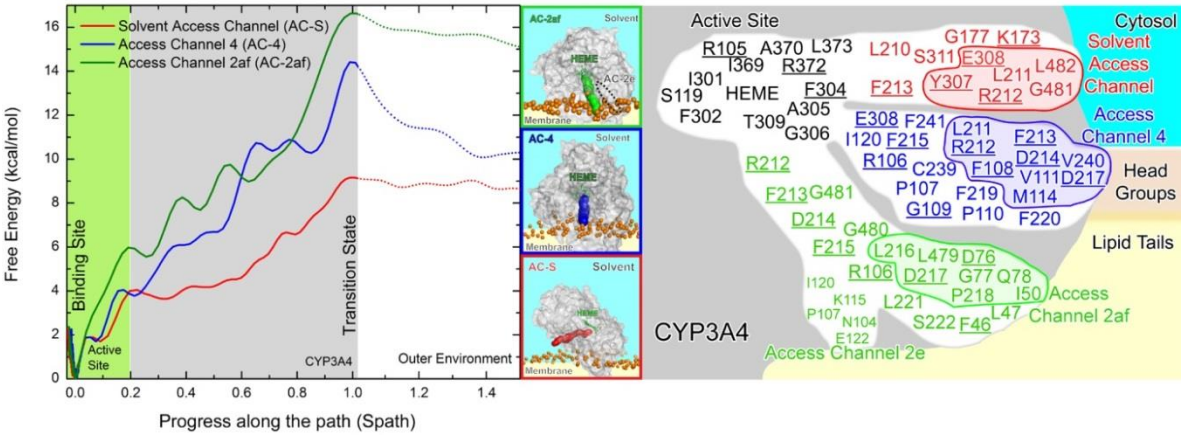

Figure 15. Left panel: Free energy profiles (left panel) of TMU passage via three channels of CYP3A4 embedded in a DOPC lipid bilayer (middle panel). CYP3A4 is represented as a gray surface, heme as green sticks and DOPC phosphates as orange spheres. Initially identified channel 2e is shown in black dots. The schematic in the right panel shows the depth of the channel entrances in the membrane and the channel lining amino acids residues. Bulky channel lining residues are underlined, whereas transition state residues within 4 Å of TMU are depicted in the bordered regions. Figure was adopted from Appendix C.

4.3.3. Permeation of the TMU through the DOPC Membrane

We also calculated the free energy profile of the TMU translocation in the DOPC membrane with using COSMOmic tool. The energy equivalent to the state where the TMU is in the membrane in respect to water phase was ~6 kcal/mol which was in good agreement with the difference of the free energy barriers of solvent channel and channel 2af which connect the active site with the cytoplasm and the membrane interior respectively. Thus the permeation through the lipophilic membrane core region is significantly disfavored for TMU.

4.3.4. Mouth Openings of Channels

The mouth opening of channels was also described by BE-META simulations. We used here the *spath* variable and radius R_m which together can describe mouth opening of the channels. R_m was described by the set of amino acids at the end point of the channel and characterizes the maximal radius of a sphere that can pass through the mouth opening (Figure 16). In case of channel 4 only small fluctuations of R_m were observed which showed that this channel mouth was rather rigid. On the other hand, channel 2af was mostly on the closed state (R_m ~0.9 Å), however the TMU permeation caused the extension ~2.5 Å of the mouth because of the peristaltic wave motion of the channel during the drug passage. Solvent channel was rather closed near the active site (R_m ~0.9 Å or ~1.7 Å) but showed high flexibility and ability to adapt to the permeating TMU. However, the channel was entirely opened with value of R_m 2.5 Å in the transition state. For comparison in the unbiased MD simulation (500 ns)

the channel remained closed (R_m ~0.85 Å) which showed that the opened and closed state can be differentiated with using biased methods such as BE-META and may also serve as the tool for the prediction of most favorable channel for individual ligand. BE-META can therefore reflect the channel malleability and allow observation of the conformational changes connected with the ligand passage through the channels which cannot be reached by classical MD or X-ray methods.

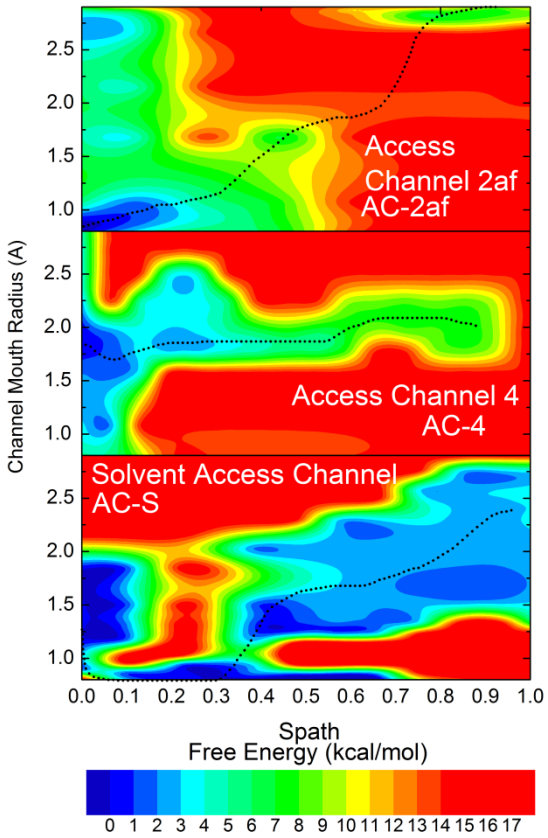

Figure 16. Free energy as a function of the mouth radius and spath variable. Red regions did not have sufficient sampling for reliable calculation of the free energy. The dashed line represents the approximate path followed by the ligand. Figure was adopted from Appendix C.

4.3.5. Transition States and Lining Amino Acids

The BE-META simulation showed also information about the transition states which can be obtained from the free energy profiles. All channels, had transition state on the edge between the protein or the environment such as in solvent channel the TMU was hydrated partially but in channel 4 only small part of TMU was hydrated and in channel 2af the TMU was not hydrated because was only in contact with membrane lipids. Similarly, the amino acids in the transition state mirrored the environment, where the TMU is localized. In case of solvent channel TMU interact with sidechains of K173, F304, E308 and Y307. The residue which can be suggested as a crucial for all movements was R212 as it

was common in all channels (Figure 17). The amino acids suggested here can be used as the interesting targets for the mutation studies.

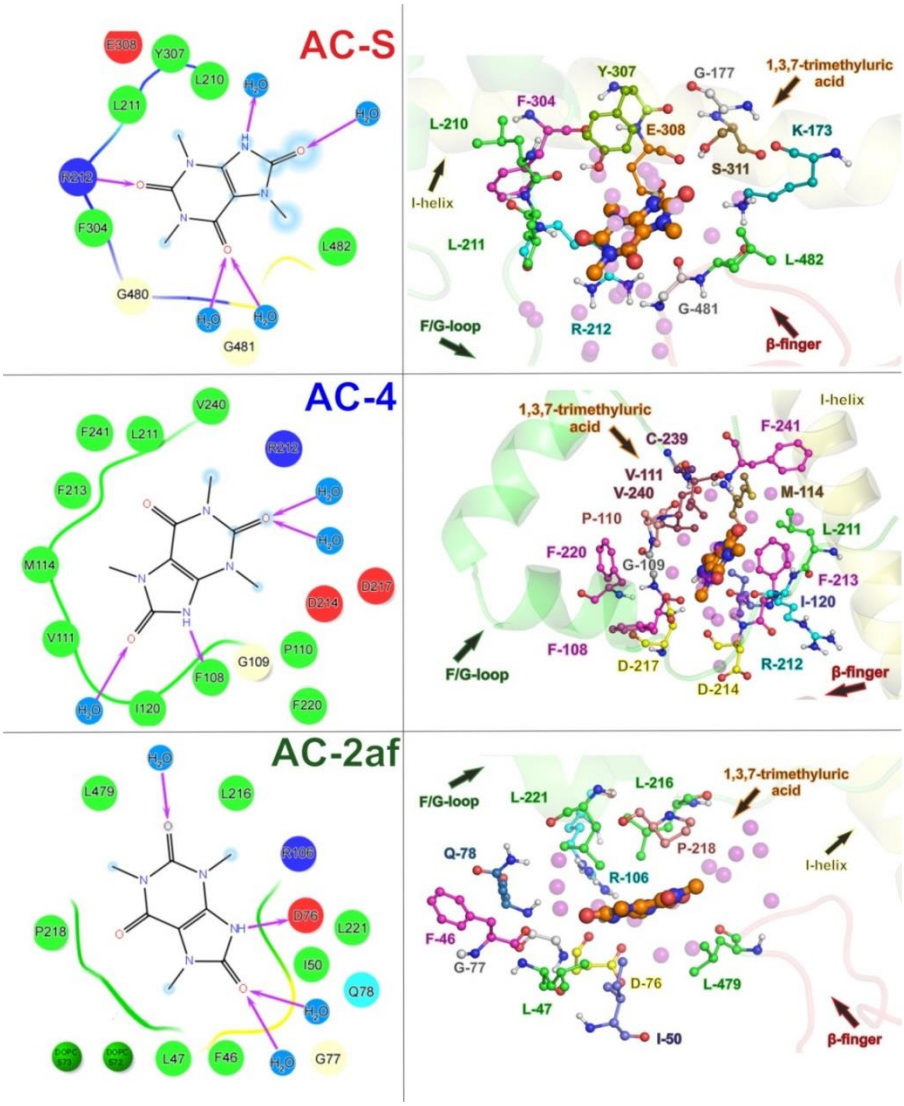

Figure 17. Amino acid residues near TMU in the transition states of studied channels in schematic representation (left) and atomic representation (right). Left panel: Blue shadow represents hydration level of TMU atoms, green curves represent non-polar contacts, yellow and blue curves show polar contacts, and magenta arrows correspond to hydrogen bonds.[78] *Right panel: Residues are shown as balls-and-sticks representations, non-polar hydrogens are not shown for clarity, secondary structural elements are represented as transparent cartoons and colored according to their position in the sequence: β-5-region (labeled as β-finger) – red, F/G loop – green, I-helix – yellow. TMU is shown as orange/blue/red balls and sticks, and water molecules as purple transparent spheres. Figure was adopted from Appendix C.*

Finally, BE-META in combination with MOLE 2.0 bioinformatic tool was used for identification of the channels of CYP3A4 and for the characterization of the egress of the 1,3,7-trimethylruric acid (TMU) from the buried active site toward the protein surface and the free energy profiles connected with this process. The synergy of these two methods and introduction of a newly defined collective

variable *spath* allowed identification of the preferred channel for TMU. Moreover, the BE-META as a biased method is able to reveal the effect of the channel flexibility. Free energy profiles also brought information about transition states and allow identification of the amino acids whose mutations may significantly change the channels opening or closing and thus the CYP3A4 catalytic activity. Briefly the BE-META in combination with MOLE 2.0 channel analysis may serve as the tool for the recognition and characterization of the multiple pathways.

4.4 The Metabolism of Persistent Organic Pollutants by Rat CYP1A1

Nowadays, the rising amount of various pollutants is observed in the environment. The most dangerous toxic compounds in the environment are persistent organic pollutants (henceforth POPs) also known as dioxins and dioxin-like compounds. POPs are known as the compounds with high lipophilicity and poor biodegradability. Due to these properties they can be easily accumulated in the hydrophobic tissues such as in visceral fat. The most dangerous dioxin is certainly 2,3,7,8-tetrachloro-dibenzo-*p*-dioxin (TCDD). TCDD cannot be metabolized by any wild type form of CYP and due to its highly lipophilic character can be accumulated in the adipose tissues in the human body as is well known from the case of Victor Yushchenko poisoning [79]. However, other POPs can be metabolized by several CYP families such as human CYP1A1, CYP1A2, CYP2C9 and also rat CYP1A1 or porcine CYP1A1 [80–83].

Whereas the human CYP1A1 cannot metabolize the TCDD, the mutant of rat CYP1A1 is capable to consume this dioxin. This assignment was observed experimentally in the mutated structure of rat CYP1A1 where the distal phenylalanine F240 was replaced by alanine. The hydroxylation experiments showed that the rat CYP1A1 mutant can slowly metabolize TCDD whereas the wild type rat CYP1A1 cannot [80] (Figure 18). This surprising experimental data came without explanation of the mechanism.

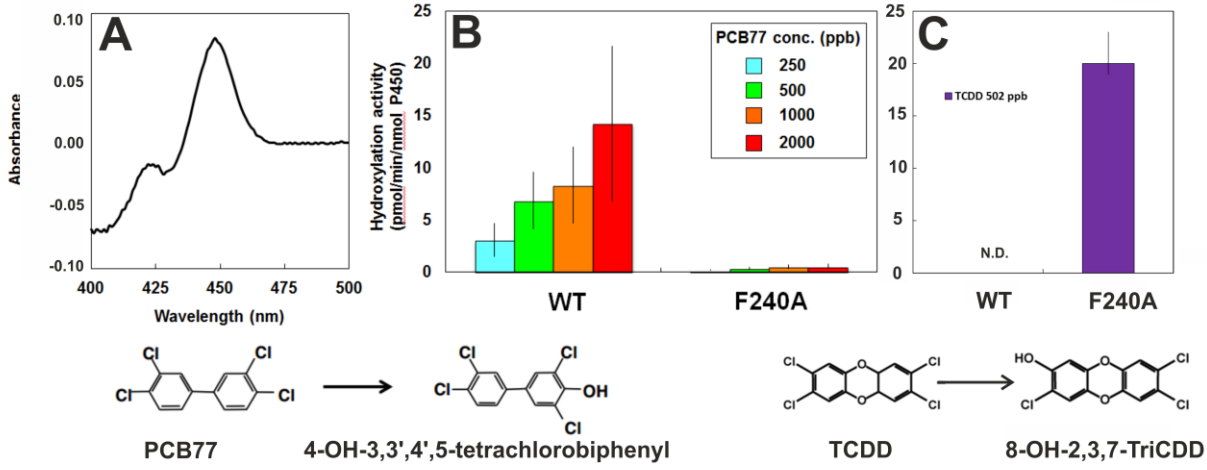

Figure 18. Experimental activities of rat CYP1A1 enzymes. Panel A shows CO difference spectrum for rat CYP1A1 F240A mutant extracted from recombinant yeast cells. Panels B and C shows the hydroxylation activity of WT and F240A mutant of rat CYP1A1 towards PCB77 (panel B) and TCDD (panel C). Data for TCDD taken from Shinkyo et al. [80] *Structures of PCB77 and TCDD are shown in the bottom together with metabolites. Figure was adopted from Appendix D.*

For purpose of description of the mechanism of hydroxylation of TCDD by rat CYP1A1 F240A mutant we carried out 200ns-long MD simulations of the complex of the ligand free rat CYP1A1 and ligand bound complex with TCDD and with PCB77. We characterized several potential reasons for

the changes of the hydroxylation activity: i) changes in the membrane positioning of the PCB77 and TCDD and access channels; ii) differences in the access channels radius (different accessibility through the channel); iii) different affinities of TCDD and PCB77 for the WT and mutant F240A.

4.4.1. Differences in Membrane Position of TCDD and PCB77 and WT and F240A

The free energies calculated along the DOPC membrane normal suggested the preferential position of the PCB77 and TCDD in the hydrophobic membrane core in the area within 1.1 nm of the membrane center with strong affinities -8.8 kcal/mol and -9.9 kcal/mol, respectively. The affinity of the PCB77 and TCDD correlates with their tendency to accumulate in the membrane which may lead to membrane disfunctions.

After the 200ns-long MD simulation the WT and mutant F240A converged to the similar position (~3.8 ± 0.2 nm) from the center of the membrane. The global common CYP fold remains unaffected in exception with small rearrangements in proximity of the mutated residue F240A in F/G loop region (Figure 4. in Appendix D).

4.4.2. Differences of the Access Channels

The F240A mutation is localized in the important region F/G loop partly immersed in the membrane which is known as a flexible region that lies between two flexible regions FR2 and FR6 [21]. Thus, mutation of the F240 to the alanine significantly affected channels in the vicinity of this area. Firstly, we compared the structures without bound POPs. In WT the most opened channels were solvent channel (S) and 2b (only channels with bottleneck radius larger than ~0.1 nm) but in case of the mutant F240A these channels were observed in reduced numbers. On the other hand, the channels 2af and 2c were more opened in the F240A mutant. It should be noted that the phenylalanine 240 as a huge aromatic residue may serves as a “lid” of the channels 2af and 2b or another neighboring channel in the proximity.

Structures with bound ligands show significantly different pattern of channels openings. Many channels were closed in WT-PCB77 complex but there is still possibility for ligand reach the active site by several channels (2b, 2d). Conversely, the WT-TCDD showed an opposite behavior because the complex is very rigid and does not allow the opening of many channels. This result is in a good correlation with previously observed in porcine CYP1A1 where the closure of the channels in case of bound TCDD was observed (other dioxins did not caused channels closure) [83]. The significant

changes were observed in the complex of the mutant F240A-TCDD where the presence of ligand induced the channels openings, especially 2af, 2b, 2c and 2d, whereas the complex WT-TCDD was rather closed (Figure 19). The different patterns of channels openings upon binding TCDD or PCB77 can be explained by the rigidifying effect of the TCDD molecules which may cause the "locking" of the active site of the WT which is in correlation with data observed for CYP2B [84].

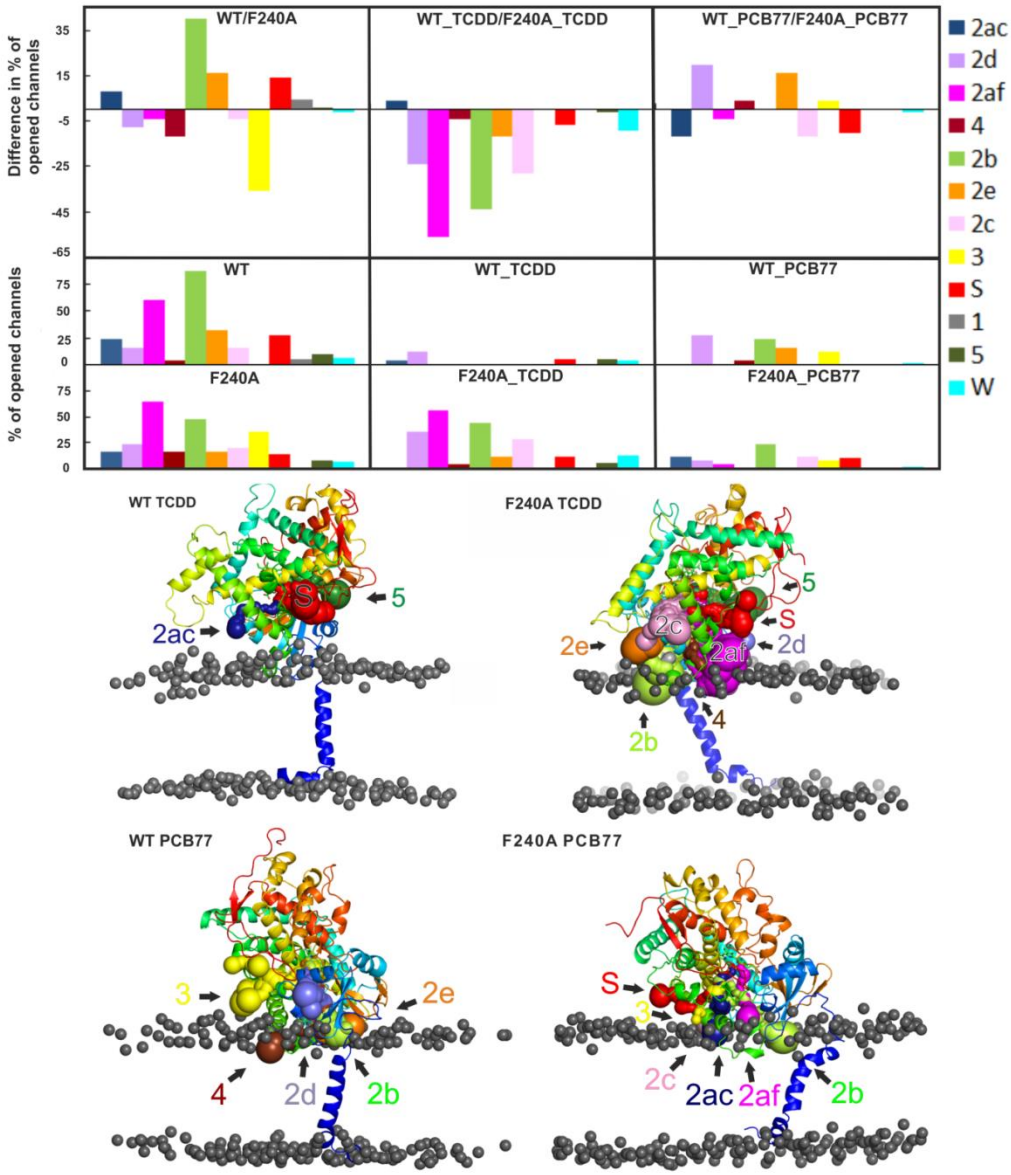

Figure 19. Top panel: Differences in channel openings between the WT enzyme and the F240A mutant, and structural overview of the channels' locations.. Bottom panel: structures of the WT and F240A mutant bound to TCDD and PCB77, showing the positions of key channel entrances. The TCDD-bound F240A complex has more open channels than the corresponding PCB77-bound complex. Detailed information see in Appendix D.

While the WT-TCDD is locked the F240A seems to prevent the active site before rigidification and did not cause the channels closure. The PCB77 molecule is smaller and more flexible than TCDD and

may cause only some conformational rearranges which leads to the changes of the channels opening/closing pattern.

4.4.3. Binding Energies of the WT and F240A with POPs

As the last step we calculated the binding energies of the WT and F240A with TCDD and PCB77 with using the MM-PBSA method [85]. According these data the binding of PCB77 to the WT was more favorable than to the F240A mutant ($\Delta\Delta G$(F240A-WT-PCB77) = +3.2 kcal/mol). Conversely, the F240A-TCDD complex showed stronger binding of TCDD than in the WT ($\Delta\Delta G$(F240A-WT-TCDD) = -1.4 kcal/mol). The data obtained by MM-PBSA nicely correlated with hydroxylation activities observed in experiments [80] where the F240A mutant catalyzed hydroxylation of TCDD but WT did not able to metabolize TCDD. The differences in hydroxylation activity and also in binding energies stem from different distribution of the π-π stacking interactions between residue F240 and surrounding phenylalanine amino acids in proximity of the BC- and FG-loops (F116, F127, F228, F255, Y236, F240; see Figure 20).

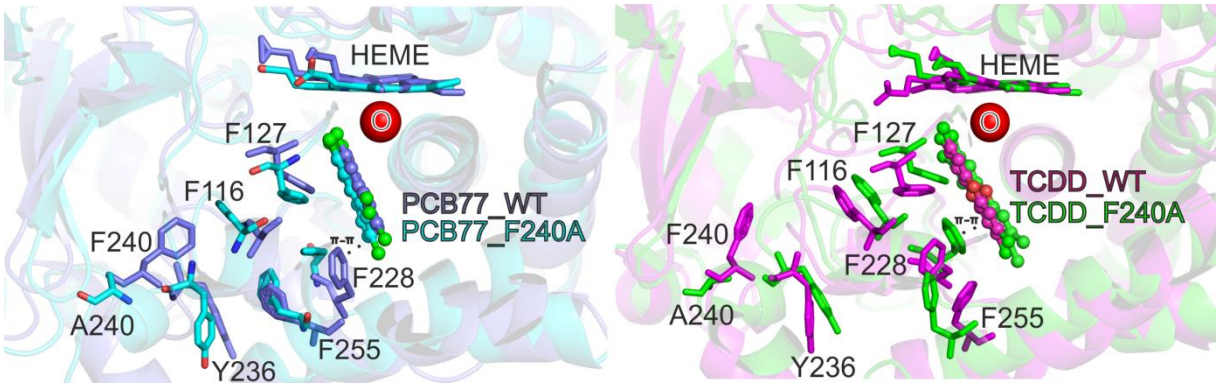

Figure 20. Detailed view of the active site with PCB77 and TCDD (average positions). Adopted from Appendix D.

MD simulations revealed that the PCB77 and TCCD accumulated in the hydrophobic part of the membrane and pre-concentrated there. Both POPs can penetrate to the CYP active site through the network of the access channels which can reach the membrane by their mouth openings and may affect the substrate access form the membrane. Mutation F240A caused significant changes in channel opening/closing and may led to the affecting of the hydroxylation activity. But this observation is only one of many pieces of this complex jigsaw.

The analysis of the binding energies added information about the differences between binding of PCB77 and TCDD and correlated with the experimental data. The main differences between binding energies of POPs comes from the structural reorganizations in the proximity of bound POP caused by mutation on the F240A position (Figure 20). These rearrangements led to the much efficient binding

of TCDD. Conversely, the presence of F240 in WT helps the PCB77 bound in catalytically efficient position while the mutant F240A led to the attenuation of PCB77 binding.

Finally, this study showed that there is the significant role in the processes connected with the uptake of substrates which can be driven by distal residues as well as the residues positioned in the active site cavity. Even the distal mutation in distance 2.5 nm from the heme cofactor may significantly change the opening/closing of the access/egress channels, conformational changes leads to the strengthening or attenuating the binding of the POPs which is finally reflected in the changes of the binding energies and hydroxylation activities as well. This information may be useful in future modulation of the POPs-metabolizing enzymes and may lead to the tailored protein engineering of the enzymes with desired properties.

5. SUMMARY

This thesis was focused on the role of important enzymes - cytochromes P450 and their behavior on the biological membranes as well as the interactions with various compounds from simulation perspective.

Firstly, we observed that the membrane affect the CYP behavior as well as CYP alter local membrane properties. The MD simulation revealed that the rising cholesterol content significantly alters the behavior of the CYP on the membrane and can even cause CYP's non-competitive inhibition by high cholesterol concentration. The membrane lipids also modify the opening or closing of access/egress channels. The electrostatic interactions between CYP and membrane change positioning and contact area of the CYP with the membrane. The various CYP isoforms may also prefer different membrane microdomains depending on the composition of membrane-immersed amino acids and surrounding membrane. Thus the membrane is not only passive environment but is also the significant player of the behavior of membrane-attached proteins.

However, the membrane play role also in the accumulation of the CYP substrates according to the character of the potential substrate e.g. highly lipophilic dioxin molecule which accumulate in the membrane from where it can be transported into the CYP active site via membrane-facing access channel. The passage of the ligand through the channel is the result of the conformational changes of the amino acids lining the channel as was shown by our biased-exchange metadynamics (BE-META) study of CYP3A4 metabolite 1,3,7-trimethyluric acid. BE-META showed not only the energetics of the ligand permeation and the classification of the most favourable channel for transportation of the individual molecule, but also how surprisingly small conformations are needed for successful ligand passage.

The substrate/metabolite passage may be affected by mutations of amino acids positioned outside the active site of the CYP. The classical mutational studies are based on the mutation in proximity of the active site cavity which is crucial for the catalytic activity of the enzyme. However, we should also consider the distal mutations whose role has not be neglected. The structural changes of the access paths and the differences in the binding energies of persistent organic pollutants explained the differences in hydroxylation activity of the rat CYP1A1 and its distal F240A mutant. The distal mutation may thus affect the activity of the enzyme given the mutation affect other functional part of the enzyme, such as access channel.

Many variables, interactions and high level of the complexity are involved in the biological processes. This work, hopefully, brought just a small piece of light to the enormous shadowy puzzle of the living cell processes.

6. SHRNUTÍ

Předmětem této disertační práce byly významné enzymy – cytochromy P450 (CYP), jejich chování v prostředí biologických membrán a také interakce těchto enzymů s různými sloučeninami, jež bylo pozorováno pomocí molekulárně dynamických simulací.

Prvně zmiňované výsledky naznačují, že přítomnost membrány může ovlivňovat chování CYP a stejně tak CYP může ovlivňovat vlastnosti membrány v místě vzájemného kontaktu. S použitím MD simulací jsme odhalili, že s rostoucím obsahem cholesterolu v membráně se významně mění chování CYP na membráně a může vést až k nekompetitivní inhibici v důsledku vysoké koncentrace cholesterolu. Membránové lipidy rovněž ovlivňují pozici a kontaktní plochu CYP s membránou. U různých izoforem CYP se mohou lišit preference vůči různým membránovým mikrodoménám, které závisí na složení v membráně zanořených aminokyselin a okolní membráně. Membrána zde tedy nehraje pouze roli jakéhosi pasivního pozorovatele, ale je významným spoluhráčem dokreslujícím chování membránově vázaných proteinů.

Membrána však hraje také roli v rámci akumulace substrátů CYP, a to na základě vlastností těchto látek např. vysoce lipofilních molekul dioxinů kumulujících se v membráně, odkud mohou být do aktivního místa CYP transportovány pomocí sítě přístupových kanálů. Průchod ligandu kanálem je výsledkem řady konformačních změn aminokyselin v okolí kanálu, jak ukázala tzv. bias-exchange metadynamika (BE-META) ve studii zaměřené transport metabolitu CYP3A4 – 1,3,7-trimethylmočové kyseliny kanály. BE-META je schopna popsat nejen energetiku permeace daného ligandu, určit kanál, který je pro průchod konkrétní molekuly nejvhodnější, ale také ukazuje, jak překvapivě malé konformační změny jsou třeba k tomu, aby byl ligand úspěšně transportován.

Transport substrátů či metabolitů může být do jisté míry také ovlivněn mutacemi aminokyselin umístěnými vně aktivního místa CYP. Klasické mutační studie jsou založeny na mutacích v blízkosti kavity aktivního místa, jež jsou zásadní pro katalytickou funkci enzymu. Měli bychom však také uvažovat význam distálních mutací, jejichž role by rozhodně neměla být přehlížena. Strukturní změny přístupových cest a rozdíly vazebných energií persistentních organických polutantů vysvětlily experimentálně zjištěné rozdíly v hodnotách hydroxylační aktivity krysího CYP1A1 a jeho mutantu F240A. Jak se zde ukázalo, distální mutace tedy může ovlivňovat aktivitu enzymu, která je dána změnou části struktury významné pro fungování proteinu, kterou představují přístupové kanály.

Velká škála proměnných, mnoho interakcí a vysoká míra komplexnosti se skrývá v rozličných biologických procesech. Doufejme, že tato disertační práce osvětlila, alespoň maličký kousíček této ohromné skládačky, z níž sestávají procesy odehrávající se v buňkách našich organismů.

7. List of Abbreviations

CYP – cytochrome P450

DOPC - 1,2-dioleoyl-sn-glycero-3-phosphocholine

DOPE - 1,2-dioleoyl-sn-glycero-3-phosphoethanolamine

DOPG - 1,2-dioleoyl-sn-glycero-3-[phospho-rac-(3-lysyl(1-glycerol))]

DOPS - 1,2-dioleoyl-sn-glycero-3-phosphoserine

POPC – 1-palmitoyl-2-oleyl-sn-glycero-3-phosphocholine

HTA – heme tilt angle

MD – molecular dynamics

CV – collective variable

BE-META – bias-exchange metadynamics

TMU – 1,3,7-trimethyluric acid

POP – persistent organic pollutants

WT – rat CYP1A1 wild type

F240A – rat CYP1A1 F240A mutant

PCB77 – 3,3',4,4'-tetrachlorobiphenyl

TCDD – 2,3,7,8-tetrachloro-dibenzo-*p*-dioxin

MM-PBSA - molecular mechanics – Poisson-Boltzmann surface area

8. Bibliography

[1] S. Rendic, F.P. Guengerich, Survey of Human Oxidoreductases and Cytochrome P450 Enzymes Involved in the Metabolism of Xenobiotic and Natural Chemicals, Chem. Res. Toxicol., 28 (2015) 38–42.

[2] T. Omura, R. Sato, A New Cytochrome in Liver Microsomes, J. Biol. Chem., 237 (1962) 1375–6.

[3] P.R.O. de Montellano, Cytochrome P450: Structure, Mechanism, and Biochemistry, 3rd ed., Kluwer Academic/Plenum Publishers, New York, 2005.

[4] P.B. Danielson, The Cytochrome P450 Superfamily : Biochemistry, Evolution and Drug Metabolism in Humans, Curr Drug Metab, 3 (2002) 561–597.

[5] F.P. Guengerich, Common and Uncommon Cytochrome P450 Reactions Related to Metabolism and Chemical Toxicity, Chem. Res. Toxicol., 14 (2001) 611–650.

[6] P. Alberts, B.; Johnson, A.; Lewis, J.; Raff, M.; Roberts, K.; Walter, B. Alberts, A. Johnson, J. Lewis, M. Raff, K. Roberts, P. Walter, Molecular Biology of THE CELL, 5th ed., New York: Garland Science, New York, 2008.

[7] K. Berka, M. Paloncýová, P. Anzenbacher, M. Otyepka, Behavior of Human Cytochromes P450 on Lipid Membranes, J. Phys. Chem. B, 117 (2013) 11556–11564.

[8] V. Cojocaru, P.J. Winn, R.C. Wade, The Ins and Outs of Cytochrome P450s, Biochim. Biophys. Acta - Gen. Subj., 1770 (2007) 390–401.

[9] R.C. Wade, P.J. Winn, I. Schlichting, Sudarko, A Survey of Active Site Access Channels in Cytochromes P450, J. Inorg. Biochem., 98 (2004) 1175–1182.

[10] P. Anzenbacher, E. Anzenbacherová, Cytochromes P450 and Metabolism of Xenobiotics, Cell. Mol. Life Sci., 58 (2001) 737–747.

[11] F.P. Guengerich, M.R. Waterman, M. Egli, Recent Structural Insights into Cytochrome P450 Function, Trends Pharmacol. Sci., 37 (2016) 625–640.

[12] M. Ekroos, T. Sjogren, Structural Basis for Ligand Promiscuity in Cytochrome P450 3A4, Proc. Natl. Acad. Sci., 103 (2006) 13682–13687.

[13] F.P. Guengerich, Intersection of the Roles of Cytochrome P450 Enzymes with Xenobiotic and Endogenous Substrates: Relevance to Toxicity and Drug Interactions, Chem. Res. Toxicol., 30 (2017) 2–12.

[14] F.P. Guengerich, T.L. Macdonald, Chemical Mechanisms of Catalysis by Cytochromes P-450: A Unified View, Acc. Chem. Res., 17 (1984) 9–16.

[15] M. Otyepka, J. Skopalík, E. Anzenbacherová, P. Anzenbacher, What Common Structural Features and Variations of Mammalian P450s are Known to Date?, Biochim. Biophys. Acta - Gen. Subj., 1770 (2007) 376–389.

[16] C. Orengo, A. Michie, S. Jones, D. Jones, M. Swindells, J. Thornton, CATH - a Hierarchic Classification of Protein Domain Structures, Structure, 17 (1997) 1093–1109.

[17] T.L. Poulos, B.C. Finzel, A.J. Howard, High-resolution Crystal Structure of Cytochrome P450cam, J. Mol. Biol., 195 (1987) 687–700.

[18] C.A. Hasemann, R.G. Kurumbail, S.S. Boddupalli, J. a Peterson, J. Deisenhofer, Structure and Function of Cytochromes P450: A Comparative Analysis of Three Crystal Structures, Structure, 3 (1995) 41–62.

[19] Schrodinger LLC, The PyMOL Molecular Graphics System, (2010).

[20] M. Subramanian, H. Tam, H. Zheng, T.S. Tracy, CYP2C9-CYP3A4 Protein-Protein Interactions: Role of the Hydrophobic N Terminus, Drug Metab. Dispos., 38 (2010) 1003–1009.

[21] J. Skopalík, P. Anzenbacher, M. Otyepka, Flexibility of Human Cytochromes P450 : Molecular Dynamics Reveals Differences between CYPs 3A4 , 2C9 , and 2A6 , which Correlate with Their Substrate Preferences, J. Phys. Chem. B, 112 (2008) 8165–8173.

[22] U.H.N. Dürr, L. Waskell, A. Ramamoorthy, The Cytochromes P450 and b5 and their Reductases—Promising Targets for Structural Studies by Advanced Solid-state NMR Spectroscopy, Biochim. Biophys. Acta - Biomembr., 1768 (2007) 3235–3259.

[23] J. Mestres, Structure Conservation in Cytochromes P450, Proteins Struct. Funct. Genet., 58 (2005) 596–609.

[24] C. Oostenbrink, A. de Ruiter, J. Hritz, N. Vermeulen, Malleability and Versatility of Cytochrome P450 Active Sites Studied by Molecular Simulations, Curr. Drug Metab., 13 (2012) 190–6.

[25] C. Hayes, D. Ansbro, M. Kontoyianni, Elucidating Substrate Promiscuity in the Human Cytochrome 3A4, J. Chem. Inf. Model., 54 (2014) 857–869.

[26] J.E. Laine, S. Auriola, M. Pasanen, R.O. Juvonen, Acetaminophen Bioactivation by Human Cytochrome P450 Enzymes and Animal Microsomes, Xenobiotica., 39 (2009) 11–21.

[27] T. Hendrychová, E. Anzenbacherová, J. Hudeček, J. Skopalík, R. Lange, P. Hildebrandt, M. Otyepka, P. Anzenbacher, Flexibility of Human Cytochrome P450 Enzymes: Molecular Dynamics and Spectroscopy Reveal Important Function-related Variations, Biochim. Biophys. Acta, 1814 (2011) 58–68.

[28] R.S. Foti, M. Honaker, A. Nath, J.T. Pearson, B. Buttrick, N. Isoherranen, W.M. Atkins, Catalytic versus Inhibitory Promiscuity in Cytochrome P450s: Implications for Evolution of New Function, Biochemistry, 50 (2011) 2387–2393.

[29] O. Gotoh, Substrate Recognition Sites in Cytochrome P450 Family 2 (CYP2) Proteins Inferred from Comparative Analyses of Amino Acid and Coding Nucleotide Sequences, J. Biol. Chem., 267 (1992) 83–90.

[30] I.G. Denisov, T.M. Makris, S.G. Sligar, I. Schlichting, Structure and Chemistry of Cytochrome P450, Chem. Rev., 105 (2005) 2253–2278.

[31] E.E. Scott, J.R. Halpert, Structures of cytochrome P450 3A4, Trends Biochem. Sci., 30 (2005) 5–7.

[32] D. Fishelovitch, S. Shaik, H.J. Wolfson, R. Nussinov, How Does the Reductase Help to Regulate the Catalytic Cycle of Cytochrome P450 3A4 Using the Conserved Water Channel?, J. Phys. Chem. B, 114 (2010) 5964–5970.

[33] C. Barnaba, K. Gentry, N. Sumangala, A. Ramamoorthy, The Catalytic Function of Cytochrome P450 is Entwined with its Membrane-bound Nature, F1000Research, 6 (2017) 662.

[34] N.A. Treuheit, M. Redhair, H. Kwon, W.D. McClary, M. Guttman, J.P. Sumida, W.M. Atkins, Membrane Interactions, Ligand-Dependent Dynamics, and Stability of Cytochrome P4503A4 in Lipid Nanodiscs, Biochemistry, 55 (2016) 1058–1069.

[35] M. Paloncýová, V. Navrátilová, K. Berka, A. Laio, M. Otyepka, Role of Enzyme Flexibility in Ligand Access and Egress to Active Site: Bias-Exchange Metadynamics Study of 1,3,7-Trimethyluric Acid in Cytochrome P450 3A4, J. Chem. Theory Comput., 12 (2016) 2101–2109.

[36] M.C.C.J.C. Ebert, S.L. Dürr, A. A. Houle, G. Lamoureux, J.N. Pelletier, Evolution of P450 Monooxygenases toward Formation of Transient Channels and Exclusion of Nonproductive Gases, ACS Catal., 6 (2016) 7426–7437.

[37] S.D. Black, Membrane Topology of the Mammalian P450 Cytochromes, FASEB J., 6 (1992) 680–685.

[38] M.J. Headlam, M.C.J. Wilce, R.C. Tuckey, The F-G loop Region of Cytochrome P450scc (CYP11A1) Interacts with the Phospholipid Membrane, Biochim. Biophys. Acta - Biomembr., 1617 (2003) 96–108.

[39] R. Shinkyo, F.P. Guengerich, Inhibition of Human Cytochrome P450 3A4 by Cholesterol, J. Biol. Chem., 286 (2011) 18426–18433.

[40] M.A. González, Force Fields and Molecular Dynamics Simulations, Collect. SFN, 12 (2011) 169–200.

[41] V. Hornak, R. Abel, A. Okur, B. Strockbine, A. Roitberg, C. Simmerling, Comparison of Multiple Amber Force Fields and Development of Improved Protein Backbone Parameters, Proteins Struct. Funct. Bioinforma., 65 (2006) 712–725.

[42] J.P.M. Jämbeck, A.P. Lyubartsev, Another Piece of the Membrane Puzzle: Extending Slipids Further, J. Chem. Theory Comput., 9 (2013) 774–784.

[43] A. Barducci, M. Bonomi, M. Parrinello, Metadynamics, Wiley Interdiscip. Rev. Comput. Mol. Sci., 1 (2011) 826–843.

[44] A. Laio, F.L. Gervasio, Metadynamics: A Method to Simulate Rare Events and Reconstruct the Free Energy in Biophysics, Chemistry and Material Science, Reports Prog. Phys., 71 (2008) 126601.

[45] I. Bisha, A. Rodriguez, A. Laio, A. Magistrato, Metadynamics Simulations Reveal a Na+ Independent Exiting Path of Galactose for the Inward-Facing Conformation of vSGLT, PLoS Comput. Biol., 10 (2014) e1004017.

[46] Y. Sugita, A. Kitao, Y. Okamoto, Multidimensional Replica-exchange Method for Free-energy Calculations, J. Chem. Phys., 113 (2000) 6042–6051.

[47] S. Piana, A. Laio, A Bias-Exchange Approach to Protein Folding, J. Phys. Chem. B, 111 (2007) 4553–4559.

[48] O.S. Smart, J.G. Neduvelil, X. Wang, B.A. Wallace, M.S.P. Sansom, HOLE: A program for the Analysis of the Pore Dimensions of Ion Channel Structural Models, J. Mol. Graph., 14 (1996) 354–360.

[49] M. Petrek, M. Otyepka, P. Banáš, P. Košinová, J. Koča, J.J. Damborský, P. Banás, P. Kosinová, J. Koca, J.J. Damborský, CAVER: A New Tool to Explore Routes from Protein Clefts, Pockets and Cavities, BMC Bioinformatics, 7 (2006) 316.

[50] M. Petřek, P. Košinová, J. Koča, M. Otyepka, MOLE: A Voronoi Diagram-Based Explorer of Molecular Channels, Pores, and Tunnels, Structure, 15 (2007) 1357–1363.

[51] E. Yaffe, D. Fishelovitch, H.J. Wolfson, D. Halperin, R. Nussinov, MolAxis: Efficient and Accurate Identification of Channels in Macromolecules, Proteins, 73 (2008) 72–86.

[52] D. Sehnal, R. Svobodová Vařeková, K. Berka, L. Pravda, V. Navrátilová, P. Banáš, C.-M.C.-M. Ionescu, M. Otyepka, J. Koča, R.S. Vařeková, K. Berka, L. Pravda, V. Navrátilová, P. Banáš, C.-M.C.-M. Ionescu, M. Otyepka, J. Koča, MOLE 20: Advanced Approach for Analysis of Biomacromolecular Channels, J. Cheminform., 5 (2013) 39.

[53] J.M. Zimmerman, N. Eliezer, R. Simha, The Characterization of Amino Acid Sequences in Proteins by Statistical Methods, J. Theor. Biol., 21 (1968) 170–201.

[54] J. Kyte, R.F. Doolittle, A Simple Method for Displaying the Hydropathic Character of a Protein, J. Mol. Biol., 157 (1982) 105–132.

[55] H. Cid, M. Bunster, M. Canales, F. Gazitúa, Hydrophobicity and Structural Classes in Proteins, Protein Eng. Des. Sel., 5 (1992) 373–375.

[56] D.T. Jones, W.R. Taylor, J.M. Thornton, The Rapid Generation of Mutation Data Matrices from Protein Sequences, Bioinformatics, 8 (1992) 275–282.

[57] J. Montero, M. Mari, A. Colell, A. Morales, G. Basañez, C. Garcia-Ruiz, J.C. Fernández-Checa, Cholesterol and Peroxidized Cardiolipin in Mitochondrial Membrane Properties, Permeabilization and Cell Death, Biochim. Biophys. Acta - Bioenerg., 1797 (2010) 1217–1224.

[58] E. Sackman, E. Sackmann, E. Sackman, Biological Membranes Architecture and Function, Struct. Dyn. Membr. From Cells to Vesicles, 1 (1995) 1–63.

[59] R.M. Epand, Cholesterol and the Interaction of Proteins with Membrane Domains, Prog. Lipid Res., 45 (2006) 279–294.

[60] J. Fantini, Interaction of Proteins with Lipid Rafts Through Glycolipid-Binding Domains:Biochemical Background and Potential Therapeutic Applications, Curr. Med. Chem., 14 (2007) 2911–2917.

[61] K. Simons, J.L. Sampaio, Membrane Organization and Lipid Rafts, Cold Spring Harb. Perspect. Biol., 3 (2011) a004697.

[62] J.L. Baylon, I.L. Lenov, S.G. Sligar, E. Tajkhorshid, Characterizing the Membrane-Bound State of Cytochrome P450 3A4: Structure, Depth of Insertion, and Orientation, J. Am. Chem. Soc., 135 (2013) 8542–8551.

[63] I.A. Pikuleva, Cholesterol-Metabolizing Cytochromes P450: Implications for Cholesterol Lowering, Expert Opin. Drug Metab. Toxicol., 4 (2008) 1403–1414.

[64] G.F. Gibbons, The Role of Cytochrome P450 in the Regulation of Cholesterol Biosynthesis, Lipids, 37 (2002) 1163–70.

[65] G. van Meer, A.I.P.M. de Kroon, Lipid Map of the Mammalian Cell, J. Cell Sci., 124 (2011) 5–8.

[66] E.F. Johnson, C.D. Stout, Structural Diversity of Eukaryotic Membrane Cytochrome P450s, J. Biol. Chem., 288 (2013) 17082–17092.

[67] I.G. Denisov, A.Y. Shih, S.G. Sligar, Structural Differences between Soluble and Membrane

Bound Cytochrome P450s, J. Inorg. Biochem., 108 (2012) 150–158.

[68] K. Berka, T. Hendrychová, P. Anzenbacher, M. Otyepka, Membrane Position of Ibuprofen Agrees with Suggested Access Path Entrance to Cytochrome P450 2C9 Active Site, J. Phys. Chem. A, 115 (2011) 11248–11255.

[69] V. Cojocaru, K. Balali-Mood, M.S.P. Sansom, R.C. Wade, Structure and Dynamics of the Membrane-Bound Cytochrome P450 2C9, PLoS Comput. Biol., 7 (2011) e1002152.

[70] J. Sgrignani, A. Magistrato, Influence of the Membrane Lipophilic Environment on the Structure and on the Substrate Access/Egress Routes of the Human Aromatase Enzyme A Computational Study, J. Chem. Inf. Model., 52 (2012) 1595–1606.

[71] K.-H. Kim, T. Ahn, C.-H. Yun, Membrane Properties Induced by Anionic Phospholipids and Phosphatidylethanolamine are Critical for the Membrane Binding and Catalytic Activity of Human Cytochrome P450 3A4, Biochemistry, 42 (2003) 15377–15387.

[72] T.A. Clarke, S.C. Im, A. Bidwai, L. Waskell, The Role of the Length and Sequence of the Linker Domain of Cytochrome b5 in Stimulating Cytochrome P450 2B4 Catalysis, J. Biol. Chem., 279 (2004) 36809–36818.

[73] A. Bridges, L. Gruenke, Y.-T. Chang, I.A. Vakser, G. Loew, L. Waskell, Identification of the Binding Site on Cytochrome P450 2B4 for Cytochrome b5 and Cytochrome P450 Reductase, J. Biol. Chem., 273 (1998) 17036–17049.

[74] J.W. Park, J.R. Reed, W.L. Backes, The Localization of Cytochrome P450s CYP1A1 and CYP1A2 into Different Lipid Microdomains Is Governed by Their N-terminal and Internal Protein Regions, J. Biol. Chem., 290 (2015) 29449–29460.

[75] L.M. Brignac-Huber, J.R. Reed, M.K. Eyer, W.L. Backes, Relationship Between CYP1A2 Localization and Lipid Microdomain Formation as a Function of Lipid Composition, Drug Metab. Dispos., 41 (2013) 1896–1905.

[76] D. Branduardi, F.L. Gervasio, M. Parrinello, From A to B in Free Energy Space, J. Chem. Phys., 126 (2007) 54103.

[77] J.C. Hackett, Membrane-embedded Substrate Recognition by Cytochrome P450 3A4, J. Biol. Chem., (2018) jbc.RA117.000961.

[78] Schrödinger Release 2015-1: Maestro, Schrödinger Release 2015-1: Maestro, (2015).

[79] O. Sorg, M. Zennegg, P. Schmid, R. Fedosyuk, R. Valikhnovskyi, O. Gaide, V. Kniazevych, J.H. Saurat, 2,3,7,8-tetrachlorodibenzo-p-dioxin (TCDD) Poisoning in Victor Yushchenko: Identification and Measurement of TCDD Metabolites, Lancet, 374 (2009) 1179–1185.

[80] R. Shinkyo, T. Sakaki, T. Takita, M. Ohta, K. Inouye, Generation of 2,3,7,8-TCDD-metabolizing Enzyme by Modifying rat CYP1A1 through Site-directed Mutagenesis, Biochem. Biophys. Res. Commun., 308 (2003) 511–517.

[81] T. Shimada, Xenobiotic-Metabolizing Enzymes Involved in Activation and Detoxification of Carcinogenic Polycyclic Aromatic Hydrocarbons, Drug Metab. Pharmacokinet., 21 (2006) 257–276.

[82] P. Urban, G. Truan, D. Pompon, High-Throughput Enzymology and Combinatorial Mutagenesis for Mining Cytochrome P450 Functions, Expert Opin. Drug Metab. Toxicol., 4 (2008) 733–747.

[83] T. Molcan, S. Swigonska, K. Orlowska, K. Myszczynski, A. Nynca, A. Sadowska, M.

Ruszkowska, J.P. Jastrzebski, R.E. Ciereszko, Structural-functional Adaptations of Porcine CYP1A1 to Metabolize Polychlorinated Dibenzo-p-dioxins, Chemosphere, 168 (2017) 205–216.

[84] H. Zhang, C. Kenaan, D. Hamdane, G.H.B. Hoa, P.F. Hollenberg, Effect of Conformational Dynamics on Substrate Recognition and Specificity as Probed by the Introduction of a de novo Disulfide Bond into Cytochrome P450 2B1, J. Biol. Chem., 284 (2009) 25678–25686.

[85] R. Kumari, R. Kumar, A. Lynn, G-mmpbsa -A GROMACS Tool for High-throughput MM-PBSA Calculations, J. Chem. Inf. Model., 54 (2014) 1951–1962.

9. List of publications

1. Šrejber, M., **Navrátilová, V.**, Paloncýová, M., Bazgier, V., Berka, K., Anzenbacher, P. and Otyepka, M. Membrane-attached Mammalian Cytochromes P450: An Overview of the Membrane's Effects on Structure, Drug Binding, and Interactions with Redox Partners. *J. Inorg. Biochem.* (**2018**), 10.1016/j.jinor gbio.2018.03.002 – *just accepted*.

   Impact Factor: 3.348

2. Pravda, L., Sehnal, D., Svobodová Vařeková, R., **Navrátilová, V.**, Toušek, D., Berka, K., Otyepka, M. and Koča, J. ChannelsDB: Database of Biomacromolecular Tunnels and Pores. *Nucleic Acids Res. 46 (D1)* (**2017**) D399-D405.

   Impact Factor: 10.162

3. **Navrátilová, V.**, Paloncýová, M., Berka, K., Mise, S., Haga, Y., Matsumura, C., Sakaki, T., Inui, H., Otyepka, M. Molecular Insights into the Role of a Distal F240A Mutation that Alters CYP1A1 Activity towards Persistent Organic Pollutants, Biochim. Biophys. Acta. – Gen. Subj. 1861 (11 Pt A) (**2017**) 2852-2860.

   Impact Factor: 4.702

4. **Navrátilová, V.**, Paloncýová, M., Berka, K., Otyepka, M. Effect of Lipid Charge on Membrane Immersion of Cytochrome P450 3A4. J. Phys. Chem. B, 120 (43) (**2016**) 11205–11213.

   Impact Factor: 3.177

5. Paloncýová, M., **Navrátilová, V.**, Berka, K., Laio, A., Otyepka, M. Role of Enzyme Flexibility in Ligand Access Egress to Active Site: Bias-Exchange Metadynamics Study of 1,3,7-Trimethyluric Acid in Cytochrome P450. J. Chem. Theory Comput., 12 (4) (**2016**) 2101-2109.

   Impact Factor: 5.245

6. Scott, E.E., Wolf, C.R., Otyepka, M., Humphreys, S.C., Reed, J.R., Henderson, C.J., McLaughlin, L.A., Paloncyova, M., **Navrátilova,V.**, Berka, K., et al. The Role of Protein-Protein and Protein-Membrane Interactions on P450 Function. Drug Metab. Dispos. 44 (4) (**2016**) 576–590.

   Impact Factor: 4.242

7. **Navrátilová, V.**, Paloncýová, M., Kajšová, M., Berka, K., Otyepka, M. Effect of Cholesterol on the Structure of Membrane-Attached Cytochrome P450 3A4. J. Chem. Inf. Model. 55 (3) (**2015**) 628–635.

Impact Factor: 3.657

8. Sehnal, D., Svobodová-Vařeková, R., Berka, K., Pravda L., **Navrátilová, V.**, Banáš, P., Ionescu, C.-M., Geidl, S., Otyepka, M., MOLE 2.0: Advanced Approach for Analysis of Biomacromolecular Channels. J. Cheminform. 5:39 (**2013**) 1-13.

   Impact Factor: 4.540

9. Berka, K., Hanák, O., Sehnal, D., Banáš, P., **Navrátilová, V.**, Jaiswal, D., Ionescu, C.-M., Svobodová-Vařeková, R., Koča, J., Otyepka, M.: MOLEonline 2.0: interactive web-based analysis of biomacromolecular channels. Nucl. Acids Res. 40 (**2012**) 222-227.

   Impact Factor: 8.278

10. Hendrychová, T., Berka, K., **Navrátilová, V.**, Anzenbacher, P., Otyepka, M. Dynamics and Hydration of the Active Sites of Mammalian Cytochromes P450 Probed by Molecular Dynamics Simulations. Curr Drug Metab. 13 (**2012**) 177-189.

    Impact Factor: 4.405

(Impact factors according to Web of Science)

10. List of appendices

A **Navrátilová, V.**, Paloncýová, M., Kajšová, M., Berka, K., Otyepka, M. Effect of Cholesterol on the Structure of Membrane-Attached Cytochrome P450 3A4, *J. Chem. Inf. Model.*, 55 (2015) 628–635.

B **Navrátilová, V.**, Paloncýová, M., Berka, K., Otyepka, M. Effect of Lipid Charge on Membrane Immersion of Cytochrome P450 3A4, *J. Phys. Chem. B,* 120 (2016) 11205–11213.

C Paloncýová, M**., Navrátilová, V.**, Berka, K., Laio, A., Otyepka, M. Role of Enzyme Flexibility in Ligand Access and Egress to Active Site: Bias-Exchange Metadynamics Study of 1,3,7-Trimethyluric Acid in Cytochrome P450 3A4, *J. Chem. Theory Comput.*, 12 (2016) 2101–2109.

D **Navrátilová, V.**, Paloncýová, M., Berka, K., Mise, S., Haga, Y., Matsumura, C., Sakaki, T., Inui, H., Otyepka, M. Molecular Insights into the Role of a Distal F240A Mutation that Alters CYP1A1 Activity towards Persistent Organic Pollutants, *Biochim. Biophys. Acta. – Gen. Subj.*, 1861 (2017) 2852–2860.

Appendices

JOURNAL OF CHEMICAL INFORMATION AND MODELING

Article

pubs.acs.org/jcim

Effect of Cholesterol on the Structure of Membrane-Attached Cytochrome P450 3A4

Veronika Navrátilová, Markéta Paloncýová, Michaela Kajšová, Karel Berka,* and Michal Otyepka*

Regional Centre of Advanced Technologies and Materials, Department of Physical Chemistry, Faculty of Science, Palacký University Olomouc, tř. 17. listopadu 12, 771 46, Olomouc, Czech Republic

Supporting Information

ABSTRACT: Cholesterol is a widely researched component of biological membranes that significantly influences membrane properties. Human cytochrome P450 3A4 (CYP3A4) is an important drug-metabolizing enzyme, wherein the catalytic domain is attached to a membrane by an N-terminal α-helical transmembrane anchor. We analyzed the behavior of CYP3A4 immersed in a 1,2-dioleoyl-*sn*-glycero-3-phosphocholine (DOPC) membrane with various amounts of cholesterol. The presence of cholesterol caused ordering and thickening of the membrane and led to greater immersion and inclination of CYP3A4 toward the membrane. Cholesterol also lowered the flexibility of and tended to concentrate around membrane-immersed parts of CYP3A4. Further, the pattern of the CYP3A4 active-site access channels was altered in the presence of cholesterol. In summary, cholesterol in the membrane affected the positioning and structural features of CYP3A4, which in turn may have implications for the activity of this enzyme in various membranes and membrane parts with different cholesterol content.

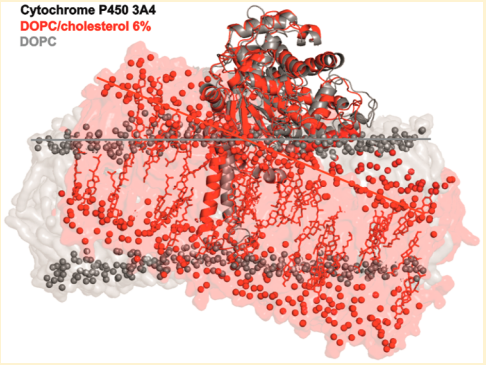

INTRODUCTION

Human cytochrome P450 (CYP) enzymes are involved in biotransformation processes of endogenous compounds and xenobiotics. Although they typically catalyze monooxygenation reactions, their catalytic potential is more diverse.[1,2] CYPs attach to membranes of the endoplasmic reticulum (ER) and mitochondria[3] by an N-terminal anchor, and their catalytic domains are partially immersed in the membrane.[4−6] It has been suggested that the membrane is not merely a passive medium but may actively contribute to the biotransformation processes by accumulation of nonpolar compounds.[7−9] Such compounds may also enter the CYP active site from the membrane via the active-site access channels.[5,6,9,10] The behavior of CYP on a membrane may be affected by the membrane composition and in turn the breathing (dynamical opening/closing) of access channels.[6,11] Moreover, CYP activity is dependent on the presence of certain redox partners, which attach to the membrane via transmembrane helices.[12,13] Thus, it is important to gain a deeper understanding of the role of membranes in the above-mentioned processes.

Direct structural insight into the behavior of membrane-anchored enzymes is still very challenging for experimental techniques. Until now, only NMR[14,15] and linear dichroism[16] measurements have been able to provide direct information on the membrane attachment of CYPs. It took more than 10 years after publication of the first X-ray structure of mammalian CYP[17] for the first crystal structure of CYP to be reported, which showed a resolved N-terminal anchor but only applied to outside the membrane environment.[18] However, it has been shown that missing information on the structural behavior of CYP on membrane can be gleaned by molecular dynamics (MD) simulations.[6,11] As the membranes of mitochondria and the ER are mainly composed of phosphatidylcholines, MD studies have so far largely focused on lipid bilayers consisting of unsaturated phospholipids, such as 1,2-dioleoyl-*sn*-glycero-3-phosphocholine (DOPC)[5,6] and 1-palmitoyl-2-oleoyl-*sn*-glycero-3-phosphocholine (POPC),[9,11,19,20] and membrane-mimicking models.[16] A recent study on membrane anchored aromatase considered the more complex composition of the ER membrane.[21] However, to date, no systematic study into the effect of membrane composition on the positioning of CYP has been published.

The ER membrane comprises glycerolipids, such as phosphatidylcholine (PC), phosphatidylethanolamine (PE), phosphatidylinositol (PI), and phosphatidylserine (PS), as well as cholesterol, cardiolipin, and sphingomyelin.[22] Among these lipids, cholesterol is known to significantly alter membrane properties by (i) enhancing the stiffness,[23] (ii) decreasing lateral diffusion,[24,25] (iii) causing "thickening" of the membrane with increasing cholesterol content,[26,27] and (iv) increasing membrane ordering.[28] The presence of cholesterol in the membrane also affects solute partitioning between the membrane and water[29,30] and interactions with proteins.[31] In eukaryotes, the membrane content of cholesterol varies depending on location: the smallest amount is present in the

Received: October 27, 2014
Published: February 5, 2015

ACS Publications © 2015 American Chemical Society

DOI: 10.1021/ci500645k
J. Chem. Inf. Model. 2015, 55, 628−635

mitochondrial membrane (3 wt%, 6 mol%), followed by the ER (6 wt%), whereas the largest amount occurs in the plasma membrane (20 wt%).[32] There is also some evidence that the concentration of cholesterol is not homogeneous in membranes and can be locally higher, i.e., in structures called lipid rafts, where cholesterol may also interact with proteins.[31,33,34] The cholesterol gradient from the ER to the cell surface can also regulate sorting of membrane proteins to their correct membrane site.[35] As cholesterol significantly influences membrane properties, it is plausible that it may also affect the structure, orientation, and dynamics of CYP on membranes and in turn the interaction of CYP with its substrates. Recently, Park and co-workers[36] showed that individual CYPs differed in localization in ordered and disordered membrane domains, which had various cholesterol concentrations.

We conducted MD simulations to analyze the structure of CYP3A4 attached to DOPC bilayers with various concentrations of cholesterol (0, 3, 6, 20, and 50 wt%). We chose CYP3A4, as it plays a prominent role in the metabolism of the more than 50% of marketed drugs and is the most abundant CYP in human hepatocytes.[37] CYP3A4 has a deeply buried, large, and malleable active site,[38−40] which can be occupied by more than one ligand.[41−43] It should be noted that cholesterol acts as a CYP3A4 substrate, undergoing 4β-hydroxylation.[44] On the other hand, cholesterol also inhibits several CYP3A4 reactions in a noncompetitive manner.[45] Our MD simulations showed that the presence of cholesterol changes the orientation and rigidifies the membrane-immersed parts of CYP3A4, which could inhibit entry of lipophilic substrates directly from the membrane.

METHODS

Structures. The structure of the catalytic domain of CYP3A4[38] was taken from the Protein Data Bank (PDB ID 1TQN), and the N-terminal anchor, which was missing in the X-ray structure, was added to the structure as an α-helix using methodology described in detail elsewhere.[6] We prepared five lipid bilayers: one consisting of pure DOPC and four composed of DOPC and various (3, 6, 20, and 50 wt%) concentrations of cholesterol. CYP3A4 was inserted into the equilibrated bilayers using the GROMACS tool g_membed.[46] CYP3A4 anchored to the bilayer was then immersed into a rectangular periodic box and solvated by SPC/E[47] explicit water molecules (~30 000). Counter ions were added to maintain a physiological concentration of 0.1 mol/L in the water phase.

MD Procedure. All simulations were carried out with using the Gromacs 4.5.4 program package.[48] We used the Berger lipid force field[49] for the membrane, which was compatible with the GROMOS 53a6[50] force field used for CYP3A4. The lipid bilayer was initially simulated without protein for 200 ns. After the protein was embedded in the membrane, all systems were minimized with the steepest descent method, followed by a short (10 ns long) MD simulation with positional restraints applied on Cα atoms. Afterward, a 200 ns long MD simulation of each system was carried out. Parameters of the MD simulations were set as follows: integration time step, 2 fs with the LINCS algorithm; Berendsen pressure coupling, semi-isotropic Berendsen barostat with pressure 1 bar; isothermal compressibility, 4.5×10^{-5} bar^{-1}; and for temperature coupling, V-rescale thermostat at 310 K with 0.1 ps time constant. The long-range electrostatics was treated with the particle mesh Ewald method, and a pair-list was generated with the group cut-off scheme.

Analysis. As equilibration of systems with CYPs requires at least 50 ns,[6] the first 100 ns of the simulation was set aside for equilibration of CYP3A4, and only data for the last 100 ns were analyzed. For analysis of the membrane properties, we used Gromacs tools.[48] The heme tilt angle was defined as the angle between the heme plane (defined by the heme nitrogens) and the lipid bilayer normal, set as the z axis.[6] Access and egress channels[51] were identified using the MOLE 2.0 tool[52] with the following setup: interior threshold and bottleneck radius, 1.0; probe radius, 8.0; surface cover radius, 3.0; origin radius, 3.0; and starting point located ~3 Å above the heme iron atom (distal side). Water molecules, hydrogens, ions, and membrane atoms were not considered in this analysis. In total, 201 structural snapshots taken every 500 ps (of the last 100 ns) were analyzed. Identified channels were sorted according to the nomenclature introduced by Wade and co-workers,[53] with the exception of channels 2a and 2f, which were united into one channel (henceforth called 2af) because of their high structural similarity.

RESULTS AND DISCUSSION

Addition of Cholesterol Changes the Basic Structural Characteristics of a DOPC Membrane. The presence of cholesterol altered the structure of the DOPC bilayer. DOPC lipid bilayers were generally thicker in the presence of cholesterol, with the headgroup−headgroup distance ($D_{(HH)}$) changing from 4.2 nm in the case of a pure DOPC membrane to 4.6 nm for a membrane containing 20 wt% cholesterol (Table 1). The area per lipid (APL) decreased from 0.59 to 0.42 nm^2. Density profiles also showed that the presence of cholesterol increased the density of the lipid plateau region in terms of the maximal density in the membrane headgroups but did not alter the density in the middle of the membrane

Table 1. Mean Distances of Phosphate (d_P), Cholesterol OH Group (d_{OH}), and Heme Cofactor (d_{heme}) from the Bilayer Center, Area Per Lipid (APL), Average Order Parameters of Lipid Tails ($S_{<CD>}$), Average Fraction of Gauche Bonds (f_g), Heme and Transmembrane (TM) Helix Tilt Angles, and Number of Amino Acid Residues (N) Buried in the Hydrophobic Membrane Interior (below DOPC Carbonyls)

	cholesterol content (wt%)				
	0%	3%	6%	20%	50%
	Membranes without CYP				
d_P (nm)	2.1	2.1	2.1	2.3	2.2
d_{OH} (nm)	–	1.6	1.6	1.8	1.9
APL (nm^2)	0.59	0.58	0.54	0.48	0.42
$S_{<CD>}$	0.182	0.190	0.219	0.259	0.294
f_g	0.157	0.156	0.154	0.150	0.147
	Membranes with CYP				
d_P (nm)	2.0	2.1	2.2	2.3	2.1
d_{OH} (nm)	–	1.5	1.5	1.8	1.8
$S_{<CD>}$	0.172	0.188	0.201	0.246	0.270
f_g	0.156	0.154	0.152	0.148	0.144
d_{heme} (nm)	3.8 ± 0.1	3.7 ± 0.1	3.5 ± 01	3.7 ± 0.1	3.5 ± 0.1
heme tilt angle (deg)	52 ± 8	59 ± 3	60 ± 4	69 ± 5	68 ± 4
TM helix tilt angle (deg)	8 ± 4	10 ± 4	11 ± 4	12 ± 5	9 ± 4
N	54	60	82	79	73

DOI: 10.1021/ci500645k
J. Chem. Inf. Model. 2015, 55, 628−635

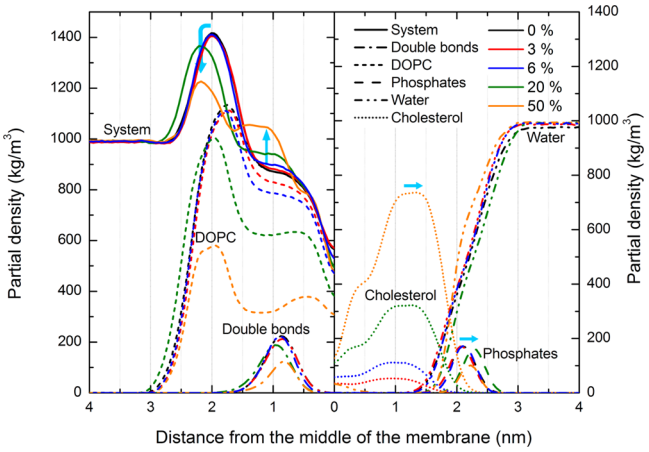

Figure 1. Density profiles of the studied membrane system (without CYP). The membrane was averaged and considered to be symmetric. However, for clarity, the partial densities of groups are shown for just one leaflet.

(Figure 1). As the concentration of cholesterol was increased, the cholesterol OH group shifted further from the membrane center. All these findings are in agreement with previous simulations[25,54,55] and experimental data[55] and confirm that the force field used adequately represented the structural properties of these mixed membranes. Thus, the membrane model was considered valid and used to study the effect of cholesterol content on CYP3A4 anchoring.

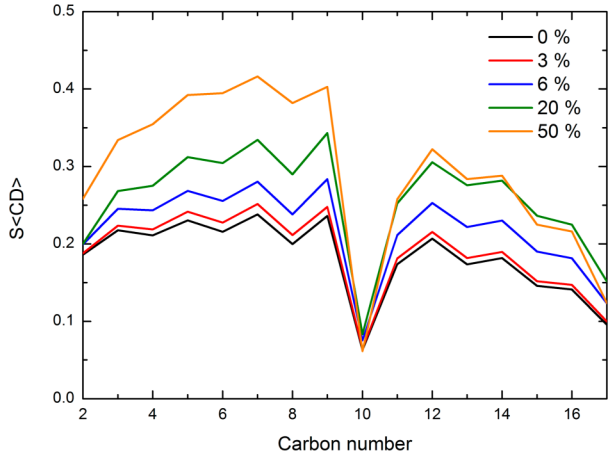

Figure 2. Average order parameter $S_{<CD>}$ for the carbon atoms of DOPC lipid tails calculated from MD simulations with varying cholesterol concentrations.

The presence of cholesterol also induced higher ordering of the DOPC lipid tails (Figure 2). A pure DOPC membrane comprises a diunsaturated lipid with a phase transition temperature of ~255 K[56] and is therefore fluid at ambient temperatures, as documented by the rather low mean order parameter $S_{<CD>}$ of 0.182. Ordering of the lipid membrane was found to increase with increasing cholesterol content, together with a decrease in the fraction of gauche torsion angles of the DOPC lipid chains (Table 1). Higher ordering (above ~0.25) can occur in a liquid-ordered lipid phase, which is generally a cholesterol-rich domain.[25,30,55,57]

Cholesterol Interacts with the N-Terminal Anchor and F/G-Loop of CYP3A4. The simulations showed that CYP3A4 was attached to the membrane by the N-terminal anchor helix, which intersected the membrane, and its catalytic domain was partially immersed in the membrane. The DOPC head groups are pushed aside and DOPC molecules form a funnel-like shape in the membrane occupied by the protein. The N-terminal helix tilt angle, i.e., angle between the helix axis and bilayer normal, was ~10° and was rather insensitive to the cholesterol content (Table 1). This angle is smaller than the transmembrane anchor tilt angle of 17° recently measured by NMR on CYP2B4 anchored to DMPC/DHPC bicelles,[15] which makes sense as the latter lipids have shorter tails and head-to-head distance than DOPC.

The radial distribution function (RDF) of the anchor and cholesterol centers of mass (COMs) showed that cholesterol had some tendency to accumulate in the vicinity of the anchor (Figure 3). Cholesterol also accumulated close to the immersed F/G loop (Figure 4). The number of hydrogen bonds between lipids and CYP3A4 rose with cholesterol content (Table S1) and cholesterol had higher capacity to make hydrogen bonds to membrane buried amino acids. Neither cholesterol nor DOPC molecules penetrated into the protein and stayed in the membrane. Fluctuations of the lipids around CYP were massively reduced (Figure S2 in Supporting Information).

Orientation and Immersion Depth of CYP3A4 on DOPC Membrane Is Affected by the Presence of Cholesterol. The presence of cholesterol in the membrane changed the penetration depth of CYP3A4 in the membrane. Besides the mentioned N-terminal anchor, the F/G loop (bearing F′ and G′ helices) was buried in the lipophilic membrane interior of the pure DOPC membrane (Figure 5). The β1 and β2-sheets, B/C loop, F and G helices, and tip of the I helix interacted with the lipid head groups in same positions as reported earlier.[6] It is worth noting that despite some differences in membrane immersion depths and orientations of individual CYPs, all recent studies have consistently reported insertion of the N-terminal, F′, and G′ helices into the membrane interior,[9,11,16,21] while the B/C loop and F and G helices in CYP3A4[11] have been reported to interact with the membrane. Figure 5 shows that with increasing content of cholesterol, the F and G helices and B/C loop become systematically sunk deeper into the membrane interior. The number of amino acids in contact with the membrane (Tables 1 and S2 in Supporting Information) was the lowest in the pure DOPC membrane and reached a maximum at 6 wt% cholesterol content.

The orientation of the CYP3A4 catalytic domain with respect to the membrane changed with the increasing content of cholesterol in the DOPC membrane (Figure 6), as evaluated from the heme tilt angle (see Methods for definition). The tilt angle systematically increased from 52° in the pure DOPC membrane to 68° in membranes containing 50 wt% cholesterol (Table 1). It should be noted that the experimentally measured tilt angle of CYP3A4 on POPC nanodiscs is $(60 \pm 4)°$.[16] A higher cholesterol content in the DOPC membrane led to increased contact of the CYP3A4 catalytic domain with the membrane, mostly in the vicinity of the F and G helices and β-finger (containing β4 and β5 sheets, and β4/β5 loop). However, the secondary structural elements of the CYP3A4 catalytic domain did not significantly change with increasing cholesterol content (Figures S1 and S3 in Supporting Information).

Cholesterol Presence in the Membrane Alters Active-Site Access Channels Openings. CYP3A4 active-site access

DOI: 10.1021/ci500645k
J. Chem. Inf. Model. 2015, 55, 628−635

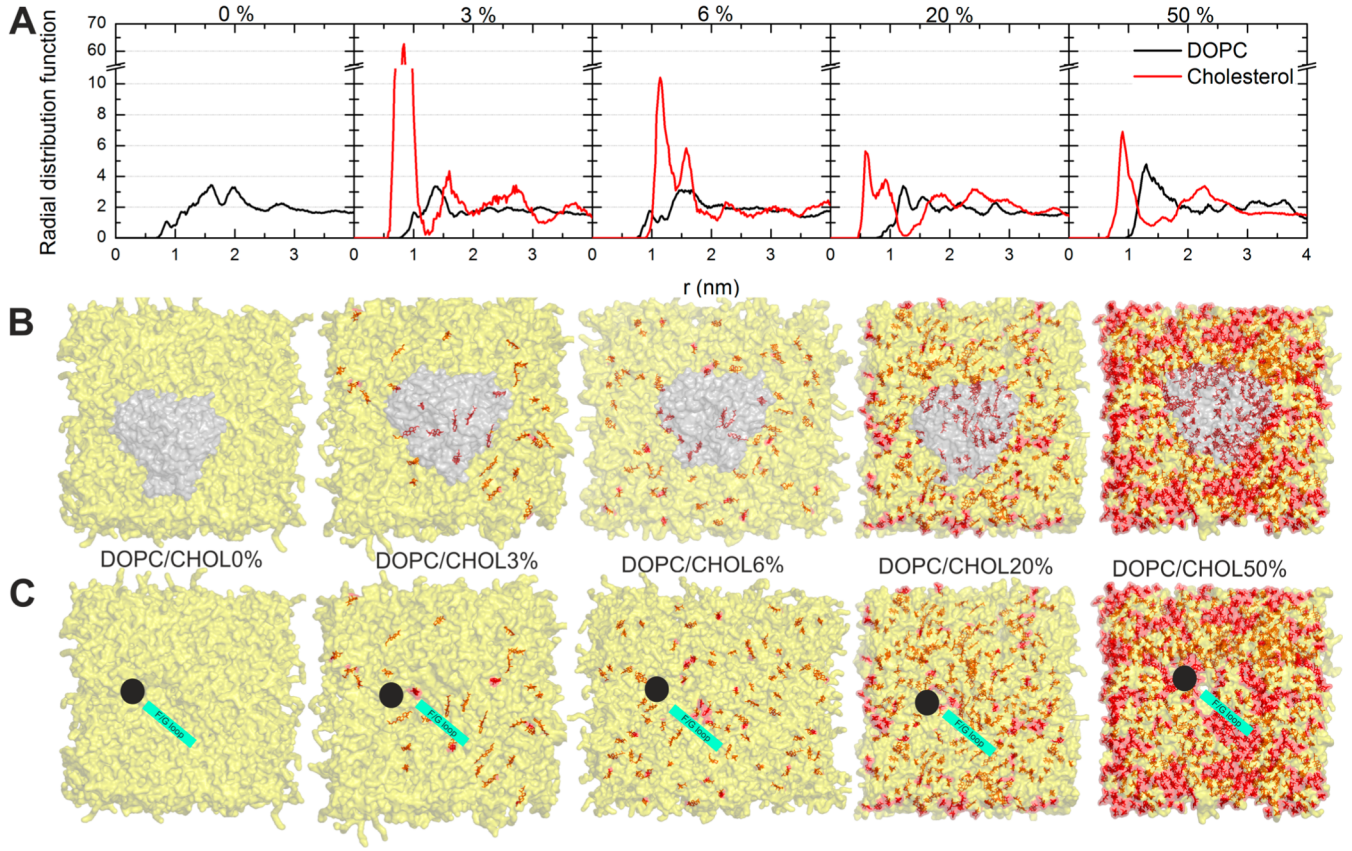

Figure 3. Distribution of cholesterol in membranes. (A) Radial distribution functions of the COMs of DOPC and cholesterol with respect to the transmembrane anchor. (B) Positions of cholesterol molecules (red) in membranes (yellow) with immersed CYP3A4 (gray); frames were taken from 200 ns snapshots. (C) The same view but with CYP3A4 deleted for clarity; positions of the CYP3A4 anchor (black circle) and F/G-loop (green) are shown. Cholesterol showed some tendency to concentrate close to the transmembrane anchor and F/G-loop.

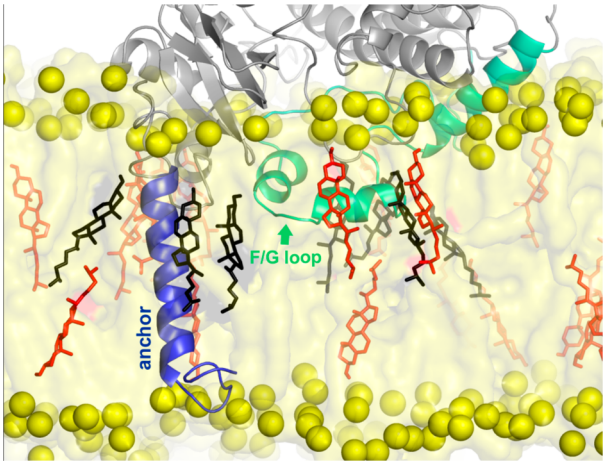

Figure 4. Snapshot taken from MD simulation of CYP3A4 embedded in 6 wt% cholesterol in DOPC membrane showing a typical view of cholesterol molecules interacting with the N-terminal anchor (blue) and F/G loop (green). Membrane phosphates are represented by yellow spheres, cholesterol molecules within 5 Å of CYP3A4 by black sticks and more distal cholesterol molecules by red sticks.

channels connected the active site to both membrane and water phases because their openings were localized inside, on and outside the membrane (Figure 7). The channels 2af, 2b, 2c (around F/G loop), and 4 (through F/G loop) pointed toward the hydrophobic membrane interior. The solvent channel (S; between F, I helices and β-finger) and channels 2e (running through B/C loop) and 3 (between F and G helices) were open to the membrane/water interface. The water channel (W; leading to the proximal side around B, C helices or B/C loop) and channels 1 (among C, H, and L helices) and 5 (between K and K′ helices) opened into the water phase. The positions of these channels are in good agreement with previously published data.[5,6,9] The channels were hydrated and enabled traffic of water molecules in/out CYP3A4 active site (Table S4).

The addition of cholesterol to the DOPC membrane changed the pattern of channel openings. At low cholesterol content (3 and 6 wt%), the water channel was closed and the solvent channel open, but there were no significant changes in the channels pointing to the membrane interior. Channels leading deepest into the membrane, i.e., channels 2af and 2b, closed when CYP was embedded into the cholesterol-rich membrane (with 20 and 50 wt% cholesterol content). The bottlenecks of membrane-exposed channels were narrower in cholesterol rich membranes (Table 2). As well as closure of the channels leading to the membrane, channels leading to the membrane/water interface, such as channels 2e or the solvent channel, opened. Channels leading toward the water phase were highly hydrated (Table S4) and enabled traffic of water molecules out/in CYP3A4 active site. A new channel, labeled 7, whose opening pointed toward the water phase, was identified. Channel 7 passed near the K helix and K/L loop to the proximal side of CYP 3A4 (Figure S2 in Supporting Information). The opening of this channel was caused by subtle movement of the F/G loop and K and L helices.

DOI: 10.1021/ci500645k
J. Chem. Inf. Model. 2015, 55, 628−635

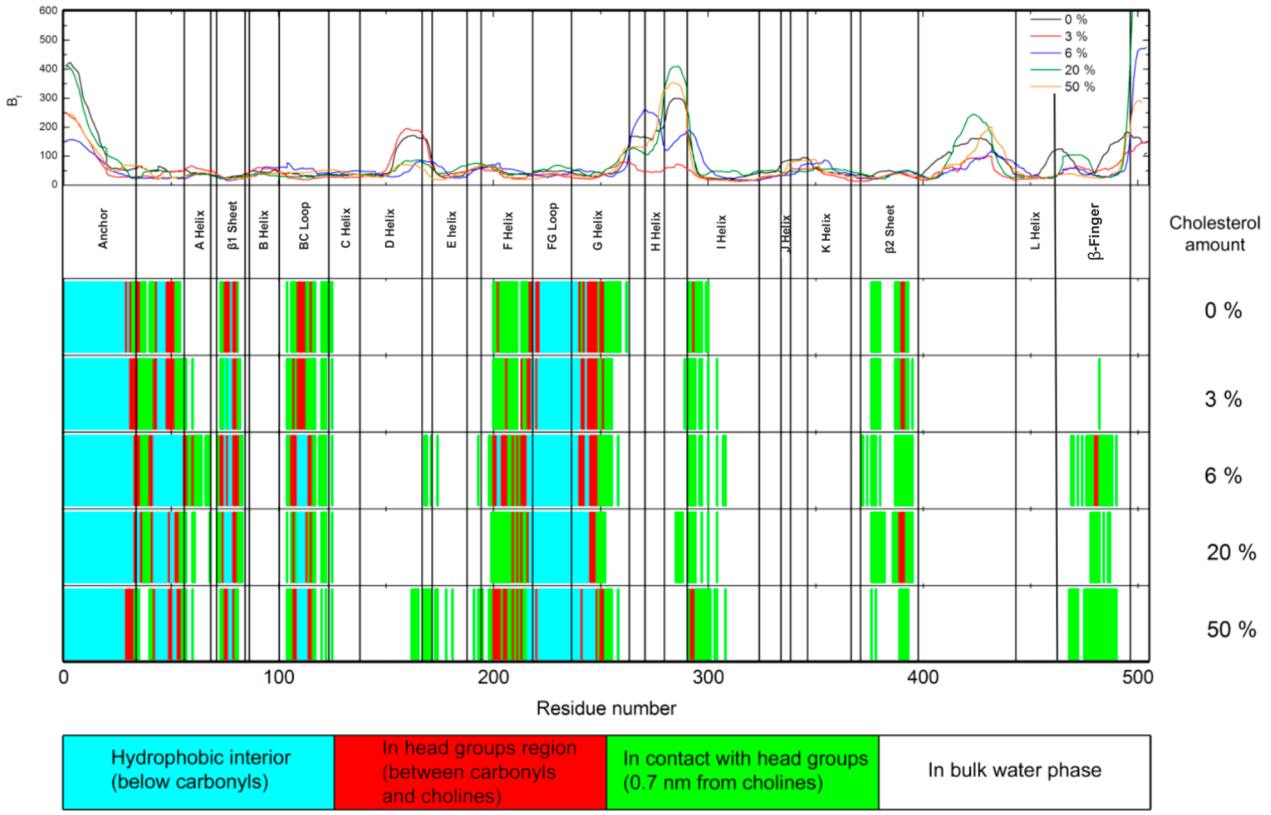

Figure 5. Structural features of CYP3A4 in different membranes. The average B-factors (upper panel) along the protein chain show that the regions in contact with water are the most flexible. The locations of residues differ with respect to the membrane composition (bottom): higher cholesterol leads to more immersed CYP structures, especially in the B/C and F/G loop regions. The colors indicate CYP3A4 parts that are in direct contact with the hydrophobic membrane interior (blue), interact with membrane head groups, i.e., between carbonyl groups and cholines (red), and contact the membrane upper layer (green). The white regions indicate parts in contact with bulk water (cytosol).

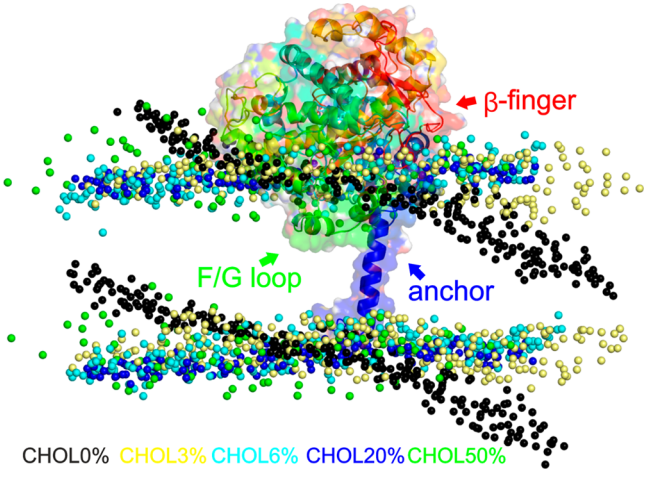

Figure 6. Effect of cholesterol on the orientation of CYP3A4 in the membrane. Structures of CYP3A4 catalytic domain have been superimposed to highlight changes in the CYP34A orientation with respect to the DOPC membrane. The membrane is represented by spheres of phosphorus atoms (for clarity) and colored according to the cholesterol content: 0 wt%, black; 3 wt%, yellow; 6 wt%, cyan; 20 wt%, blue; and 50 wt%, green. CYP3A4 is shown as a cartoon with transparent surfaces.

Generally, conformational changes of channel lining amino acid residues and small variations in arrangement of secondary structural elements, which bear the channel lining amino acids can cause channel opening/closing. The subtle movement of the F/G loop toward the membrane and concurrent opening of the K and L helix region in the CYP structures immersed in membranes containing cholesterol lead to opening of the channel 7. Solvent channel opening and closing was mostly connected with the orientation of R212, which closed solvent channel of CYP3A4 immersed to membranes with 0% and 3% of cholesterol, whereas the channel was open in the membrane containing 20% cholesterol.

CONCLUSION

We studied the effect of increasing the cholesterol content in a DOPC membrane on the behavior of membrane-anchored cytochrome P450 3A4 (CYP3A4). The presence of cholesterol in the lipid membrane significantly changed the membrane thickness, ordering, and diffusion. The position and orientation of CYP3A4 on the membrane were also affected by the cholesterol content. With increasing cholesterol concentration, CYP3A4 was immersed about 0.4 nm deeper into the membrane and was more inclined toward the membrane. In addition, the contact area between the catalytic domain and membrane increased. As a result, about 34% more CYP3A4 amino acids were in contact with the membrane. The presence of cholesterol in the membrane also affected opening of the active-site access channels, but the most pronounced changes occurred for high (20 and 50 wt%) cholesterol concentrations. One can hypothesize that the above-discussed changes might also contribute to the noncompetitive inhibition of CYP3A4 by cholesterol observed by Shinkyo and Guengerich.[45] Our results show that cholesterol content significantly influences the

DOI: 10.1021/ci500645k
J. Chem. Inf. Model. 2015, 55, 628−635

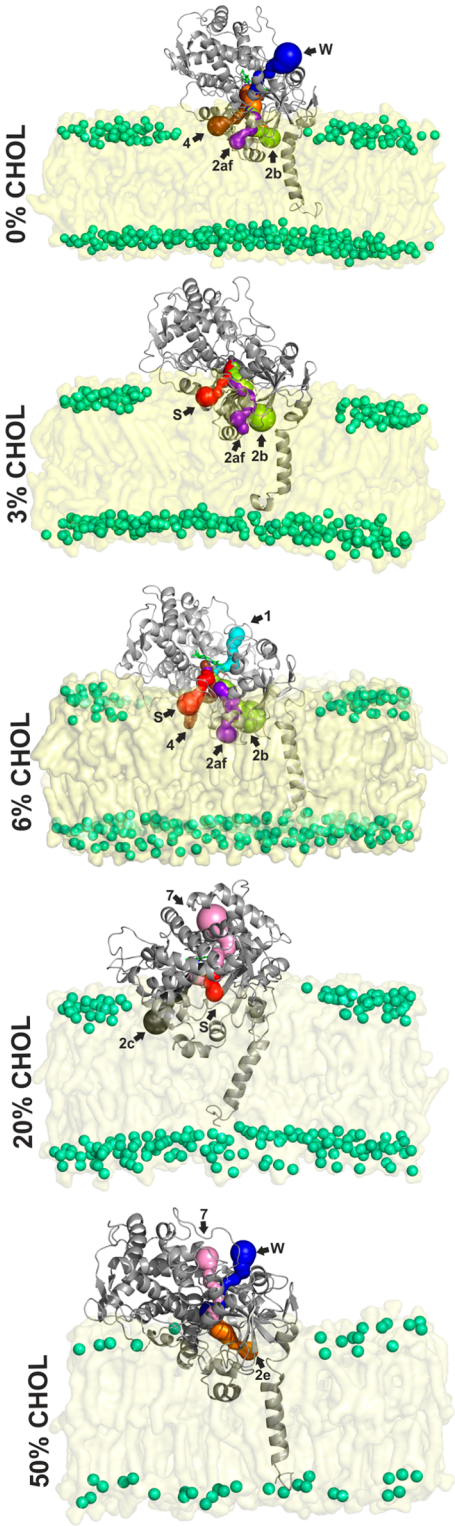

Figure 7. Channel openings (highlighted by arrows) of CYP3A4 active-site access channels (open with bottleneck radius of 1 Å and higher in 15% of frames) are shown in DOPC membranes with increasing cholesterol content. Access channels are labeled according to the nomenclature introduced by Wade and co-workers,[53] and colored as follows: 1, cyan; 4, brown; 7, pink; W, blue; S, red; 2af, magenta; 2b, bright green; 2c, gray; 2e, orange. Membrane lipids are represented as transparent surfaces and phosphates in green spheres; CYP3A4 is shown as a cartoon.

Table 2. Normalized Frequency of CYP Channel Opening (nfreq) and Average Radius (Rmax) of Bottlenecks[a]

		chol 0%		chol 3%		chol 6%		chol 20%		chol 50%	
	#	nfreq	Rmax	nfreq	Rmax	nfreq	Rmax	nfreq	Rmax	nfreq	Rmax
membrane	2af	47	1.46	30	1.45	29	1.39	2	1.19	4	1.24
	2b	76	1.73	95	1.64	88	1.53	1	1.09	10	1.41
	4	18	1.29	8	1.26	17	1.31	1	1.16	11	1.31
interface	2c	5	1.42	1	1.13			21	1.43	4	1.26
	2e	33	1.61	1	1.01	2	1.13	78	1.77	62	1.59
	S			27	1.28	45	1.47	75	1.89	5	1.17
	3	5	1.22			2	1.01	2	1.05	1	1.2
	5							9	1.39	5	1.23
water	1	10	1.25	2	1.17	20	1.36	10	1.47	10	1.24
	W	56	1.38	5	1.27	3	1.07	1	1.01	21	1.36
	7					11	1.62	34	1.57	78	1.55
	r	0.74		0.89		0.62		0.92		0.90	

[a]Rmax values are colored according to their bottleneck radius, from dark green for the most open to red for the most closed channels. According to the Rmax and nfreq values, the most frequently occurring channels were also the most open, whereas rarely observed channels tended to have rather narrow bottlenecks. The last line shows the correlation coefficients between nfreq and Rmax.

structural features of a membrane-anchored enzyme, which in turn may affect the substrate preferences and catalytic efficiency of the respective membranes or membrane domains. The described changes may influence biotransformation processes in different membrane parts and various cellular compartments, which differ in membrane composition and cholesterol content.

■ ASSOCIATED CONTENT

Supporting Information

Root-mean-square fluctuations of the systems with different cholesterol content (Figure S1); detailed view of newly observed channel 7 (Figure S2); number of hydrogen bonds between lipids, protein, and water (Table S1); numbers of protein residues located in various parts of the membrane and potentially interacting with the membrane (Table S2); numbers of solvent and ions in the simulated system (Table S3); number of water molecules in various channels (Table S4); evolution of secondary structure elements (Figure S3); overview of all channels found in the CYPs in membranes with different cholesterol content (Figure S4). This material is available free of charge via the Internet at http://pubs.acs.org.

■ AUTHOR INFORMATION

Corresponding Authors

*K.B.: phone +420 585634769, fax +420 585634761, E-mail karel.berka@upol.cz.

*M.O.: phone +420 585634756, fax +420 585634761, E-mail michal.otyepka@upol.cz.

Notes

The authors declare no competing financial interest.

■ ACKNOWLEDGMENTS

This research was supported by the Operational Program Research and Development for Innovations—European Social Fund (CZ.1.07/2.4.00/31.0130 ChemPharmNet) from the Ministry of Education Youth and Sports, Czech Republic. We acknowledge support from the Czech Grant Agency through the projects P303/12/P019 to K.B. and P208/12/G016 to M.O. We also acknowledge support from a student project of Palacký University Olomouc (IGA_PrF_2014023) to M.P. and V.N. The authors gratefully acknowledge support through the

DOI: 10.1021/ci500645k
J. Chem. Inf. Model. 2015, 55, 628−635

project LO1305 of the Ministry of Education, Youth and Sports of the Czech Republic.

■ ABBREVIATIONS

CYP, cytochrome P450; ER, endoplasmic reticulum; DOPC, 1,2-dioleoyl-*sn*-glycero-3-phosphocholine; POPC, 1-palmitoyl-2-oleoyl-*sn*-glycero-3-phosphocholine; MD, molecular dynamics; PC, phosphatidylcholine; PE, phosphatidylethanolamine; PI, phosphatidylinositol; PS, phosphatidylserine; APL, area per lipid; TM, transmembrane; DMPC, 1,2-dimyristoyl-*sn*-glycero-3-phosphocholine; DHCP, 1,2-diheptanoyl-*sn*-glycero-3-phosphocholine; CHOL, cholesterol; RDF, radial distribution function; COM, center of mass

■ REFERENCES

(1) Guengerich, F. P. Common and Uncommon Cytochrome P450 Reactions Related to Metabolism and Chemical Toxicity. *Chem. Res. Toxicol.* **2001**, *14*, 611−650.
(2) Ortiz de Montellano, P. R., Ed. *Cytochrome P450: Structure, Mechanism, and Biochemistry*, 3rd ed.; Kluwer Academic/Plenum Publishers: New York, 2005; Vol. *21*, p 690.
(3) Black, S. D. Membrane Topology of the Mammalian P450 Cytochromes. *FASEB J.* **1992**, *6*, 680−685.
(4) Williams, P. A.; Cosme, J.; Sridhar, V.; Johnson, E. F.; McRee, D. E. Microsomal Cytochrome P450 2C5: Comparison to Microbial P450s and Unique Features. *J. Inorg. Biochem.* **2000**, *81*, 183−190.
(5) Berka, K.; Hendrychová, T.; Anzenbacher, P.; Otyepka, M. Membrane Position of Ibuprofen Agrees with Suggested Access Path Entrance to Cytochrome P450 2C9 Active Site. *J. Phys. Chem. A* **2011**, *115*, 11248−11255.
(6) Berka, K.; Paloncýová, M.; Anzenbacher, P.; Otyepka, M. Behavior of Human Cytochromes P450 on Lipid Membranes. *J. Phys. Chem. B* **2013**, *117*, 11556−11564.
(7) Endo, S.; Escher, B. I.; Goss, K.-U. Capacities of Membrane Lipids to Accumulate Neutral Organic Chemicals. *Environ. Sci. Technol.* **2011**, *45*, 5912−5921.
(8) Paloncýová, M.; Devane, R.; Murch, B.; Berka, K.; Otyepka, M. Amphiphilic Drug-Like Molecules Accumulate in a Membrane below the Head Group Region. *J. Phys. Chem. B* **2014**, *118*, 1030−1039.
(9) Cojocaru, V.; Balali-Mood, K.; Sansom, M. S. P.; Wade, R. C. Structure and Dynamics of the Membrane-Bound Cytochrome P450 2C9. *PLoS Comput. Biol.* **2011**, *7*, No. e1002152.
(10) Kingsley, L. J.; Lill, M. a Ensemble Generation and the Influence of Protein Flexibility on Geometric Tunnel Prediction in Cytochrome P450 Enzymes. *PLoS One* **2014**, *9*, No. e99408.
(11) Denisov, I. G.; Shih, a Y.; Sligar, S. G. Structural Differences between Soluble and Membrane Bound Cytochrome P450s. *J. Inorg. Biochem.* **2012**, *108*, 150−158.
(12) Sündermann, A.; Oostenbrink, C. Molecular Dynamics Simulations Give Insight into the Conformational Change, Complex Formation, and Electron Transfer Pathway for Cytochrome P450 Reductase. *Protein Sci.* **2013**, *22*, 1183−1195.
(13) Yamamoto, K.; Dürr, U. H. N.; Xu, J.; Im, S.-C.; Waskell, L.; Ramamoorthy, A. Dynamic Interaction between Membrane-Bound Full-Length Cytochrome P450 and Cytochrome b5 Observed by Solid-State NMR Spectroscopy. *Sci. Rep.* **2013**, *3*, No. 2538.
(14) Dürr, U. H. N.; Waskell, L.; Ramamoorthy, A. The Cytochromes P450 and b5 and their Reductases—Promising Targets for Structural Studies by Advanced Solid-State NMR Spectroscopy. *Biochim. Biophys. Acta* **2007**, *1768*, 3235−3259.
(15) Yamamoto, K.; Gildenberg, M.; Ahuja, S.; Im, S.-C.; Pearcy, P.; Waskell, L.; Ramamoorthy, A. Probing the Transmembrane Structure and Topology of Microsomal Cytochrome-P450 by Solid-State NMR on Temperature-Resistant Bicelles. *Sci. Rep.* **2013**, *3*, No. 2556.
(16) Baylon, J. L.; Lenov, I. L.; Sligar, S. G.; Tajkhorshid, E. Characterizing the Membrane-Bound State of Cytochrome P450 3A4: Structure, Depth of Insertion and Orientation. *J. Am. Chem. Soc.* **2013**, *135*, 8542−8551.
(17) Williams, P. A.; Cosme, J.; Sridhar, V.; Johnson, E. F.; McRee, D. E. Mammalian Microsomal Cytochrome P450 Monooxygenase: Structural Adaptations for Membrane Binding and Functional Diversity. *Mol. Cell* **2000**, *5*, 121−131.
(18) Monk, B. C.; Tomasiak, T. M.; Keniya, M. V.; Huschmann, F. U.; Tyndall, J. D. A. Architecture of a Single Membrane Spanning Cytochrome P450 Suggests Constraints that Orient the Catalytic Domain Relative to a Bilayer. *Proc. Natl. Acad. Sci. U.S.A.* **2014**, *111*, 3865−3870.
(19) Jiang, W.; Ghosh, D. Motion and Flexibility in Human Cytochrome P450 Aromatase. *PLoS One* **2012**, *7*, No. e32565.
(20) Sgrignani, J.; Magistrato, A. Influence of the Membrane Lipophilic Environment on the Structure and on the Substrate Access/Egress Routes of the Human Aromatase Enzyme. A Computational Study. *J. Chem. Inf. Model.* **2012**, *52*, 1595−1606.
(21) Park, J.; Czapla, L.; Amaro, R. Molecular Simulations of Aromatase Reveal New Insights into the Mechanism of Ligand Binding. *J. Chem. Inf. Model.* **2013**, *53*, 2047−2056.
(22) Van Meer, G.; de Kroon, A. I. P. M. Lipid Map of the Mammalian Cell. *J. Cell Sci.* **2011**, *124*, 5−8.
(23) Needham, D.; McIntosh, T.; Evans, E. Thermomechanical and Transition Properties of Dimyristoylphosphatidylcholine/Cholesterol Bilayers. *Biochemistry* **1988**, 4668−4673.
(24) Evans, E.; Needham, D. Physical Properties of Surfactant Bilayer Membranes: Thermal Transitions, Elasticity, Rigidity, Cohesion and Colloidal Interactions. *J. Phys. Chem.* **1987**, *2*, 4219−4228.
(25) Ohvo-Rekilä, H.; Ramstedt, B.; Leppimäki, P.; Slotte, J. P. Cholesterol Interactions with Phospholipids in Membranes. *Prog. Lipid Res.* **2002**, *41*, 66−97.
(26) Raffy, S.; Teissié, J. Control of Lipid Membrane Stability by Cholesterol Content. *Biophys. J.* **1999**, *76*, 2072−2080.
(27) Drolle, E.; Kučerka, N.; Hoopes, M. I.; Choi, Y.; Katsaras, J.; Karttunen, M.; Leonenko, Z. Effect of Melatonin and Cholesterol on the Structure of DOPC and DPPC Membranes. *Biochim. Biophys. Acta* **2013**, *1828*, 2247−2254.
(28) Hung, W.-C.; Lee, M.-T.; Chen, F.-Y.; Huang, H. W. The Condensing Effect of Cholesterol in Lipid Bilayers. *Biophys. J.* **2007**, *92*, 3960−3967.
(29) Trandum, C.; Westh, P.; Jorgensen, K.; Mouritsen, O. G. A Thermodynamic Study of the Effects of Cholesterol on the Interaction Between Liposomes and Ethanol. *Biophys. J.* **2000**, *78*, 2486−2492.
(30) Wennberg, C. L.; Spoel, D. Van Der; Hub, J. S. Large Influence of Cholesterol on Solute Partitioning into Lipid Membranes. *J. Am. Chem. Soc.* **2012**, *134*, 5351−5361.
(31) Pike, L. J. The Challenge of Lipid Rafts. *J. Lipid Res.* **2009**, *50* (Suppl), S323−328.
(32) Sackman, E. Biological Membranes Architecture and Function. In *Structure and Dynamics of Membranes From Cells to Vesicles*; Lipowsky, R., Sackmann, E., Eds.; Elsevier: Amsterdam, 1995; pp 1−63.
(33) Epand, R. M. Cholesterol and the Interaction of Proteins with Membrane Domains. *Prog. Lipid Res.* **2006**, *45*, 279−294.
(34) Fantini, J. Interaction of Proteins with Lipid Rafts through Glycolipid-Binding Domains: Biochemical Background and Potential Therapeutic Applications. *Curr. Med. Chem.* **2007**, *14*, 2911−2917.
(35) Coskun, Ü.; Simons, K. Cell Membranes: the Lipid Perspective. *Structure* **2011**, *19*, 1543−1548.
(36) Park, J. W.; Reed, J. R.; Brignac-Huber, L. M.; Backes, W. L. Cytochrome P450 System Proteins Reside in Different Regions of the Endoplasmic Reticulum. *Biochem. J.* **2014**, *464*, 241−249.
(37) Anzenbacher, P.; Anzenbacherová, E. Cytochromes P450 and Metabolism of Xenobiotics. *Cell. Mol. Life Sci.* **2001**, *58*, 737−747.
(38) Yano, J. K.; Wester, M. R.; Schoch, G. A.; Griffin, K. J.; Stout, C. D.; Johnson, E. F. The Structure of Human Microsomal Cytochrome P450 3A4 Determined by X-ray Crystallography to 2.05-A Resolution. *J. Biol. Chem.* **2004**, *279*, 38091−38094.

DOI: 10.1021/ci500645k
J. Chem. Inf. Model. 2015, 55, 628−635

(39) Otyepka, M.; Skopalík, J.; Anzenbacherová, E.; Anzenbacher, P. What Common Structural Features and Variations of Mammalian P450s Are Known to Date? *Biochim. Biophys. Acta* **2007**, *1770*, 376−389.
(40) Hendrychová, T.; Anzenbacherová, E.; Hudeček, J.; Skopalík, J.; Lange, R.; Hildebrandt, P.; Otyepka, M.; Anzenbacher, P. Flexibility of Human Cytochrome P450 Enzymes: Molecular Dynamics and Spectroscopy Reveal Important Function-Related Variations. *Biochim. Biophys. Acta* **2011**, *1814*, 58−68.
(41) Bren, U.; Oostenbrink, C. Cytochrome P450 3A4 Inhibition by Ketoconazole: Tackling the Problem of Ligand Cooperativity Using Molecular Dynamics Simulations and Free-Energy Calculations. *J. Chem. Inf. Model.* **2012**, *52*, 1573−1582.
(42) Bren, U.; Fuchs, J. E.; Oostenbrink, C. Cooperative Binding of Aflatoxin B 1 by Cytochrome P450 3A4: A Computational Study. *Chem. Res. Toxicol.* **2014**, *27*, 2136−2147.
(43) Davydov, D. R.; Halpert, J. R. Allosteric P450 Mechanisms: Multiple Binding Sites, Multiple Conformers, or Both? *Exp. Opin. Drug Metab. Toxicol.* **2008**, *4*, 1523−1535.
(44) Bodin, K.; Bretillon, L.; Aden, Y.; Bertilsson, L.; Broomé, U.; Einarsson, C.; Diczfalusy, U. Antiepileptic Drugs Increase Plasma Levels of 4beta-Hydroxycholesterol in Humans: Evidence for Involvement of Cytochrome P450 3A4. *J. Biol. Chem.* **2001**, *276*, 38685−38689.
(45) Shinkyo, R.; Guengerich, F. P. Inhibition of Human Cytochrome P450 3A4 by Cholesterol. *J. Biol. Chem.* **2011**, *286*, 18426−18433.
(46) Wolf, M. G.; Hoefling, M.; Aponte-Santamaría, C.; Grubmüller, H.; Groenhof, G. g _ membed: Efficient Insertion of a Membrane Protein into an Equilibrated Lipid Bilayer with Minimal Perturbation. *J. Comput. Chem.* **2010**, *31*, 2160−2174.
(47) Berendsen, H. The Missing Term in Effective Pair Potentials. *J. Phys. Chem.* **1987**, *91*, 6269−6271.
(48) Hess, B.; Kutzner, C.; van der Spoel, D.; Lindahl, E. GROMACS 4: Algorithms for Highly Efficient, Load-Balanced, and Scalable Molecular Simulation. *J. Chem. Theory Comput.* **2008**, *4*, 435−447.
(49) Berger, O.; Edholm, O.; Jahnig, F. Molecular Dynamics Simulations of a Fluid Bilayer of Dipalmitoylphosphatidylcholine at Full Hydration, Constant Pressure and Constant Temperature. *Biophys. J.* **1997**, *72*, 2002−2013.
(50) Oostenbrink, C.; Villa, A.; Mark, A. E.; van Gunsteren, W. F. A Biomolecular Force Field Based on the Free Enthalpy of Hydration and Solvation: the GROMOS Force-Field Parameter Sets 53A5 and 53A6. *J. Comput. Chem.* **2004**, *25*, 1656−1676.
(51) Pravda, L.; Berka, K.; Svobodová Vařeková, R.; Sehnal, D.; Banáš, P.; Laskowski, R. A.; Koča, J.; Otyepka, M. Anatomy of enzyme channels. *BMC Bioinformatics* **2014**, *15*, 379.
(52) Sehnal, D.; Svobodová Vařeková, R.; Berka, K.; Pravda, L.; Navrátilová, V.; Banáš, P.; Ionescu, C.-M.; Otyepka, M.; Koča, J. MOLE 2.0: Advanced Approach for Analysis of Biomacromolecular Channels. *J. Cheminform.* **2013**, *5*, 39.
(53) Cojocaru, V.; Winn, P. J.; Wade, R. C. The Ins and Outs of Cytochrome P450s. *Biochim. Biophys. Acta* **2007**, *1770*, 390−401.
(54) Hofsäss, C.; Lindahl, E.; Edholm, O. Molecular Dynamics Simulations of Phospholipid Bilayers with Cholesterol. *Biophys. J.* **2003**, *84*, 2192−2206.
(55) Róg, T.; Pasenkiewicz-Gierula, M.; Vattulainen, I.; Karttunen, M. Ordering Effects of Cholesterol and its Analogues. *Biochim. Biophys. Acta* **2009**, *1788*, 97−121.
(56) Koynova, R.; Caffrey, M. Phases and Phase Transitions of the Phosphatidylcholines. *Biochim. Biophys. Acta* **1998**, *1376*, 91−145.
(57) Rawicz, W.; Smith, B. A.; McIntosh, T. J.; Simon, S. A.; Evans, E. Elasticity, Strength, and Water Permeability of Bilayers that Contain Raft Microdomain-Forming Lipids. *Biophys. J.* **2008**, *94*, 4725−4736.

DOI: 10.1021/ci500645k
J. Chem. Inf. Model. 2015, 55, 628−635

THE JOURNAL OF PHYSICAL CHEMISTRY B

Article

pubs.acs.org/JPCB

Effect of Lipid Charge on Membrane Immersion of Cytochrome P450 3A4

Veronika Navrátilová, Markéta Paloncýová, Karel Berka, and Michal Otyepka*

Regional Centre of Advanced Technologies and Materials, Department of Physical Chemistry, Faculty of Science, Palacký University Olomouc, tř. 17. listopadu 12, 771 46 Olomouc, Czech Republic

Supporting Information

ABSTRACT: Microsomal cytochrome P450 enzymes (CYPs) are membrane-attached enzymes that play indispensable roles in biotransformations of numerous endogenous and exogenous compounds. Although recent progress in experiments and simulations has allowed many important features of CYP−membrane interactions to be deciphered, many other aspects remain underexplored. Using microsecond-long molecular dynamics simulations, we analyzed interaction of CYP3A4 with bilayers composed of lipids differing in their polar head groups, i.e., phosphatidylcholine, phosphatidylethanolamine, phosphatidylserine, and phosphatidylglycerol. In the negatively charged lipids, CYP3A4 was immersed more deeply and was more inclined toward the membrane because of favorable electrostatic and hydrogen bonding interactions between the CYP catalytic domain and lipid polar head groups. We showed that electrostatics significantly contributes to positioning and orientation of CYP on the membrane and might contribute to the experimentally observed preferences of individual CYP isoforms to distribute in (dis)ordered membrane microdomains.

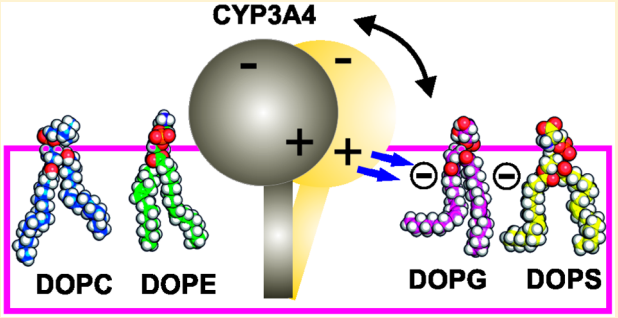

INTRODUCTION

The microsomal cytochrome P450 (CYP) enzymes are membrane-anchored proteins involved in many biotransformation processes of drugs and other endogenous and exogenous compounds.[1,2] They are known to metabolize more than 50% of marketed drugs[2] and are responsible for some adverse effects of drugs, e.g., drug−drug interactions. Thus, CYPs have been a focus of pharmacology and drug development. The catalytic domains of CYPs contain a deeply buried active site housing a heme cofactor,[3] which is connected to the environment by a complex network of channels.[4] The CYP catalytic domain sits on the cytoplasmic side of the endoplasmic reticulum (ER) membrane and is embedded to it by an N-terminal transmembrane α-helical anchor.[5−9]

Membrane orientations of CYPs have been studied by various methods. Molecular dynamics (MD) simulations[5−9] have identified common hydrophobic regions of CYPs that interact with membranes (N-terminal, A′, F′, and G′ helices), with only small variations among individual CYP isoforms.[10] The proposed orientation agreed with experimental evidence obtained from atomic force microscopy,[11,12] tryptophan fluorescence scanning,[13] epitope labeling,[14,15] and NMR experiments.[16] These findings about CYP membrane orientation were recently corroborated by the first published X-ray structures of CYP with a resolved transmembrane N-terminal anchor from *Saccharomyces cerevisiae*.[17,18] In addition, there is growing evidence that the membrane is not just a passive environment but affects the CYP orientation, localization, ligand binding, and catalytic activity. Individual CYP isoforms differ in their localization in the ordered and disordered microdomains of the ER membrane.[19−21] Whereas CYP1A1 and CYP2E1 have been shown to prefer disordered domains, CYP1A2 and CYP reductase (CPR) prefer ordered domains and CYP2B4 is equally distributed in both domains.[19−25] This difference in localization could affect the catalytic efficiency of individual CYPs. For instance, excessive addition of the order-inducing cholesterol lipid has been shown to significantly suppress the activity of CYP3A4.[26,27]

The activity of CYP also depends on the membrane lipid composition. Addition of phosphatidylethanolamine (PE) to phosphatidylcholine (PC) has been shown to increase the catalytic activity of CYP2B4,[28] whereas it had a stabilization effect on CYP1A2.[29] The catalytic activity of CYP1A2 was found to increase by 2−3-fold in the presence of anionic lipids, i.e., 50% addition of phosphatidic acid (PA) or phosphatidylserine (PS).[30] When CYP3A4 was attached to a mixed phosphatidylcholine/phosphatidylserine membrane, an increase in maximal velocity V_{max} for nifedipine oxidation was observed, but the Michaelis constant, K_m, was unchanged.[31] The enzymatic activity of CYP3A4 in the presence of anionic lipids was shown to increase by ∼6-fold at 50 mol% of PS in comparison with a pure PC membrane. Further increasing the PS concentration (above 60%) led to a rapid decrease of the

Received: October 6, 2016
Published: October 10, 2016

ACS Publications © 2016 American Chemical Society

DOI: 10.1021/acs.jpcb.6b10108
J. Phys. Chem. B 2016, 120, 11205−11213

enzyme activity.[32] As the rate of NADPH oxidation was found to be unaffected by the presence of anionic lipids, it was suggested that negatively charged membrane lipids might affect the electron flow between CYP and redox partners.[31−34] However, the mechanism by which lipids mediate the electron transfer remains unclear.[11] Thus, despite the apparent influence of the membrane on the catalytic function of CYP, there is still a lack of information regarding the structural details of the interaction of CYPs with various membranes and reasons for the pronounced role of the membrane composition in CYP biophysics.

In this work, we describe interactions between CYP3A4 and various membrane lipids differing in the headgroup region. We chose to study dioleoyl phospholipids and examined the influence of differently charged head groups on CYP3A4 interaction with the membranes (Figure 1). We observed

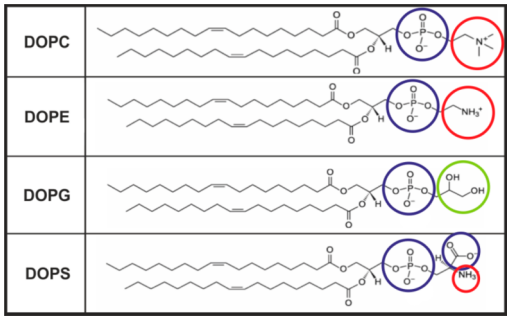

Figure 1. Lipids of biological membranes addressed in this study: 1,2-dioleoyl-*sn*-glycero-3-phosphocholine (DOPC), 1,2-dioleoyl-*sn*-glycero-3-phosphoethanolamine (DOPE), 1,2-dioleoyl-*sn*-glycero-3-[phospho-*rac*-(3-lysyl(1-glycerol))] (DOPG), and 1,2-dioleoyl-*sn*-glycero-3-phosphoserine (DOPS). The charges are highlighted by circles in the following colors: blue, negative; red, positive; green, neutral polar.

significant differences in the structure, position, and orientation of CYP3A4 in membranes with variously charged lipids. We considered the implications of the observations in the context of the activity and charges of CYPs. We hypothesized that the charge of CYP might induce electrostatic interactions between CYP and (negatively charged) membranes, which may influence not only the catalytic efficiency and access or egress of substrates/metabolites but also CYP localization in membrane microdomains.

METHODS

We prepared membrane models using four different lipid bilayers, each composed of pure dioleoylphosphoglycerolipid (DOPx) containing 121 molecules per leaflet. We used 1,2-dioleoyl-*sn*-glycero-3-phosphocholine (DOPC), 1,2-dioleoyl-*sn*-glycero-3-phosphoethanolamine (DOPE), 1,2-dioleoyl-*sn*-glycero-3-[phospho-*rac*-(3-lysyl(1-glycerol))] (DOPG), and 1,2-dioleoyl-*sn*-glycero-3-phosphoserine (DOPS). The lipids differed only in the head groups (Figure 1) in order to separate the role of the head groups from the effect of the lipid tails. The Slipids[35] force field was applied for the lipids, and the membrane bilayers were hydrated with the TIP3P water model.[36] The bilayer models were initially equilibrated for 200 ns.

We used the all-atom structure of CYP3A4 pre-equilibrated on the DOPC membrane obtained from our previous study.[37] CYP3A4 was attached into each of the four different equilibrated bilayers using the Gromacs tool g_membed.[38] CYP3A4 attached to the membrane was then inserted into a rectangular box and solvated with the TIP3P water model.[36] After solvation, Na^+ and Cl^- ions were added to neutralize the system and obtain a physiological concentration of 0.1 mol/L (see Table S1 in Supporting Information).

All simulations were performed using Gromacs package 5.0.[39] The AMBER ff99SB[40] force field was used for CYP3A4, which is compatible with the Slipids force field.[35] Parameters developed by Cheatham et al.[41] were used for the heme cofactor, whereas parameters developed by Aqvist and Applequist et al.[42,43] were used for the ions. Each system was energy minimized using the steepest descent method. After the initial minimization, a short 10-ns-long MD simulation with positional restraints applied for C_α atoms was executed. Afterward, a 200-ns-long equilibration MD simulation of each membrane with CYP3A4 was performed with the following parameters: 2-fs-long time step (LINCS algorithm[44]); semi-isotropic Berendsen barostat[45] with pressure of 1 bar; V-rescale thermostat at 310 K. Trajectories were collected from a 1000+-ns-long production run using the following parameters for [*N*, *p*, *T*] MD simulations: 2-fs-long time step, Nosé−Hoover thermostat[46,47] set to 310 K, Parrinello−Rahman barostat[48] set to 1.013 bar with semi-isotropic conditions, isothermal compressibility of 4.5×10^{-5} bar^{-1}, and pair-list generated with the group cut-off scheme. The particle Mesh Ewald method[49] was to treat electrostatics interactions from 1 nm, and van der Waals interactions were switched off between 0.8 and 1.0 nm. Constraints were applied on all bonds with hydrogens. Periodic boundary conditions were applied in all directions.

All analyses were performed over the last 500 ns of the MD simulations. For analysis of CYP3A4 and the membrane properties, Gromacs tools were used.[39] To measure the distances between CYP, parts of CYP, and the membrane, the g_dist tool was used to calculate the centers of masses of individual moieties. The g_sgangle tool was used to compute the heme tilt angle, which was defined as the angle between the heme plane and membrane normal (*z*-axis).[10] The heme plane was represented by a set of three nitrogen atoms of the heme porphyrin. A similar approach was used for calculation of CYP tilt angle represented by a vector pointing from middle of I-helix (T309) to β1-sheet (I383). The area per lipid (APL) was calculated from the size of the plane and number of lipids. The monolayer thickness ($D_{HH}/2$) was calculated from the *z*-distance between the maximum densities of phosphate group in each leaflet obtained using the g_density tool. Amino acids located below the level of membrane head groups and above them were analyzed from the density distribution of individual amino acids along the *z*-axis. Amino acids were sorted into three groups: (1) located below the level of membrane head groups, (2) further from the membrane center than group 1, but closer than 7 Å above the headgroup level, (3) distant amino acids. Density profiles of amino acids were also used for calculation of CYP3A4 height above the membrane (the distance of the furthest amino acid was taken, cf., Figure S1 in Supporting Information). Deuterium order parameters were measured using the g_order tool. Radial distribution functions of terminal nitrogens (in the case of DOPG, terminal oxygen), phosphorus atoms, ions, and water molecules around the surface of CYP3A4 were calculated using the g_rdf tool. The root-mean-square deviation (RMSD) was calculated using the g_rms tool. Figures were rendered by PyMOL (PyMOL Molecular Graphics System, Version 1.8 Schrödinger, LLC). The analysis of contacts between CYP3A4 amino acid residues

DOI: 10.1021/acs.jpcb.6b10108
J. Phys. Chem. B 2016, 120, 11205−11213

(within 6 Å between heavy atoms) and membrane lipid head groups and tails was performed by gromacs tool g_mindist. Analysis of CYP charges was perfomed by Pymol script *FindSurfaceResidues.py* script from Pymol Scripts repository (https://github.com/Pymol-Scripts/Pymol-script-repo/raw/master/findSurfaceResidues.py).

RESULTS

We embedded CYP3A4 into four different DOPx bilayers (Figure 2) and carried out 1-μs-long MD simulations in order

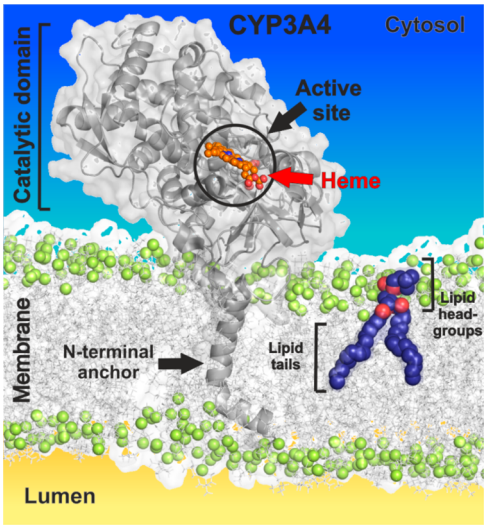

Figure 2. Structural view of CYP3A4 attached to a DOPC membrane. CYP3A4 is represented as a gray cartoon and transparent surface; the active site is shown by a black circle and the heme cofactor as orange (carbons) and red (oxygens) spheres. The detail of an individual DOPC lipid (blue spheres) shows the position of the lipid headgroup and tails in the bilayer; oxygens are represented as red spheres and phosphate atoms as pale green spheres.

to explain the role of the lipid headgroup on the interaction of CYP3A4 with the membrane. The structural details of the pure membranes (without CYP3A4) are listed in Table 1, and a schematic view of the measured characteristics is depicted in Figure S1 in Supporting Information. The area per lipid (APL) of the pure membranes varied from 0.59 nm^2 (DOPE) to 0.70 nm^2 (DOPG) and was negatively linearly correlated (r^2 = 0.96) with the membrane thickness varying from 4.2 nm (DOPE) to 3.6 nm (DOPG). The DOPE membrane was significantly more ordered (average deuterium order parameters $S_{\langle CD\rangle}$ of 0.16) than the other lipids and exhibited a significantly increased $S_{\langle CD\rangle}$ on its sn-2 chain (Figure S2 in Supporting Information). Differences in chain ordering between the sn-1 and sn-2 chains were observed near the head groups, but with the exception of DOPE, $S_{\langle CD\rangle}$ values for the lipids chains in the membrane cores were similar. These observations agree with previous literature[50−52] and indicate that the used parameters and protocols provided relevant data for further interpretation.

The embedded CYP3A4 catalytic domain kept its native fold as RMSD of C_α atoms from the last frame to the X-ray structure below 0.4 nm, with the notable exception of CYP3A4 on the DOPS membrane (Figures S3 and S4 in Supporting Information), and the systems achieved convergence after 500 ns of production simulation. The difference of RMSD in the case of CYP3A4 on the DOPS membrane was caused by modification of a small portion of a CYP3A4 secondary structural element of membrane-attached parts, i.e., C, F, G, H helices, but the majority of secondary structure remained conserved. As a result, former C and H helices sunk toward the membrane, dragging along the I-helix and causing a kink in the middle part of the I-helix. During 1 μs of unbiased simulations, the center of mass of CYP3A4 structural elements reached a stable distance from the center of the membrane (Table S2 in Supporting Information). CYP3A4 was anchored to the membrane by its N-terminal transmembrane helix but also by the tip of the F/G loop; A, F, and G helices; and partially the B/C loop (Figures 3 and 4), in good agreement with previous observations.[5−10] In the DOPS membrane, additional contacts of the K-helix with the membrane head groups were found, whereas in the DOPG membrane, β3−β5 sheets (β-finger) were in contact with the membrane. The membrane adapted to the presence of CYP by forming a funnel-like hydrophobic protrusion, with lipids' head groups pushed to the edge of the funnel (see Figure S5). These additional contacts in DOPG or

Table 1. Measured Properties from Lipid Membrane Simulations

	pure membrane			membrane with CYP3A4									
					AA in contact with membrane[d]			AA located in membrane layers[e]					
lipid type	APL[a] [nm^2]	$D_{HH}/2$[b] [nm]	$S_{\langle CD\rangle}$	dCM[c] [nm]	L1	L2	total	L1	L2	av no. H bonds of CYP3A4 to lipids[f]	HTA[g] [deg]	CTA[h] [deg]	CYP height[i] [nm]
DOPC	0.69	1.89	0.11	3.77 ± 0.14	57	80	97	47	38	12.7	63.6 ± 6.1	85.4 ± 4.5	5.0
DOPE	0.59	2.12	0.16	3.83 ± 0.14	60	79	98	52	34	25.3	73.2 ± 5.6	84.4 ± 6.1	4.5
DOPG	0.70	1.80	0.10	3.10 ± 0.11	68	107	121	112	98	40.3	77.3 ± 5.0	98.5 ± 3.1	4.1
DOPS	0.65	1.97	0.13	3.58 ± 0.15	55	97	117	68	46	32.1	68.6 ± 5.2	102.8 ± 3.9	4.6

[a]Area per lipid (APL). [b]Monolayer thickness ($D_{HH}/2$) calculated as half the headgroup−headgroup distance of lipid bilayers in pure bilayer simulations. [c]dCM, CYP center-of-mass distance from the membrane. [d]Number of CYP3A4 AA residues located in contact with the membrane within 6 Å (between heavy atoms) from lipid tails (L1) or polar head groups (L2) and the total number of unique AA residues interacting with the membrane (i.e., removes duplicates of AA interacting simultaneously with lipid tails and head groups). [e]AA located in various membrane layers, below the level of lipid head groups (L1) or 7 Å above the level of lipid head groups (L2). [f]Average number of hydrogen bonds between CYP3A4 and lipids. [g]Heme tilt angle (HTA). [h]CYP tilt angle (CTA). [i]Height of CYP was calculated as a distance between the position of the furthest amino acid of CYP3A4 above the membrane surface (taken as $D_{HH}/2$ from the membrane center). Each analysis here includes the whole CYP3A4, including 27 amino acids from anchor.

DOI: 10.1021/acs.jpcb.6b10108
J. Phys. Chem. B 2016, 120, 11205−11213

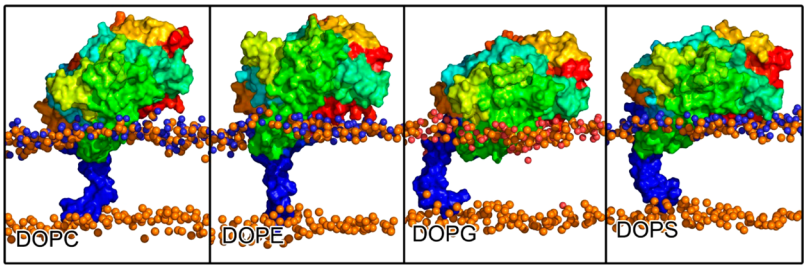

Figure 3. CYP3A4 on different membranes adopting different orientations and depths of the embedding. In the lipids, phosphates are shown as orange balls, whereas in the upper layer of the membrane, the nitrogens and glycerol oxygens (in DOPG) are shown as blue and pink balls, respectively.

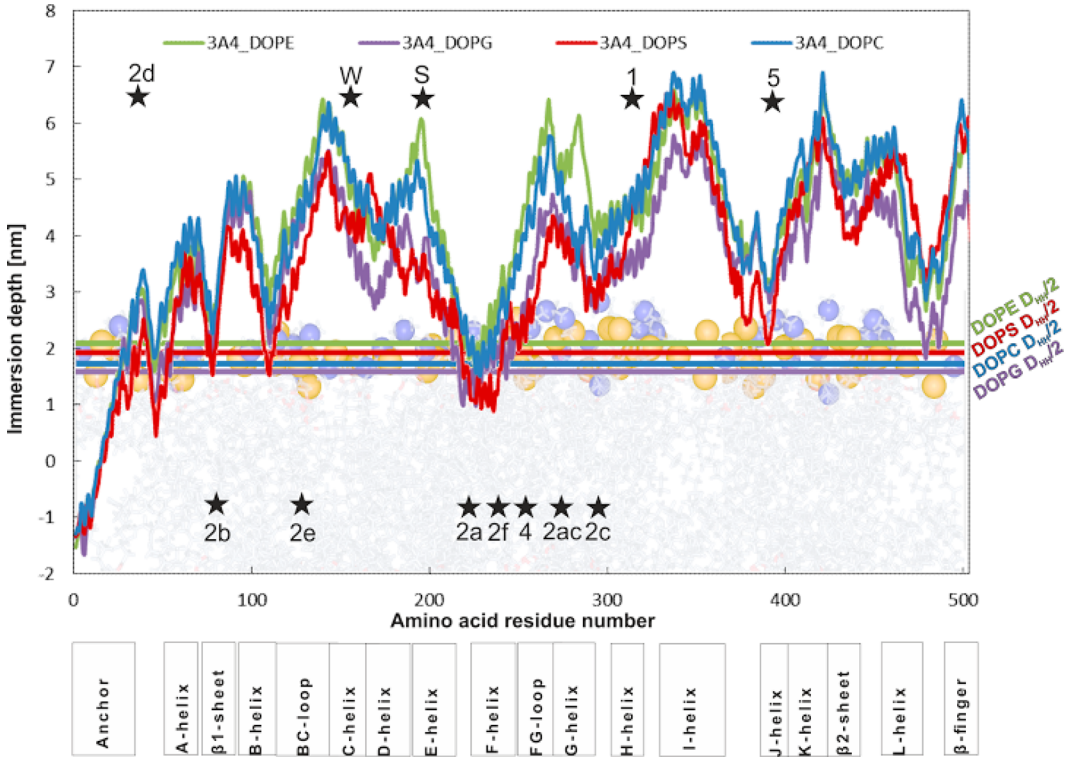

Figure 4. Distribution of amino acids in contact with the membrane. The different systems are represented by the following colors: CYP3A4-DOPC, blue; CYP3A4-DOPE, green; CYP3A4-DOPG, purple; CYP3A4-DOPS, red. Boxes below the graph show the position of secondary structural features of CYP3A4. The colored lines depict the monolayer thickness according to $D_{HH}/2$ values (from Table 1). Black stars depict the positions of mouth openings of active site access channels (2a, 2ac, 2b, 2c, 2d, 2e, 2f, 1, 4, 5), water (W), and solvent (S) channels (Wade et al. nomenclature[4] was used).

DOPS membranes (Table 1) indicated deeper immersion of CYP3A4 into the respective membranes. Consequently, the mouth openings of the active site access/egress channels were located deeper in the negatively charged membranes (Figure 4 and Figure S6).

The position of CYP3A4 in the DOPx membranes correlated with the number of CYP3A4 amino acid (AA) residues embedded below the membrane surface (r^2 = 0.98; Table 1). We evaluated the distance of CYP center of mass from the middle of the membrane (dCM) as a global metric for CYP immersion. The deepest immersion of CYP3A4 was observed in the DOPG membrane (dCM = 3.1 ± 0.1 nm) followed by DOPS (dCM = 3.6 ± 0.1 nm; Table 1, and Table S2 and Figure S7 in Supporting Information). In the neutral DOPC and DOPE membranes, CYP3A4 was located significantly further from the membrane center (dCM ∼ 3.8 ± 0.1 nm in both cases). We also monitored the distance from CPR binding AA residues (N441−R446) to the membrane center and identified similar trends as described for dCM (Figure S8 in Supporting Information). The number of hydrogen bonds between CYP3A4 and the membrane head groups increased with decreasing dCM (r^2 = 0.67; Table 1); the same applies for the number of interacting amino acids with the membrane.

The type of lipid in the membrane influenced, besides the position, the orientation of CYP3A4 on the membrane (Figure 3). The different orientations of the catalytic domain can be analyzed in terms of the heme tilt angle (HTA, Figure 5), which defines the orientation of the heme cofactor plane with respect to the membrane plane and can be experimentally determined from linear dichroism measurements.[53] The highest heme tilt angle of CYP3A4 was observed in the DOPG membrane (77 ± 5°), indicating the largest inclination toward the membrane. The heme tilt angle then decreased gradually in the order DOPG > DOPE > DOPS > DOPC. The smallest angle was

DOI: 10.1021/acs.jpcb.6b10108
J. Phys. Chem. B 2016, 120, 11205−11213

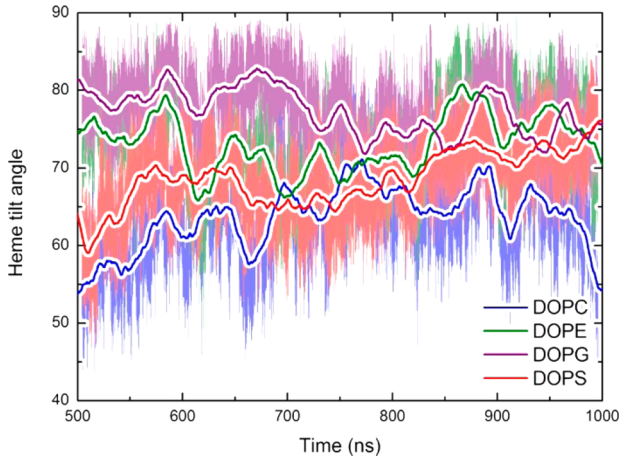

Figure 5. Heme tilt angle of CYP3A4 on different membranes (DOPC, blue; DOPE, green; DOPG, purple; DOPS, red) obtained from the last 500 ns of MD simulations. The thick lines represent smooth development of the heme tilt angle, and the background shows the detailed trajectory analysis.

obtained with DOPC (64 ± 6°, Table 1), which agrees (within the error bars) with the experimentally obtained value of 60 ± 4° measured for CYP3A4 on 1-palmitoyl-2-oleoyl-*sn*-glycero-3-phosphocholine (POPC) nanodiscs.[53] Though HTA can be experimentally measured, it does not fully describe the orientation of CYP in the membrane. We used CYP tilt angle as another metric for evaluation of the CYP orientation, which is the angle between an axis defined by the middle of I-helix and β1-sheet and *z*-axis (Figure S9). The CYP tilt angle was selected to be orthogonal to both HTA and I-helix (whose orientation against *z*-axis is almost invariant, data not shown). The CYP tilt angle clearly showed a more inclined orientation of CYP toward DOPS and DOPG membranes (Table 1). In all cases, the heme tilt angle displayed larger fluctuations than the CYP tilt angle on the ∼100 ps time scale, and both fluctuated significantly on the ∼100 ns time scale during the MD simulations (Figure 5).

DISCUSSION

The goal of this study was to investigate the structural and dynamical features of CYP3A4 interaction with membranes consisting of lipids differing in their polar headgroup. Most in silico CYP studies published so far were carried out on PC membranes. The position and orientation of CYP3A4 on the DOPC membrane observed here agree well with previous structures and experiments.[17,53,54] In our model, CYP3A4 was embedded in the DOPC membrane according to a typical membrane binding pattern represented by immersed structural motifs, i.e., N-terminal α-helix, tips of F/G loop and B/C loop, and parts of F and G loops (Figures 2 and 4).[55]

The orientation of CYP3A4 on DOPC, evaluated from the heme tilt angle, was consistent with the experimentally determined value for CYP3A4 on POPC nanodiscs,[53] supporting the validity of our model. Higher heme tilt angle values were connected with a lower number of hydrogen bonds between CYP3A4 and the membrane (Table 1). The number of hydrogen bonds was also connected with the depth of immersion of CYP3A4 into the membrane (Figure S10). However, we observed large fluctuations with slow frequency in the characteristics of dCM and orientation of CYP3A4 on all membranes. Although the systems were allowed to relax for 200 ns, as previously considered sufficient time for equilibration,[56] analysis of the first 500 ns of our production simulation (i.e., after 700 ns of MD simulation since the start) revealed time evolution of the distribution of the heme tilt angle, e.g., relaxation of the DOPE system (Figure S11 in Supporting Information). As we defined the heme tilt angle by a small region, tiny fluctuations or reversible deformations of the heme were reflected in fluctuations on a picosecond time scale without significant influence on the whole CYP3A4 structure. On the other hand, longer scale fluctuations, on a 100 ns+ time scale, reflected the enzyme orientation changes on the membrane. CYP tilt angle also fluctuated significantly, but clearly showed more inclined orientation of CYP3A4 on DOPG and DOPS membranes (Figure S9, Table 1). These observations indicate that membrane-attached proteins such as CYP3A4 undergo slow floating motions, which can be observed on 100+ ns time scales. Hence, we recommend executing MD simulations of membrane-attached proteins on at least a 500 ns time scale in order to observe such motions. However, for the sake of completeness, we cannot rule out that some relevant motion was not detected owing to the relatively short time scale of the simulations compared to those in actual biophysical and biochemical experiments.

In our simulations, we observed changes in CYP3A4 depth and orientation on membranes that might affect the activity of CYP3A4 in various membranes depending on the chemical properties of the lipid head groups. For example, regarding the neutral lipids, DOPE has a small headgroup (ethanolamine) terminated by a charged ammonium group, which can serve as a hydrogen bond proton donor, whereas DOPC with the charged choline group is unable to form hydrogen bonds. Thus, the DOPE bilayer was more ordered than DOPC and was able to form more hydrogen bonds with CYP3A4 (Table 1). The negatively charged DOPG and DOPS lipids may serve as both proton donors and acceptors for hydrogen bonds. DOPG possesses a single negative charge on a phosphoryl group terminated by a neutral glycerol moiety. In contrast, DOPS bears a zwitterion serine moiety attached to the phosphoryl group, and therefore has three charged groups that can interact more strongly via electrostatic interactions. The different binding properties of the lipid head groups were reflected in the total number of hydrogen bonds to CYP3A4, which was highest for DOPG, followed by DOPS and DOPE, and lowest for DOPC (Table 1). Clearly, the ability of DOPG to form an extensive network of hydrogen bonds induced CYP3A4 to bend toward the membrane (Figure 3).

Contacts between CYP3A4 and lipids differed depending on the membrane composition, as is apparent from their radial distribution functions (RDF, Figure S12 in Supporting Information). In all four cases, a clear peak in the RDF between the CYP3A4 surface and phosphorus atoms could be seen at approximately the same position (∼0.30 nm). In DOPS, the lipid head groups were more organized than in the other membranes owing to stronger interactions, and the second headgroup layer was observed at a distance of ∼0.45 nm. The position of the terminal nitrogen (in the case of DOPG, terminal oxygen) was the same (∼0.27 nm) except for DOPC, which cannot form hydrogen bonds as its nitrogen is shielded by methyl groups, and it is located at ∼0.38 nm. In DOPG, we observed an additional shoulder in the RDF function close to the CYP3A4 surface (at ∼0.20 nm), which reflected close hydrogen bonding interactions between the uncharged terminal hydroxyl group of the DOPG glycerol with CYP3A4. In DOPG

DOI: 10.1021/acs.jpcb.6b10108
J. Phys. Chem. B 2016, 120, 11205−11213

and DOPS, we also observed a high concentration of Na^+ cations interacting with the negatively charged head groups, whereas the water pattern was similar in all cases. Thus, the different orientation and depth of CYP3A4 creates a unique environment in the contact region, rich in hydrogen bonds, ions, and charged head groups (Figure S5 in Supporting Information).

CYP3A4 was immersed more deeply in the negatively charged membranes (DOPG and DOPS) than in the neutral ones (DOPC and DOPE). This is consistent with the fact that the distal side of the CYP3A4, which is in direct contact with the membrane (see Figure 6), is positively charged, and

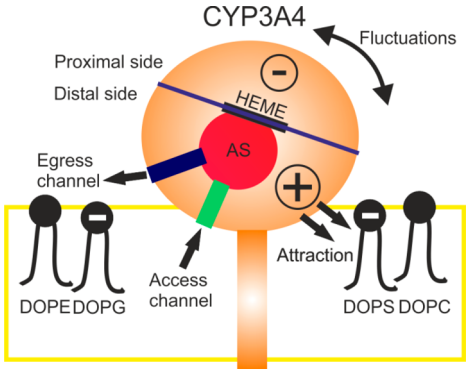

Figure 6. Schematic view of CYP3A4–membrane lipid interactions and possible effects on CYP function. CYP3A4 is represented as an orange circle and the N-terminal transmembrane anchor as an orange rectangle. The CYP active site (AS) is shown as a red circle, whereas blue and green rectangles denote the egress and access channels, respectively. The membrane is depicted as a yellow box, and membrane lipids are shown in black. The distal side of CYP3A4 is positively charged, which enhances attraction between the catalytic domain and negatively charged membrane lipids (in this case, DOPS and DOPG) and may also influence substrate access and product release by changes of opening/closing access/egress channels (Figure S6). In addition, interaction of the membrane lipids with the CYP catalytic domain causes fluctuations of CYP on the membrane surface.

therefore strongly attracted to the negatively charged lipids. DOPG showed the deepest immersion of CYP3A4 into the membrane as its negatively charged group had a deeper position than that of the serine carboxylic acid in DOPS. Experimentally, a 6-fold increase in the CYP3A4 activity was observed in 50% PS membrane. Further increase in PS concentration (60%) leads, however, to a loss of CYP3A4 activity, which was attributed to lipid vesicles aggregation.[32] Unfortunately, no direct experimental information about activity of CYP3A4 in pure PS membrane is currently available. Though the secondary structure was conserved in all lipids, simulations revealed that the surplus of negatively charged lipids in DOPS caused a kink on I-helix in the CYP3A4 structure. Without any doubt, experimental observations as well as simulations document that the electrostatic interactions between CYP and the membrane may have an impact on the catalytic activity of the enzyme, due to numerous reasons including also changes in positioning of CYP access channels mouth openings. These openings were localized deeper in negatively charged membranes (cf. Figure 4 and Figure S6), while the positions of substrates and metabolites of CYP3A4 in the membranes did not significantly differ (Figure S13).

Overall, the differences in the interactions between CYPs with the membranes can be tracked to their respective charges. Lipid membranes involved, e.g., in the human body, contain differently charged lipids: from neutral ones (e.g., PC, PE) to negatively charged ones (e.g., PS, PG). Lipid types also differentiate in their ordering, ability to form hydrogen bonds, etc. Individual CYP isoforms differ in their charge from negatively charged CYP2D6 to highly positively charged CYP1A2 (Table 2). In addition, the charge is unevenly distributed between the distal and proximal sides of the catalytic domain, and more than 90% of charge residues lie on the CYP surface (Table S3). The proximal side is usually negatively charged, which is consistent with the structures of its redox partners interacting in this area.[55,57,58] In contrast, the distal side, which makes up the majority of the CYP3A4–membrane interface, is usually positively charged. A different preference for ordered and disordered membrane domains has been observed for the very homologous CYP isoforms 1A1 and 1A2.[20,21] As these two CYP isoforms have significantly different total charge, we suggest that the different membrane localization could be controlled not only directly by the lipid ordering, but also by the charge of the CYP catalytic domain. The preference of CYPs for various membrane domains can

Table 2. Preferences of CYP Membrane Domains Based on the Charge for Important Mammalian CYPs[a]

CYP	total[b]	distal[c]	proximal[c]	TM helix[c]	PDBID	domain
rabbit 1A2	12	N/A	N/A	N/A	N/A	ordered,[21,22,24,25] anionic-rich[60]
human 1A2	10	2	7	1	2hi4	
human 2C8	9	10	−4	3	2nnj	
rabbit 2B4	6	6	−1	1	1po5	disordered + ordered[20]
human 1A1	5	4	−1	2	4i8v	
rabbit 1A1	3	N/A	N/A	N/A	N/A	disordered[20,21,25]
rabbit 2E1	3	N/A	N/A	N/A	N/A	disordered[20]
human 2C9	3	4	−1	0	1r9o	
human 2B6	3	5	−2	0	3ua5	
human 2E1	3	3	0	0	3koh	
human 3A4	3	6	0	−3	1tqn	
human 2C19	0	−2	1	1	4gqs	
human 2D6	−2	1	−5	2	3qm4	

[a]For charge distribution over the CYP surface, see Table S3 in Supporting Information. [b]Total charge was calculated from the UNIPROT canonical sequence. [c]Distribution of the charge between the distal or proximal side was calculated from the crystal structure resembling the most native form; TM helix means charge of transmembrane helix. Charges were estimated on the basis of the presence of Arg, Lys, Asp, and Glu amino acids.

DOI: 10.1021/acs.jpcb.6b10108
J. Phys. Chem. B 2016, 120, 11205−11213

also be affected by many other factors such as temperature, lipid composition, presence of divalents, etc. In any case, the data in Table 2 (and more detailed Table S3) show that CYPs with positive total charge prefer the ordered membrane domains, which might contain a surplus of anionic lipids.[59]

CONCLUSION

We studied the influence of lipid membrane composition on the behavior of human CYP3A4. CYP3A4 was found to be anchored to the membrane in N-terminal α-helix, F/G loop, and neighboring hydrophobic regions. The embedding depth and orientation depended on the membrane lipid charge. As CYP3A4 is positively charged, it was more attracted to the negatively charged rather than neutral lipid membrane lipids, as reflected by the calculated membrane immersion depth and orientation. Hence, the CYP3A4−membrane interaction seemed to be affected by electrostatics and hydrogen bonding, which are believed to be responsible for the observed structural changes of CYP3A4−membrane complexes. We suggest that the structural features of the CYP−membrane interaction might be further reflected in the differing CYP function and membrane microdomain localization, as already observed for CYP1A1 and CYP1A2. These findings indicate that CYP−membrane interactions are rather complex (Figure 6) and the specific nature of the membrane may affect many biophysical and biochemical aspects of CYP function, i.e., enzyme immersion depth, orientation, access/egress channels opening or closing, interaction with its redox partners and substrates, and membrane domain localization. We suggest that the membrane is not merely a passive environment but may contribute to regulation of CYP function.

ASSOCIATED CONTENT

Supporting Information

The Supporting Information is available free of charge on the ACS Publications website at DOI: 10.1021/acs.jpcb.6b10108.

Additional data including numbers of ions and water molecules in simulations, view of CRP characteristics, order parameters, and further information (PDF)

AUTHOR INFORMATION

Corresponding Author

*Phone: +420 585634756. Fax: +420 585634761. E-mail: michal.otyepka@upol.cz.

Notes

The authors declare no competing financial interest.

ACKNOWLEDGMENTS

This research was supported by the Czech Grant Agency through Project P208/12/G016. M.P. and V.N. acknowledge support from a student project of Palacký University Olomouc (IGA_PrF_2016_028). The authors gratefully acknowledge support through Project LO1305 of the Ministry of Education, Youth and Sports of the Czech Republic.

ABBREVIATIONS

AA, amino acid
CPR, cytochrome P450 reductase
CTA, CYP tilt angle
CYP, cytochrome P450
dCM, CYP center-of-mass distance from the membrane
DOPC, 1,2-dioleoyl-*sn*-glycero-3-phosphocholine
DOPE, 1,2-dioleoyl-*sn*-glycero-3-phosphoethanolamine
DOPG, 1,2-dioleoyl-*sn*-glycero-3-[phospho-*rac*-(3-lysyl(1-glycerol))]
DOPS, 1,2-dioleoyl-*sn*-glycero-3-phosphoserine
DOPx, phospho-(choline, ethanolamine, glycerol, serine)
HTA, heme tilt angle
MD, molecular dynamics
POPC, 1-palmitoyl-2-oleoyl-*sn*-glycero-3-phosphocholine
PC, phosphocholine
PA, phosphatidyl acid
PE, phosphoethanolamine
PS, phosphoserine

REFERENCES

(1) de Montellano, P. R. O. *Cytochrome P450: Structure, Mechanism, and Biochemistry*, 3rd ed.; Ortiz de Montellano, P. R., Ed.; Kluwer Academic/Plenum Publishers: New York, 2005.
(2) Anzenbacher, P.; Anzenbacherová, E. Cytochromes P450 and Metabolism of Xenobiotics. *Cell. Mol. Life Sci.* **2001**, *58*, 737−747.
(3) Shaik, S.; Kumar, D.; de Visser, S. P.; Altun, A.; Thiel, W. Theoretical Perspective on the Structure and Mechanism of Cytochrome P450 Enzymes. *Chem. Rev.* **2005**, *105*, 2279−2328.
(4) Cojocaru, V.; Winn, P. J.; Wade, R. C. The Ins and Outs of Cytochrome P450s. *Biochim. Biophys. Acta, Gen. Subj.* **2007**, *1770*, 390−401.
(5) Sgrignani, J.; Magistrato, A. Influence of the Membrane Lipophilic Environment on the Structure and on the Substrate Access/Egress Routes of the Human Aromatase Enzyme. A Computational Study. *J. Chem. Inf. Model.* **2012**, *52*, 1595−1606.
(6) Cojocaru, V.; Balali-Mood, K.; Sansom, M. S. P.; Wade, R. C. Structure and Dynamics of the Membrane-Bound Cytochrome P450 2C9. *PLoS Comput. Biol.* **2011**, *7*, e1002152.
(7) Berka, K.; Hendrychová, T.; Anzenbacher, P.; Otyepka, M. Membrane Position of Ibuprofen Agrees with Suggested Access Path Entrance to Cytochrome P450 2C9 Active Site. *J. Phys. Chem. A* **2011**, *115*, 11248−11255.
(8) Denisov, I. G.; Shih, A. Y.; Sligar, S. G. Structural Differences between Soluble and Membrane Bound Cytochrome P450s. *J. Inorg. Biochem.* **2012**, *108*, 150−158.
(9) Johnson, E. F.; Stout, C. D. Structural Diversity of Eukaryotic Membrane Cytochrome P450s. *J. Biol. Chem.* **2013**, *288*, 17082−17092.
(10) Berka, K.; Paloncýová, M.; Anzenbacher, P.; Otyepka, M. Behavior of Human Cytochromes P450 on Lipid Membranes. *J. Phys. Chem. B* **2013**, *117*, 11556−11564.
(11) Bayburt, T. H.; Sligar, S. G. Single-molecule Height Measurements on Microsomal Cytochrome P450 in Nanometer-Scale Phospholipid Bilayer Disks. *Proc. Natl. Acad. Sci. U. S. A.* **2002**, *99*, 6725−6730.
(12) Nussio, M. R.; Voelcker, N. H.; Miners, J. O.; Lewis, B. C.; Sykes, M. J.; Shapter, J. G. AFM Study of the Interaction of Cytochrome P450 2C9 with Phospholipid Bilayers. *Chem. Phys. Lipids* **2010**, *163*, 182−189.
(13) Ozalp, C.; Szczesna-Skorupa, E.; Kemper, B. Identification of Membrane-Contacting Loops of the Catalytic Domain of Cytochrome P450 2C2 by Tryptophan Fluorescence Scanning. *Biochemistry* **2006**, *45*, 4629−37.
(14) Black, S. S. Membrane Topology of the Mammalian P450 Cytochromes. *FASEB J.* **1992**, *6*, 680−685.
(15) Von Wachenfeldt, C.; Johnson, E. F. Structures of Eukaryotic Cytochrome P450 Enzymes. In *Cytochrome P450*; de Montellano, P. R. O., Ed.; Springer US: Boston, MA, 1995; pp 183−223.
(16) Yamamoto, K.; Dürr, U. H. N.; Xu, J.; Im, S.-C.; Waskell, L.; Ramamoorthy, A. Dynamic Interaction Between Membrane-Bound Full-Length Cytochrome P450 and Cytochrome b5 Observed by Solid-State NMR Spectroscopy. *Sci. Rep.* **2013**, *3*, 2538.

(17) Monk, B. C.; Tomasiak, T. M.; Keniya, M. V.; Huschmann, F. U.; Tyndall, J. D. A.; O'Connell, J. D.; Cannon, R. D.; McDonald, J. G.; Rodriguez, A.; Finer-Moore, J. S.; et al. Architecture of a Single Membrane Spanning Cytochrome P450 Suggests Constraints That Orient the Catalytic Domain Relative to a Bilayer. *Proc. Natl. Acad. Sci. U. S. A.* **2014**, *111*, 3865−3870.
(18) Sagatova, A. A.; Keniya, M. V.; Wilson, R. K.; Monk, B. C.; Tyndall, J. D. A. Structural Insights into Binding of the Antifungal Drug Fluconazole to Saccharomyces Cerevisiae Lanosterol 14α-Demethylase. *Antimicrob. Agents Chemother.* **2015**, *59*, 4982−4989.
(19) Reed, J. R.; Backes, W. L. Formation of P450·P450 Complexes and Their Effect on P450 Function. *Pharmacol. Ther.* **2012**, *133*, 299−310.
(20) Park, J. W.; Reed, J. R.; Brignac-Huber, L. M.; Backes, W. L. Cytochrome P450 System Proteins Reside in Different Regions of the Endoplasmic Reticulum. *Biochem. J.* **2014**, *464*, 241−249.
(21) Park, J. W.; Reed, J. R.; Backes, W. L. The Localization of Cytochrome P450s CYP1A1 and CYP1A2 into Different Lipid Microdomains Is Governed by Their N-terminal and Internal Protein Regions. *J. Biol. Chem.* **2015**, *290*, 29449−29460.
(22) Brignac-Huber, L. M.; Reed, J. R.; Eyer, M. K.; Backes, W. L. Relationship Between CYP1A2 Localization and Lipid Microdomain Formation as a Function of Lipid Composition. *Drug Metab. Dispos.* **2013**, *41*, 1896−1905.
(23) Berman, H.; Henrick, K.; Nakamura, H.; Markley, J. L. The Worldwide Protein Data Bank (wwPDB): Ensuring a Single, Uniform Archive of PDB Data. *Nucleic Acids Res.* **2007**, *35*, D301−D303.
(24) Brignac-Huber, L.; Reed, J. R.; Backes, W. L. Organization of NADPH-Cytochrome P450 Reductase and CYP1A2 in the Endoplasmic Reticulum—Microdomain Localization Affects Monooxygenase Function. *Mol. Pharmacol.* **2011**, *79*, 549−557.
(25) Scott, E. E.; Wolf, C. R.; Otyepka, M.; Humphreys, S. C.; Reed, J. R.; Henderson, C. J.; McLaughlin, L. A.; Paloncyova, M.; Navratilova, V.; Berka, K.; et al. The Role of Protein-Protein and Protein-Membrane Interactions on P450 Function. *Drug Metab. Dispos.* **2016**, *44*, 576−590.
(26) Navrátilová, V.; Paloncýová, M.; Kajšová, M.; Berka, K.; Otyepka, M. Effect of Cholesterol on the Structure of Membrane-Attached Cytochrome P450 3A4. *J. Chem. Inf. Model.* **2015**, *55*, 628−635.
(27) Shinkyo, R.; Guengerich, F. P. Inhibition of Human Cytochrome P450 3A4 by Cholesterol. *J. Biol. Chem.* **2011**, *286*, 18426−18433.
(28) Ingelman-Sundberg, M.; Haaparanta, T.; Rydström, J. Membrane Charge as Effector of Cytochrome P-450LM2 Catalyzed Reactions in Reconstituted Liposomes. *Biochemistry* **1981**, *20*, 4100−4106.
(29) Ahn, T.; Yun, C. H.; Oh, D. B. Involvement of Nonlamellar-Prone Lipids in the Stability Increase of Human Cytochrome P450 1A2 in Reconstituted Membranes. *Biochemistry* **2005**, *44*, 9188−9196.
(30) Ahn, T.; Guengerich, F. P.; Yun, C.-H. Membrane Insertion of Cytochrome P450 1A2 Promoted by Anionic Phospholipids. *Biochemistry* **1998**, *37*, 12860−12866.
(31) Ingelman-Sundberg, M.; Hagbjork, A. L.; Ueng, Y. F.; Yamazaki, H.; Guengerich, F. P. High Rates of Substrate Hydroxylation by Human Cytochrome P450 3A4 in Reconstituted Membranous Vesicles: Influence of Membrane Charge. *Biochem. Biophys. Res. Commun.* **1996**, *221*, 318−322.
(32) Kim, K.-H.; Ahn, T.; Yun, C.-H. Membrane Properties Induced by Anionic Phospholipids and Phosphatidylethanolamine are Critical for the Membrane Binding and Catalytic Activity of Human Cytochrome P450 3A4. *Biochemistry* **2003**, *42*, 15377−15387.
(33) Macdonald, P. M.; Seelig, J. Anion Binding to Neutral and Positively Charged Lipid Membranes. *Biochemistry* **1988**, *27*, 6769−6775.
(34) Laursen, T.; Jensen, K.; Møller, B. L. Conformational Changes of the NADPH-Dependent Cytochrome P450 Reductase in the Course of Electron Transfer to Cytochromes P450. *Biochim. Biophys. Acta, Proteins Proteomics* **2011**, *1814*, 132−138.
(35) Jämbeck, J. P. M.; Lyubartsev, A. P. Another Piece of the Membrane Puzzle: Extending Slipids Further. *J. Chem. Theory Comput.* **2013**, *9*, 774−784.
(36) Mahoney, M. W.; Jorgensen, W. L. A Five-Site Model for Liquid Water and the Reproduction of the Density Anomaly by Rigid, Nonpolarizable Potential Functions. *J. Chem. Phys.* **2000**, *112*, 8910.
(37) Paloncýová, M.; Navrátilová, V.; Berka, K.; Laio, A.; Otyepka, M. Role of Enzyme Flexibility in Ligand Access and Egress to Active Site: Bias-Exchange Metadynamics Study of 1,3,7-Trimethyluric Acid in Cytochrome P450 3A4. *J. Chem. Theory Comput.* **2016**, *12*, 2101−2109.
(38) Wolf, M. G.; Hoefling, M.; Aponte-Santamaría, C.; Grubmüller, H.; Groenhof, G. g_membed: Efficient Insertion of a Membrane Protein into an Equilibrated Lipid Bilayer with Minimal Perturbation. *J. Comput. Chem.* **2010**, *31*, 2169−2174.
(39) Van Der Spoel, D.; Lindahl, E.; Hess, B.; Groenhof, G.; Mark, A. E.; Berendsen, H. J. C. GROMACS: Fast, flexible, and free. *J. Comput. Chem.* **2005**, *26*, 1701−1718.
(40) Hornak, V.; Abel, R.; Okur, A.; Strockbine, B.; Roitberg, A.; Simmerling, C. Comparison of Multiple Amber Force Fields and Development of Improved Protein Backbone Parameters. *Proteins: Struct., Funct., Genet.* **2006**, *65*, 712−725.
(41) Shahrokh, K.; Orendt, A.; Yost, G. S.; Cheatham, T. E., III. Quantum Mechanically Derived AMBER-Compatible Heme Parameters for Various States of the Cytochrome P450 Catalytic Cycle. *J. Comput. Chem.* **2012**, *33*, 119−133.
(42) Åqvist, J. Ion-Water Interaction Potentials Derived from Free Energy Perturbation Simulations. *J. Phys. Chem.* **1990**, *94*, 8021−8024.
(43) Applequist, J.; Carl, J. R.; Fung, K. An Atom Dipole Interaction Model for Molecular Polarizability. Application to Polyatomic Molecules and Determination. *J. Am. Chem. Soc.* **1972**, *94*, 2952−2960.
(44) Hess, B.; Bekker, H.; Berendsen, H. J. C.; Fraaije, J. G. E. M. LINCS: A Linear Constraint Solver for Molecular Simulations. *J. Comput. Chem.* **1997**, *18*, 1463−1472.
(45) Berendsen, H. J. C.; Postma, J. P. M.; van Gunsteren, W. F.; DiNola, A.; Haak, J. R. Molecular Dynamics with Coupling to an External Bath. *J. Chem. Phys.* **1984**, *81*, 3684−3690.
(46) Nosé, S. A Unified Formulation of the Constant Temperature Molecular Dynamics Methods. *J. Chem. Phys.* **1984**, *81*, 511.
(47) Hoover, W. G. Canonical Dynamics: Equilibrium Phase-Space Distributions. *Phys. Rev. A: At., Mol., Opt. Phys.* **1985**, *31*, 1695−1697.
(48) Parrinello, M.; Rahman, A. Polymorphic Transitions in Single Crystals: A New Molecular Dynamics Method. *J. Appl. Phys.* **1981**, *52*, 7182−7190.
(49) Darden, T.; York, D.; Pedersen, L. Particle Mesh Ewald: An N.log(N) Method for Ewald Sums in Large Systems. *J. Chem. Phys.* **1993**, *98*, 10089.
(50) Kucerka, N.; Nagle, J. F.; Sachs, J. N.; Feller, S. E.; Pencer, J.; Jackson, A.; Katsaras, J. Lipid Bilayer Structure Determined by the Simultaneous Analysis of Neutron and X-ray Scattering Data. *Biophys. J.* **2008**, *95*, 2356−67.
(51) Tristram-Nagle, S.; Nagle, J. F. Lipid bilayers: Thermodynamics, Structure, Fluctuations, and Interactions. *Chem. Phys. Lipids* **2004**, *127*, 3−14.
(52) Petrache, H. I.; Tristram-Nagle, S.; Gawrisch, K.; Harries, D.; Parsegian, V. A.; Nagle, J. F. Structure and Fluctuations of Charged Phosphatidylserine Bilayers in the Absence of Salt. *Biophys. J.* **2004**, *86*, 1574−1586.
(53) Baylon, J. L.; Lenov, I. L.; Sligar, S. G.; Tajkhorshid, E. Characterizing the Membrane-Bound State of Cytochrome P450 3A4: Structure, Depth of Insertion, and Orientation. *J. Am. Chem. Soc.* **2013**, *135*, 8542−8551.
(54) Strandberg, E.; Tiltak, D.; Ehni, S.; Wadhwani, P.; Ulrich, A. S. Lipid Shape is a Key Factor for Membrane Interactions of Amphipathic Helical Peptides. *Biochim. Biophys. Acta, Biomembr.* **2012**, *1818*, 1764−76.
(55) Otyepka, M.; Skopalík, J.; Anzenbacherová, E.; Anzenbacher, P. What Common Structural Features and Variations of Mammalian

DOI: 10.1021/acs.jpcb.6b10108
J. Phys. Chem. B 2016, 120, 11205−11213

P450s are Known to Date? *Biochim. Biophys. Acta, Gen. Subj.* **2007**, *1770*, 376−389.
(56) Freddolino, P. L.; Liu, F.; Gruebele, M.; Schulten, K. Ten-Microsecond Molecular Dynamics Simulation of a Fast-Folding WW domain. *Biophys. J.* **2008**, *94*, L75−L77.
(57) Clarke, T. A.; Im, S. C.; Bidwai, A.; Waskell, L. The Role of the Length and Sequence of the Linker Domain of Cytochrome b5 in Stimulating Cytochrome P450 2B4 Catalysis. *J. Biol. Chem.* **2004**, *279*, 36809−36818.
(58) Bridges, A.; Gruenke, L.; Chang, Y.-T.; Vakser, I. A.; Loew, G.; Waskell, L. Identification of the Binding Site on Cytochrome P450 2B4 for Cytochrome b5 and Cytochrome P450 Reductase. *J. Biol. Chem.* **1998**, *273*, 17036−17049.
(59) Himeno, H.; Shimokawa, N.; Komura, S.; Andelman, D.; Hamada, T.; Takagi, M. Charge-Induced Phase Separation in Lipid Membranes. *Soft Matter* **2014**, *10*, 7959−7967.
(60) Ahn, T.; Kim, M.; Yun, C.; Chae, H. Functional Regulation of Hepatic Cytochrome P450 Enzymes by Physicochemical Properties of Phospholipids in Biological Membranes. *Curr. Protein Pept. Sci.* **2007**, *8*, 496−505.

DOI: 10.1021/acs.jpcb.6b10108
J. Phys. Chem. B 2016, 120, 11205−11213

JCTC Journal of Chemical Theory and Computation

Article

pubs.acs.org/JCTC

Role of Enzyme Flexibility in Ligand Access and Egress to Active Site: Bias-Exchange Metadynamics Study of 1,3,7-Trimethyluric Acid in Cytochrome P450 3A4

Markéta Paloncýová,[†,#] Veronika Navrátilová,[†,#] Karel Berka,[#] Alessandro Laio,[*,∥] and Michal Otyepka[*,#]

[#]Regional Centre of Advanced Technologies and Materials, Department of Physical Chemistry, Faculty of Science, Palacký University Olomouc, tř. 17 Listopadu 12, 771 46 Olomouc, Czech Republic

[∥]SISSA - Scuola Internazionale Superiore di Studi Avanzati, via Bonomea 265, 34136 Trieste, Italy

Supporting Information

ABSTRACT: Although the majority of enzymes have buried active sites, very little is known about the energetics and mechanisms associated with substrate and product channeling in and out. Gaining direct information about these processes is a challenging task both for experimental and theoretical techniques. Here, we present a methodology that enables following of a ligand during its passage to the active site of cytochrome P450 (CYP) 3A4 and mapping of the free energy associated with this process. The technique is based on a combination of a bioinformatics tool for identifying access channels and bias-exchange metadynamics and provides converged free energies in good agreement with experimental data. In addition, it identifies the energetically preferred escape routes, limiting steps, and amino acids residues lining the channel. The approach was applied to mapping of a complex channel network in a complex environment, i.e., CYP3A4 attached to a lipid bilayer mimicking an endoplasmic reticulum membrane. The results provided direct information about the energetics and conformational changes associated with the ligand channeling. The methodology can easily be adapted to study channeling through other flexible biomacromolecular channels.

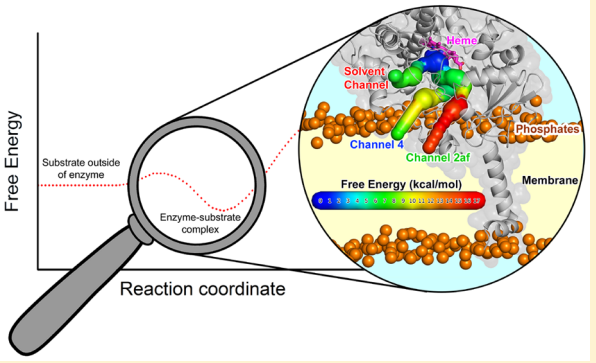

INTRODUCTION

Enzyme catalyzed biotransformation processes take place in active sites,[1−3] which are usually either localized in surface pockets or buried within the protein, as shown for more than 60% of annotated enzymes.[4] Hence, substrates and products (henceforth referred to as ligands) must typically access the enzyme's active site through access channels (ACs),[5] which connect the site with the surrounding environment.[6] The amino acids lining such channels contribute to the substrate specificity and enzyme efficiency[7−9] because they determine the channel geometry, physical-chemical properties, and flexibility. Thus, identification of ACs and AC lining amino acids is important for understanding the enzyme substrate specificity, which in turn can be used for the rational design of biocatalysts in biotechnology and sensing applications.[9,10] In addition ACs may behave as uniform pathways which connect the buried active site with the protein surface or form a complex channel network where the channels may either merge into the others or branch.[11] This can hinder the ACs description. Nonetheless, the identification of ACs and AC lining amino acids and evaluation of their behavior and role in ligand permeation are challenging tasks for both experimental techniques and theoretical tools.

Unfortunately, traditional structural methods, i.e., single crystal X-ray diffraction and NMR spectrometry, do not provide a sufficient picture of the ligand passage. X-ray diffraction provides mostly a static view of the enzyme and its ACs from either analysis of enzyme structures by dedicated software tools (e.g., MOLE 2.0,[12] CAVER 3.0,[13] and MolAxis,[14] to name a few) or comparison of enzyme structures with and without bound ligands.[15,16] However, NMR techniques can reveal information on multiple time-scales about the conformational enzyme dynamics,[17] e.g., product release during an isomerization reaction.[18] Yet another view is provided by single molecule fluorescence spectroscopy, which can be used to describe the structural dynamics and fluctuations of enzymes at molecular resolution.[19,20] Fluorescence spectroscopy has also successfully been applied in studies of catalytic properties of enzymes with buried active sites.[21,22] Apart from spectroscopy methods, the role of specific amino acids in the ACs or active site on the activity of enzymes can be evaluated by mutational studies.[23−27] However, such experimental techniques have so far provided only limited details of the mechanism of ligand

Received: January 21, 2016
Published: March 11, 2016

ACS Publications © 2016 American Chemical Society

DOI: 10.1021/acs.jctc.6b00075
J. Chem. Theory Comput. 2016, 12, 2101−2109

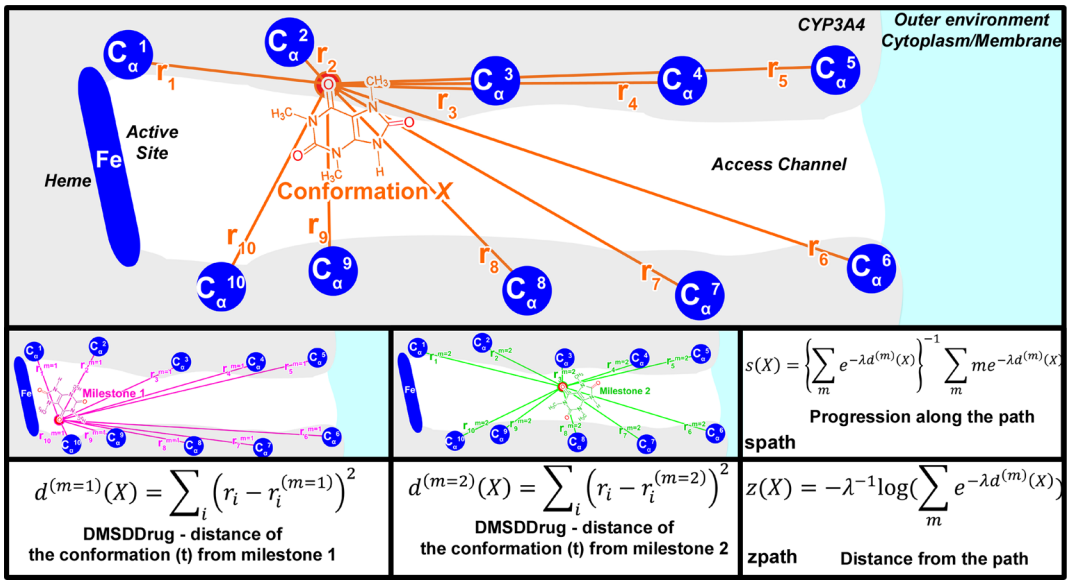

Figure 1. Schematic representation of 1,3,7-trimethyluric acid (TMU) passage through one of the CYP3A4 enzyme channels. The path through the channel (spath) was defined by several milestones—reference structures equally distributed in the chosen space. The metric defining the milestones was the drug distance mean square deviation (DMSDDrug) (one of the pair of atoms used for DMSDDrug enumeration was a TMU heavy atom (red), the other was the C_α atom of the channel lining residues or heme atoms (blue), for clarity we only show contacts to one oxygen atom of the ligand). The value of spath determines the position along the path (for conformation in time t (orange) in the figure spath ∼1.5—between milestones 1 and 2). The value of zpath determines the distance from the path.

passage through ACs and degree of adaptive conformation changes of ACs associated with ligand passage.

The identification and characterization of ACs and lining amino acids by theoretical methods are also a nontrivial task as channels may dynamically open/close in response to water or ligand passage and enzyme breathing motions.[28−30] Random acceleration (originally termed expulsion) molecular dynamics (RAMD)[31] and steered molecular dynamics (SMD)[11,32,33] are two techniques developed to identify potential ACs.[34,35] These techniques are derived from classical molecular dynamics (MD) and use an additional force to pull the ligand molecule through the channel. They can suggest the mechanism of ligand passage and assess free energies of ligand binding ΔG^{bind} and the transition state $\Delta G^{\#}$, which are related to the experimentally observed Michaelis constant and rate constant of ligand binding and unbinding, respectively. However, it should be noted, that the latter methods tend to overestimate the free energies associated with ligand passage[33,36−38] as they do not sample the configurational space effectively. A recently published approach, based on Hamiltonian replica exchange molecular dynamics (HREMD), allows studying the process of pulling the ligand from the active site or binding the ligand to the protein cavity obtaining results in the good agreement with experiments.[39,40] Its use with a newly defined variable−distance field distance−allowed studying binding of aspirin to a shallow active pocket in PLA_2 enzyme without the exact prior definition of the path.[41] Nevertheless, to our best knowledge, these methods were never applied to systems with a complex network of malleable ACs, such as those identified in cytochrome P450 (CYP) enzymes: the passage from one state to another in such complicated systems can depend on several collective variables and sampling of such a multidimensional space is not possible by simply pulling the ligand out of the active site. In recent years, metadynamics with a well chosen set of collective variables has been shown to allow sampling the configurational space of complex systems and provide converged free energies.[47,48] This approach was introduced in 2002, building on ideas from other free energy methods, such as the Wang−Landau algorithm[42] and adaptive force bias,[43] and conformational search methods such as Tabu search,[46] conformational flooding,[45] and local elevation.[44] However, metadynamics has not yet been applied to such highly flexible systems as CYPs. Overall, an efficient and robust method capable of providing information about the passage of ligands through multiple flexible channels has not been described yet.

Human cytochrome P450 (CYP) enzymes are membrane anchored proteins that catalyze biotransformation processes of many endogenous and exogenous compounds.[49] They are important targets of pharmacological studies, being responsible for transformations of more than 60% of marketed drugs[50,51] and many drug−drug interactions.[52] CYP active sites are deeply buried in compact catalytic domains[53−55] and are connected to the outside via a complex network of flexible ACs.[34,56] The CYP3A4 isoform is a prominent member of the CYP family[15] owing to its promiscuity and relevance in drug metabolism.[50,57] Despite its importance, CYP3A4 represents a challenge for molecular dynamics simulations (MD): the catalytic cycle involving the heme cofactor is complex[58] and the enzyme is flexible and most frequently anchored to an endoplasmic reticulum membrane. MD simulations of membrane attached CYP3A4 have been published very recently[59,60] mostly thanks to advances in force field development and membrane simulations. The above-mentioned features make CYP3A4 a highly challenging but ideal touchstone of theoretical methods for the identification of ACs, their lining amino acids and free energy changes accompanying ligand passage through flexible ACs.

Here, we present a synergy of the standard structure-based approach for identifying ACs (MOLE) and bias-exchange metadynamics (BE-META) to study the mechanism of ligand passage through the malleable ACs of CYP3A4. As the ligand we used one of the CYP3A4 caffeine metabolites,

DOI: 10.1021/acs.jctc.6b00075
J. Chem. Theory Comput. 2016, 12, 2101−2109

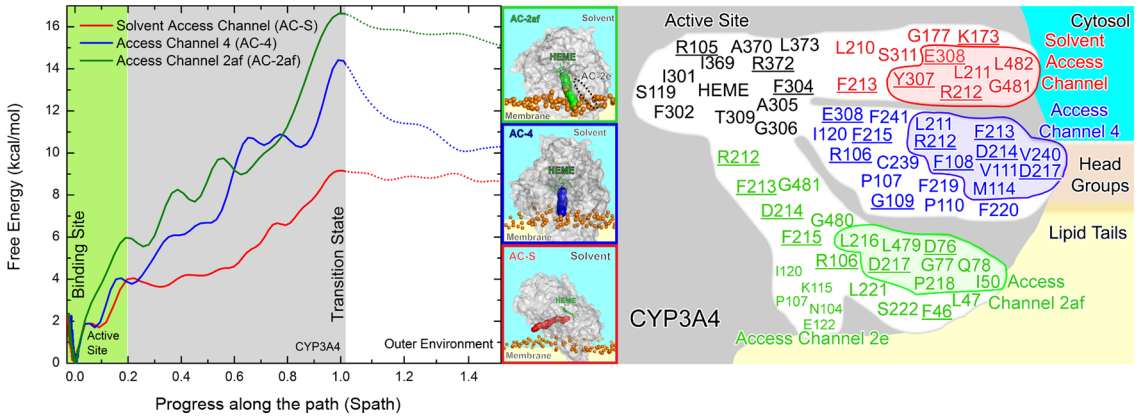

Figure 2. Free energy profiles (left panel) of TMU passage via three ACs of CYP3A4 embedded in a DOPC lipid bilayer (middle panel). CYP3A4 is shown as a gray surface, heme as green sticks, and DOPC phosphates as orange balls. Initially identified AC-2e is shown in black dots. The schematic in the right panel shows the depth of the channel entrances in the membrane and the channel lining amino acids residues. Bulky channel lining residues are underlined, whereas transition state residues within 4 Å of TMU are depicted in the bordered regions.

1,3,7-trimethyluric acid (TMU). For this purpose, we developed a new metric describing the movement of a ligand along a highly flexible AC, named *DMSDDrug* (Figure 1). Using *DMSDDrug* together with a set of other collective variables (CVs), we obtained converged free energy profiles along three independent ACs valid for both access and egress of a ligand. Using these profiles, we identified the preferred AC, transition states for all three ACs and lining and gate-keeping amino acids, whose mutations may alter enzyme function. We observed adaptive conformational changes of CYP3A4 during ligand passage and demonstrated that the flexibility and adaptability of ACs are crucial for ligand passage. The knowledge gained into the ligand passage mechanism represents a key step forward for rational enzyme design, and the presented technique could be easily adapted to analyze other enzymes.

METHODS

We prepared the model of CYP3A4 using the X-ray structure 1TQN according to the procedure described elsewhere[60] (see also the Supporting Information). We then inserted CYP3A4 into a pre-equilibrated 1,2-dioleoyl-*sn*-glycero-3-phosphocholine (DOPC) bilayer and performed 100 ns of unbiased MD simulation with GROMACS 4.5.5.[61] Using the MD trajectory, we identified potential access channels by MOLE 2.0.[12] Among the 7 channels found by this algorithm (see Table S1), we selected three channels that were open (bottleneck radius larger than 1 Å) in total for more than 1 ns during the whole MD run. The channels satisfying this criterion are depicted in Figure 2: the channel depicted in black (AC-2e) joins the enzymatic cavity with the hydrophobic core of the membrane; the one depicted in blue (AC-4) ends in the headgroup region of the phospholipids; and finally, the one depicted in red ends in the cytoplasm.

We then performed MD simulations for a total of approximately 6 μs and computed the free energy associated with the passage of 1,3,7-trimethyluric acid (TMU, Figure S1) through the three channels using bias-exchange metadynamics (BE-META).[62] This technique is based on running in parallel a large number of metadynamics,[48] each biasing a different collective variable (CV). Exchanges between the replicas are attempted at regular time intervals according to a replica-exchange scheme. As a consequence of the exchanges, this procedure enhances the convergence of the free energy estimates on each replica and allows multidimensional free energy landscapes associated with complex biochemical processes to be computed, e.g., protein folding.[63]

In BE-META simulations, choosing the correct CVs is crucial for reaching convergence. BE-META has already been applied for studying the translocation of a ligand through a channel.[64] Building on this work, we introduced a metric (named *DMSDDrug*) specifically tailored for studying the translocation of ligands through very flexible and faintly defined channels. The metric was used for enumeration of the path collective variable introduced in ref 65. In ref 64 it was shown that in some cases the distance CV does not allow reaching convergence, and only by using a suitably defined spath variable it is possible to reconstruct a meaningful free energy landscape.[64] Progression along the channel was defined by 5−10 *milestones*, in which the ligand was placed in a regularly spaced sequence of configurations between the enzymatic cavity and mouth of the channel. These milestones were generated by docking the ligand in the channel identified by MOLE 2.0[12] by AutoDock Vina[66] (see the Supporting Information). To estimate the value of *DMSDDrug* on configuration X, the distance between X and milestone m was computed as follows

$$d^{(m)}(X) = \frac{1}{N_{\text{ligand}} N_{\text{channel}}} \sum_{i=1}^{N_{\text{ligand}}} \sum_{j=1}^{N_{\text{channel}}} (r_{ij} - r_{ij}^{(m)})^2$$

where r_{ij} and $r_{ij}^{(m)}$ are the distance between atom i and j in configuration X and the configuration of milestone m, respectively. The sums on i and j run from 1 to N_{ligand} atoms belonging to the ligand and N_{channel} atoms belonging to the channel wall, respectively (see Figure 1). This is the main difference to the *DMSD* metric detailed in ref 65, for which both sums run over the same set of atoms. This modification was crucial for using a *spath* variable for the process studied in this work because in the original formulation, the value of $d^{(m)}$ was dominated by fluctuations in the distance between the atoms of the channel wall, making its value a noisy measure of the position of the ligand. Following ref 65, we then defined the channel *spath* collective variable as follows

DOI: 10.1021/acs.jctc.6b00075
J. Chem. Theory Comput. 2016, 12, 2101−2109

$$s(X) = \frac{\sum_m m e^{-\lambda d^{(m)}(X)}}{\sum_m e^{-\lambda d^{(m)}(X)}}$$

The set of CVs used for the three BE-META simulations of the three channels included the *spath* variable defined above (CV1) and seven other variables aimed at describing the orientation of the ligand, the size of the channel and chemical nature of the interaction of the ligand with the channel walls: CV2 and CV3 covered the number of hydrophobic and hydrophilic contacts between the ligand and channel, CV4 and CV5 described the orientation of the ligand with respect to the channel axis, CV6 was the radius of gyration (R_g) of the channel mouth/s, CV7 was the distance from the heme, and CV8 was the *zpath* variable defined according to ref 65 (see the Supporting Information and Table S2 for exact definition and Figure S2). For increasing the sampling in channel AC-2af and its R_g (see later) we performed another 130 ns BE-META simulation with 5 replicas − AC-2e spath and zpath, distance from the heme, R_g of AC-2af, and contacts with AC-2e. The sampling and convergence is discussed in the Supporting Information (see Figures S10−S15).

RESULTS AND DISCUSSION

We studied the thermodynamics of TMU permeation through membrane-attached CYP3A4 via its access channels. Based on MOLE 2.0 analysis of an unbiased simulation (Table S1), we chose channels AC-S, AC-2e, and AC-4 for further study. We then defined a set of eight collective variables (CV1−CV8) for BE-META calculations as using multiple CVs in BE-META simulations was shown to increase the convergence rate.[62] Since we aimed at monitoring the translocation of TMU through different channels, the simple distance from the heme was insufficient for this purpose. Therefore, and owing to the flexibility of the channels, we employed the new *DMSDDrug* metric for *spath* CV, which allowed distinguishing the motion of a ligand and motion of the channel (see Methods). For each channel, we performed ∼2 μs of BE-META simulations. By a detailed analysis of the trajectories of the individual replicas we observed that for some of them (especially those biased on the orientation of TMU with respect to the channel direction) the sampling was produced almost entirely with the TMU in the active site and therefore we discarded these replicas from further analysis (Figures S12−14). In other words, these CVs (two orientation CV replicas, hydrophobic contacts replica and hydrophilic contacts replica in AC-2af) contribute to the final free energy results only by enhancing the convergence of the other replicas (for example by generating configurations with the TMU in different orientations). The zpath CV was introduced in order to control the distance from the predefined path. In the case of AC-S, a soft potential wall on this variable was introduced in order to keep a drug within the channel for an initial part of the simulation; however, finally this appeared to be useful only in the case of very disfavored channels. In principle, we would recommend keeping as many CV replicas as possible, because it leads to convergent BE-META simulations of a rather complex system and enabled enough flexibility for similar simulations; however, in the case of need the discarded replicas could be under consideration and the CVs can be mapped afterward. During the analysis, we noticed that in the simulation of TMU transport through AC-2e, the ligand preferred to permeate through the nearby channel AC-2af. Therefore, we interpreted the results of this simulation as for AC-2af.

In Figure 2, free energy profiles are plotted as a function of the *spath* variable, which describes the progress of TMU along the channels. All the free energy profiles showed a minimum in the active site. For all three cases after this minimum, we observed a low barrier of 4−6 kcal/mol related to the unbinding of TMU from the active site. After this barrier, the free energy progressively increased up to the transition state, which was localized just below the CYP3A4 surface in all three cases, with barriers of 10.2 ± 0.6 kcal/mol for AC-S, 14.5 ± 0.9 for AC-4, and 16.5 ± 0.9 for AC-2af. This shows that TMU is released preferentially through the AC-S channel. The computational setup did not allow computing the binding free energy ΔG^{bind}. Indeed, the milestones used in *spath* only properly describe the translocation through the channels, though some milestones were located also outside of the channels (dotted line in Figure 2). However, by using the milestones we cannot take into account the entropy gain deriving from releasing the confinement effect of the channel. Thus, to compute ΔG^{bind}, one should perform another free energy calculation with different collective variables aimed at describing the detachment of the ligand from the transition state at the channel mouth, add a correction to the entropic gain (e.g., using the method described in ref 67), or perform alchemical free energy calculation. For amphiphilic molecules, the free energy of the transition state of AC-S provides an upper bound for ΔG^{bind}. The ΔG^{bind} calculated by the alchemical simulation (see the Supporting Information) was −10.4 ± 2.5 kcal/mol, which is in good agreement with ΔG of the transition state.

Apart from BE-META, we also computed the free energy profile associated with the translocation of TMU through a DOPC membrane by COSMOmic[68] (see Figure S3). The state in which TMU was solvated in water was favored by ∼6 kcal/mol with respect to the membrane core, consistent with the difference between the free energy barriers for the AC-S and the AC-2af channels connecting the active site with the cytoplasm and membrane interior. This indicates that the pathway toward the hydrophobic tail region is strongly disfavored for this ligand. Interestingly, COSMOmic also predicted that TMU can localize close to the headgroup region (notice the minimum at z = 1.5 nm in Figure S3). Remarkably, the barrier for channel AC-4 directing TMU to the region below the head groups was significantly higher than for the channel leading to the solvent; however, the free energy profiles after the transition states (outside of protein) suggest a small free energy decrease as TMU samples both solvent and headgroup region. Our calculations also unambiguously demonstrate that two of the channels (AC-S and AC-2af) of CYP3A4 are remarkably flexible and change their conformations in response to the passage of TMU.

In Figure 3, we plot the free energy for each channel as a function of the mouth opening (henceforth mouth) radius R_m and the *spath* variable. R_m represents the maximal radius of a sphere docked to the mouth opening at the end point of the channel starting from the active site and leading to the respective mouth as calculated by MOLE 2.5[12] software with a probe radius 5.0 Å. End points of channels were defined by the same amino acids as those used for the definition of R_g (Figure 3, Figure S6). We observed small changes in R_m during TMU permeation through AC-4, indicating that this specific channel is rather rigid, at least in the mouth region. The mouth of

DOI: 10.1021/acs.jctc.6b00075
J. Chem. Theory Comput. 2016, 12, 2101−2109

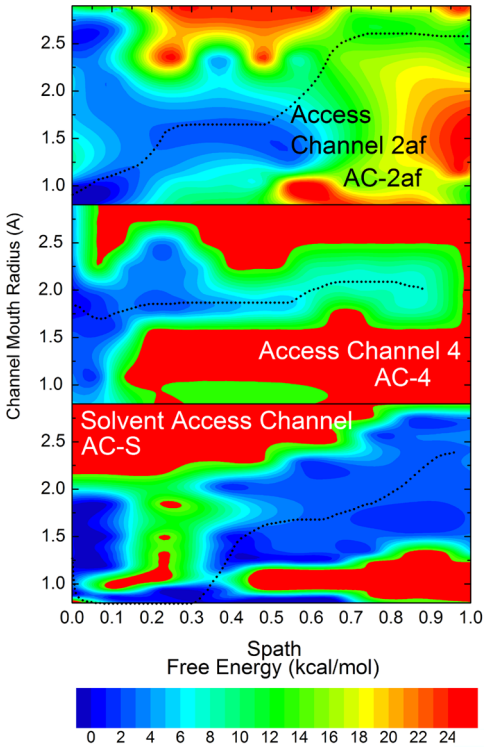

Figure 3. Free energy as a function of the mouth radius and spath variable. Red regions did not have sufficient sampling for reliable calculation of the free energy. The dashed line represents the approximate path followed by the ligand.

AC-2af was rather in a closed state when TMU was in the active site with $R_m \sim 0.9$ Å, but TMU permeation opened the channel mouth to $R_m \sim 2.5$ Å. It should be remarked that the initially studied channel AC-2e did not open sufficiently for TMU permeation. Indeed, the one-dimensional free energy profile of R_g of channel AC-2e showed a high free energy barrier for its opening (see Figure S4). Interestingly, both AC-4 and AC-2e lead through CYP3A4 F/G or B/C loops with defined backbone lengths, and the adjustment of these loops to the presence of ligand is rather limited. The AC-S channel was very flexible and gradually adjusted its geometry in response to the ligand passage. When TMU was in the active site, the channel was either closed ($R_m \sim 0.9$ Å) or moderately open ($R_m \sim 1.7$ Å), as indicated also by the one-dimensional free energy profile (see Figures S4, S5, and Figure 3). As soon as the ligand left the active site, the channel stayed closed ($R_m \sim 0.9$ Å). Finally, at the transition state, the channel opened completely, and R_m reached 2.5 Å. In a free unbiased simulation with TMU in the active site, the channel remained closed ($R_m \sim 0.85$ Å) for the whole simulation (500 ns, Figure S7), indicating that the open state is separated from the closed state by a significant free energy barrier associated with a variable not directly related to R_g and therefore not visible in the free energy projections of Figures 3 and S4. The results clearly indicate that biased MD simulations directly addressing passage of a ligand may identify different preferred access channels than analyses based on classical MD simulations or X-ray structures. This is demonstrated by the fact that in the free simulations, channel AC-S appeared to open very rarely, whereas with BE-META, it was the most favorable channel. In other words, the enzyme access channels are malleable,[55,69−72] reflecting ligand passage, and such adaptive conformation changes of access channels may not necessarily be reflected in structures taken from X-ray analysis and classical MD simulations.

The multidimensional free energy profiles obtained from the BE-META simulations allowed identification of the transition states for the release of TMU via the three channels (Figure 4). In all three cases, the transition states corresponded to configurations where TMU was at least partially in contact with the surrounding environment, i.e., either water or lipids. The nature of the environment outside the individual ACs differed significantly, especially in terms of hydration level: TMU in the transition state of AC-S was partially hydrated, in AC-4, the hydration was localized on a small part of TMU, and in AC-2af, TMU was not in contact with bulk water but in contact with lipids (Figure 4). The amino acid residues of the transition states also reflected the nature of the local environment: in AC-S, TMU made polar contacts with E308, Y307, and the backbone of L211; in AC-4, a hydrogen bond was formed between TMU and the backbone of F108; and in AC-2af, the only polar contact was with the backbone of D76 and otherwise TMU was surrounded by nonpolar residues. A common residue of transition states for two of the three channels (AC-S and AC-4) was R212. This residue was also present close to the transition state of AC-2af, and therefore it seems to play an important role in channel opening. The mentioned residues and also other residues important to the transition states are depicted in Figure 4. Mutations of these amino acid residues may alter access channel properties and, in turn, enzyme substrate preferences, as shown also for other enzymes.[9]

Large amino acids lining the channels, such as R106, E308, F213, D214, and D217, are also perspective candidates for mutation (Figures 2, S8, and S9), as their size and ability for forming hydrogen bonds can significantly affect the malleability of ACs. The importance of some of these residues has been confirmed experimentally (Appendix #1, Supporting Information).[23−26,74,75] We identified that the enzyme flexibility is a crucial property for ligand permeation, and therefore reducing the flexibility (especially in AC-S) may reduce the AC permeability. Hence, mutation of residues on loops forming the mouth of AC-S (glycines 480−481 or leucines 210−211) to other residues (especially forming a hydrogen bond with the I-helix or larger amino acids blocking AC entrance) may restrict the opening of AC-S. Indeed, mutation of L211 to tyrosine has been shown to decrease the affinity toward several xenobiotics.[76]

These results show that the presented method is not only capable of predicting the free energy of release of a ligand from the binding site but also of finding new access channels not detectable by the analysis of the enzyme structure, which usually focuses on lining amino acids or on the AC diameter.[38,56,77,78] In our approach the identification and characterization of the ACs is based on a synergy between the structural bioinformatics tool, MOLE 2.0, and BE-META simulation. Here, it was possible to achieve a satisfactory statistical accuracy only by using a newly employed metric used in the *spath* variable. Unlike other in silico techniques for free energy calculations of ligand passage through enzyme ACs[31,79,80] that drive the ligand from the active site and usually overestimate the free energy barrier, the proposed BE-META approach allowed several permeations of TMU to be observed through ACs and provided converged free energy profiles valid both for access and egress. Previous studies employing the BE-META method to analyze ligand passage have only focused on

DOI: 10.1021/acs.jctc.6b00075
J. Chem. Theory Comput. 2016, 12, 2101−2109

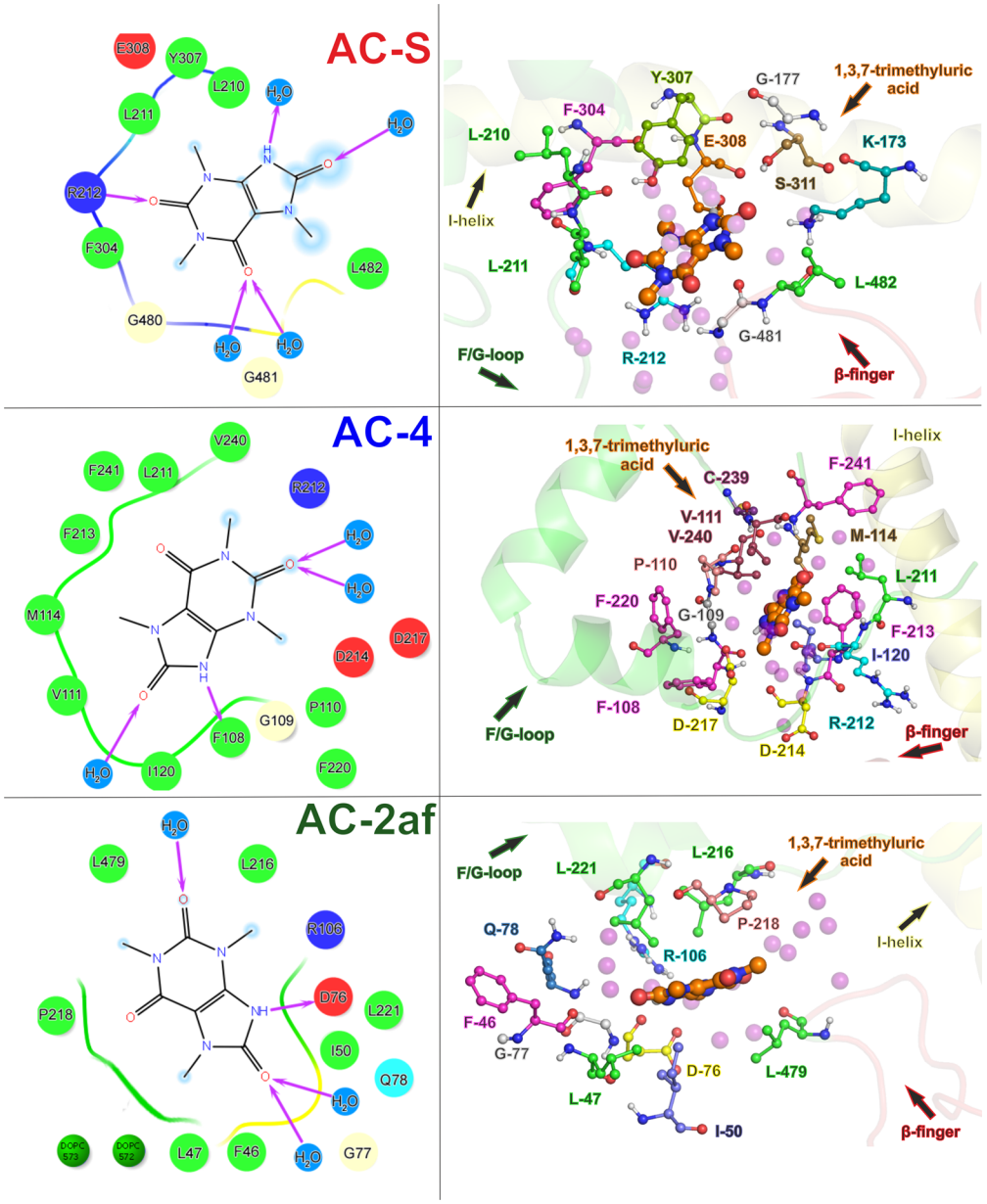

Figure 4. Amino acid residues near TMU in the transition states of studied ACs in schematic representation (left) and atomic representation (right). **Left**: Blue shadow represents hydration level of TMU atoms, green curves represent nonpolar contacts, yellow and blue curves show polar contacts, and magenta arrows correspond to hydrogen bonds.[73] **Right**: Residues are shown as balls-and-sticks representations, nonpolar hydrogens are not shown for clarity, secondary structural elements are represented as transparent cartoons and colored according to their position in the sequence: β-5-region (labeled as β-finger) – red, F/G loop–green, I-helix–yellow. TMU is shown as orange/blue/red balls and sticks, and water molecules are shown as purple transparent spheres.

rigid and clearly defined pathways through enzymes.[64,81] However, we have shown that the approach presented here also allows identification of mutable AC-lining residues and analysis of their function in malleable enzyme ACs.

CONCLUSION

We have presented a method for studying ligand passage through malleable enzyme ACs and applied it to the passage of 1,3,7-trimethyluric acid (TMU) through membrane attached CYP3A4 ACs. We used a synergy of the MOLE 2.0 bioinformatics tool for identifying access channels and bias-exchange metadynamics (BE-META). This combination of methods allowed differentiating well between multiple ACs and allowed performing a detailed thermodynamic and structural analysis without the restriction to previously identified channels. To achieve convergence, it was necessary to introduce a new metric for *spath* enumeration (*DMSDDrug*), which was shown to closely describe the position of TMU in the ACs.

Our results suggested that CYP3A4 flexibility has a significant influence on the permeation ability of TMU. Whereas MOLE 2.0 analysis of a classical MD simulation identified AC-2e and AC-4 as the mostly opened channels, the BE-META simulation suggested that TMU does not pass through AC-2e, mostly due to the rigidity and insufficient size of its mouth. Further, we analyzed a channel (AC-S) that opened very rarely during the classical MD simulation. BE-META indicated that AC-S was the most favorable channel for TMU release, followed by AC-4 and AC-2af. From analysis of

DOI: 10.1021/acs.jctc.6b00075
J. Chem. Theory Comput. 2016, 12, 2101–2109

transition states located on the CYP3A4 surface and the channel lining residues, we identified several amino acids (R212, E308, F304, S119 and F108, F213, D214, D217) whose mutations may significantly affect CYP3A4 activity. Some of these residues have already been identified experimentally as amino acids altering CYP3A4 function.[23−26,74,75] These results provide new insights into the mechanism of ligand release from CYP3A4. Overall, the approach presented here appears to be robust, transferable, and capable of distinguishing between multiple pathways. We anticipate it will be a valuable tool for enzymatic studies and rational enzyme design.

■ ASSOCIATED CONTENT

Supporting Information

The Supporting Information is available free of charge on the ACS Publications website at DOI: 10.1021/acs.jctc.6b00075.

Detailed description of simulation protocol. Figure S1: C8 hydroxylation/oxylation of caffeine in CYP3A4. Figure S2: Scheme showing used collective variables. Figure S3: Free energy profile of caffeine and TMU on a DOPC membrane calculated by COSMOmic. Figure S4: One dimensional free energy profiles for radius of gyration of channel mouths. Figure S5: 3D chart of free energy above all monitored radii of gyration and S-path variable. Figure S6: Recalculation of radius of gyration mouth radius Rg into physical mouth radius Rm (radius of maximally inscribed ball calculated by MOLE 2.0). Figure S7: Development of radii of gyration of monitored mouths during an unbiased simulation. Figure S8: Channel lining residues of the respective channels. Figure S9: Binding state in atomic and schematic representation. Figure S10. Free energy profiles along the spath with estimated errors. Figure S11. Monitoring spath variable during the BE-META simulation in spath replica. Figures S12−14: Monitoring of other CVs in all replicas. Figure S15: The history dependent potential along the time extracted from BE-META simulations. Figure S16: Multiple free simulations starting from various positions in channel AC-S. Table S1: Frequency of channel opening during free simulation analyzed by MOLE 2.0. Table S2: Amino acid residues defining the milestones, contacts, and mouths. Appendix #1: Mutation studies. Appendix #2: Input files for Plumed calculation (PDF)

Modified source codes of Plumed 2.1 (ZIP)

■ AUTHOR INFORMATION

Corresponding Authors

*E-mail: michal.otyepka@upol.cz.

*E-mail: laio@sissa.it.

Author Contributions

†Both authors contributed equally to this paper.

Notes

The authors declare no competing financial interest.

■ ACKNOWLEDGMENTS

We gratefully acknowledge support through Project LO1305 of the Ministry of Education, Youth and Sports of the Czech Republic. M.O. acknowledges support from the Czech Grant Agency through Project P208/12/G016. V.N. and M.P. acknowledge support from a student project of Palacký University Olomouc (IGA_PrF_2016_028).

■ REFERENCES

(1) Garcia-Viloca, M.; Gao, J.; Karplus, M.; Truhlar, D. G. How Enzymes Work: Analysis by Modern Rate Theory and Computer Simulations. *Science* **2004**, *303*, 186−195.

(2) Benkovic, S. J.; Hammes-Schiffer, S. A Perspective on Enzyme Catalysis. *Science* **2003**, *301*, 1196−1202.

(3) Koeller, K. M.; Wong, C. H. Enzymes for Chemical Synthesis. *Nature* **2001**, *409*, 232−240.

(4) Pravda, L.; Berka, K.; Svobodová Vařeková, R.; Sehnal, D.; Banáš, P.; Laskowski, R. A.; Koča, J.; Otyepka, M. Anatomy of Enzyme Channels. *BMC Bioinf.* **2014**, *15*, 379.

(5) Bui, J. M.; Tai, K.; McCammon, J. A. Acetylcholinesterase: Enhanced Fluctuations and Alternative Routes to the Active Site in the Complex with Fasciculin-2. *J. Am. Chem. Soc.* **2004**, *126*, 7198−7205.

(6) Bailey, L. J.; McCoy, J. G.; Phillips, G. N.; Fox, B. G. Structural Consequences of Effector Protein Complex Formation in a Diiron Hydroxylase. *Proc. Natl. Acad. Sci. U. S. A.* **2008**, *105*, 19194−19198.

(7) Lindberg, R. L.; Negishi, M. Alteration of Mouse Cytochrome P450coh Substrate Specificity by Mutation of a Single Amino-Acid Residue. *Nature* **1989**, *339*, 632−634.

(8) Scrutton, N. S.; Berry, A.; Perham, R. N. Redesign of the Coenzyme Specificity of a Dehydrogenase by Protein Engineering. *Nature* **1990**, *343*, 38−43.

(9) Pavlova, M.; Klvana, M.; Prokop, Z.; Chaloupkova, R.; Banas, P.; Otyepka, M.; Wade, R. C.; Tsuda, M.; Nagata, Y.; Damborsky, J. Redesigning Dehalogenase Access Tunnels as a Strategy for Degrading an Anthropogenic Substrate. *Nat. Chem. Biol.* **2009**, *5*, 727−733.

(10) Bernhardt, R.; Urlacher, V. B. Cytochromes P450 as Promising Catalysts for Biotechnological Application: Chances and Limitations. *Appl. Microbiol. Biotechnol.* **2014**, *98*, 6185−6203.

(11) Kingsley, L. J.; Lill, M. a Including Ligand-Induced Protein Flexibility into Protein Tunnel Prediction. *J. Comput. Chem.* **2014**, *35*, 1748−1756.

(12) Sehnal, D.; Svobodová Vařeková, R.; Berka, K.; Pravda, L.; Navrátilová, V.; Banáš, P.; Ionescu, C.-M.; Otyepka, M.; Koča, J. MOLE 2.0: Advanced Approach for Analysis of Biomacromolecular Channels. *J. Cheminf.* **2013**, *5*, 39.

(13) Chovancova, E.; Pavelka, A.; Benes, P.; Strnad, O.; Brezovsky, J.; Kozlikova, B.; Gora, A.; Sustr, V.; Klvana, M.; Medek, P.; et al. CAVER 3.0: a Tool for the Analysis of Transport Pathways in Dynamic Protein Structures. *PLoS Comput. Biol.* **2012**, *8*, e1002708.

(14) Yaffe, E.; Fishelovitch, D.; Wolfson, H. J.; Halperin, D.; Nussinov, R. MolAxis: Efficient and Accurate Identification of Channels in Macromolecules. *Proteins: Struct., Funct., Genet.* **2008**, *73*, 72−86.

(15) Ekroos, M.; Sjögren, T. Structural Basis for Ligand Promiscuity in Cytochrome P450 3A4. *Proc. Natl. Acad. Sci. U. S. A.* **2006**, *103*, 13682−13687.

(16) Zhao, Y.; White, M. A.; Muralidhara, B. K.; Sun, L.; Halpert, J. R.; Stout, C. D. Structure of Microsomal Cytochrome P450 2B4 Complexed with the Antifungal Drug Bifonazole: Insight into P450 Conformational Plasticity and Membrane Interaction. *J. Biol. Chem.* **2006**, *281*, 5973−5981.

(17) Henzler-Wildman, K. A.; Lei, M.; Thai, V.; Kerns, S. J.; Karplus, M.; Kern, D. A Hierarchy of Timescales in Protein Dynamics is Linked to Enzyme Catalysis. *Nature* **2007**, *450*, 913−916.

(18) Rozovsky, S.; Jogl, G.; Tong, L.; McDermott, A. E. Solution-state NMR Investigations of Triosephosphate Isomerase Active Site Loop Motion: Ligand Release in Relation to Active Site Loop Dynamics. *J. Mol. Biol.* **2001**, *310*, 271−280.

(19) Ha, T.; Ting, A. Y.; Liang, J.; Caldwell, W. B.; Deniz, A. A.; Chemla, D. S.; Schultz, P. G.; Weiss, S. Single-Molecule Fluorescence Spectroscopy of Enzyme Conformational Dynamics and Cleavage Mechanism. *Proc. Natl. Acad. Sci. U. S. A.* **1999**, *96*, 893−898.

(20) Weiss, S. Measuring Conformational Dynamics of Biomolecules by Single Molecule Fluorescence Spectroscopy. *Nat. Struct. Biol.* **2000**, *7*, 724−729.

(21) Yang, H. Protein Conformational Dynamics Probed by Single-Molecule Electron Transfer. *Science* **2003**, *302*, 262−266.

(22) Sykora, J.; Brezovsky, J.; Koudelakova, T.; Lahoda, M.; Fortova, A.; Chernovets, T.; Chaloupkova, R.; Stepankova, V.; Prokop, Z.; Smatanova, I. K.; et al. Dynamics and Hydration Explain Failed Functional Transformation in Dehalogenase Design. *Nat. Chem. Biol.* **2014**, *10*, 428−430.
(23) Davydov, D. R.; Rumfeldt, J. a O.; Sineva, E. V.; Fernando, H.; Davydova, N. Y.; Halpert, J. R. Peripheral Ligand-binding Site in Cytochrome P450 3A4 Located with Fluorescence Resonance Energy Transfer (FRET). *J. Biol. Chem.* **2012**, *287*, 6797−6809.
(24) Domanski, T. L.; He, Y. a.; Khan, K. K.; Roussel, F.; Wang, Q.; Halpert, J. R. Phenylalanine and Tryptophan Scanning Mutagenesis of CYP3A4 Substrate Recognition Site Residues and Effect on Substrate Oxidation and Cooperativity. *Biochemistry* **2001**, *40*, 10150−10160.
(25) Sevrioukova, I. F.; Poulos, T. L. Structural and Mechanistic Insights into theInteraction of Cytochrome P4503A4 with Bromoergocryptine, a Type I Ligand. *J. Biol. Chem.* **2012**, *287*, 3510−3517.
(26) Yamaguchi, Y.; Khan, K. K.; He, Y. A.; He, Y. Q.; Halpert, J. R. Topological Changes in the CYP3A4 Active Site Probed with Phenyldiazene: Effect of Interaction with NADPH-Cytochrome P450 Reductase and Cytochrome b 5 and of Site-Directed Mutagenesis. *Drug Metab. Dispos.* **2004**, *32*, 155−161.
(27) Urban, P.; Truan, G.; Pompon, D. Access Channels to the Buried Active Site Control Substrate Specificity in CYP1A P450 Enzymes. *Biochim. Biophys. Acta, Gen. Subj.* **2015**, *1850*, 696−707.
(28) Hendrychová, T.; Berka, K.; Navrátilová, V.; Anzenbacher, P.; Otyepka, M. Dynamics and Hydration of the Active Sites of Mammalian Cytochromes P450 Probed by Molecular Dynamics Simulations. *Curr. Drug Metab.* **2012**, *13*, 177−189.
(29) Scorciapino, M. A.; Robertazzi, A.; Casu, M.; Ruggerone, P.; Ceccarelli, M. Breathing Motions of a Respiratory Protein Revealed by Molecular Dynamics Simulations. *J. Am. Chem. Soc.* **2009**, *131*, 11825−11832.
(30) Shen, T.; Tai, K.; Mccammon, J. A. Molecular Dynamics Simulations of Acetylcholinesterase. *Acc. Chem. Res.* **2002**, *35*, 332−340.
(31) Lüdemann, S. K.; Lounnas, V.; Wade, R. C. How Do Substrates Enter and Products Exit the Buried Active Site of Cytochrome P450cam? 1. Random Expulsion Molecular Dynamics Investigation of Ligand Access Channels and Mechanisms. *J. Mol. Biol.* **2000**, *303*, 797−811.
(32) Isralewitz, B.; Gao, M.; Schulten, K. Steered Molecular Dynamics and Mechanical Functions of Proteins. *Curr. Opin. Struct. Biol.* **2001**, *11*, 224−230.
(33) Fishelovitch, D.; Shaik, S.; Wolfson, H. J.; Nussinov, R. Theoretical Characterization of Substrate Access/Exit Channels in the Human Cytochrome P450 3A4 Enzyme: Involvement of Phenylalanine Residues in the Gating Mechanism. *J. Phys. Chem. B* **2009**, *113*, 13018−13025.
(34) Wade, R. C.; Winn, P. J.; Schlichting, I.; Sudarko. A Survey of Active Site Access Channels in Cytochromes P450. *J. Inorg. Biochem.* **2004**, *98*, 1175−1182.
(35) Kalyaanamoorthy, S.; Chen, Y. P. P. Exploring Inhibitor Release Pathways in Histone Deacetylases Using Random Acceleration Molecular Dynamics Simulations. *J. Chem. Inf. Model.* **2012**, *52*, 589−603.
(36) Li, W.; Liu, H.; Luo, X.; Zhu, W.; Tang, Y. Possible Pathway (s) of Metyrapone Egress from the Active Site of Cytochrome P450 3A4: a Molecular Dynamics Simulation. *Drug Metab. Dispos.* **2007**, *35*, 689−696.
(37) Li, W.; Liu, H.; Scott, E. E.; Gräter, F.; Halpert, J. R.; Luo, X.; Shen, J.; Jiang, H. Possible Pathway(s) of Testosterone Egress from the Active Site of Cytochrome P450 2B1: A Steered Molecular Dynamics Simulation. *Drug Metab. Dispos.* **2005**, *33*, 910−919.
(38) Shen, Z.; Cheng, F.; Xu, Y.; Fu, J.; Xiao, W.; Shen, J.; Liu, G.; Li, W.; Tang, Y. Investigation of Indazole Unbinding Pathways in CYP2E1 by Molecular Dynamics Simulations. *PLoS One* **2012**, *7*, e33500.
(39) Oostenbrink, C.; de Ruiter, A.; Hritz, J.; Vermeulen, N. Malleability and Versatility of Cytochrome P450 Active Sites Studied by Molecular Simulations. *Curr. Drug Metab.* **2012**, *13*, 190−6.
(40) Venhorst, J.; Onderwater, R. C.; Meerman, J. H. N.; Commandeur, J. N. M.; Vermeulen, N. P. E. Influence of N-Substitution of 7-Methoxy-4- (Aminomethyl) -Coumarin on Cytochrome P450 Metabolism and Selectivity. *Drug Metab. Dispos.* **2000**, *28*, 1524−1532.
(41) de Ruiter, A.; Oostenbrink, C. Protein − Ligand Binding from Distancefield Distances and Hamiltonian Replica Exchange Simulations. *J. Chem. Theory Comput.* **2013**, *9*, 883−892.
(42) Wang, F.; Landau, D. P. Efficient, Multiple-Range Random Walk Algorithm to Calculate the Density of States. *Phys. Rev. Lett.* **2001**, *86*, 2050−2053.
(43) Darve, E.; Pohorille, A. Calculating Free Energies Using Average Force. *J. Chem. Phys.* **2001**, *115*, 9169.
(44) Huber, T.; Torda, A. E.; van Gunsteren, W. F. Local Elevation: A Method for Improving the Searching Properties of Molecular Dynamics Simulation. *J. Comput.-Aided Mol. Des.* **1994**, *8*, 695−708.
(45) Grubmüller, H. Predicting Slow Structural Transitions in Macromolecular Systems: Conformational Flooding. *Phys. Rev. E: Stat. Phys., Plasmas, Fluids, Relat. Interdiscip. Top.* **1995**, *52*, 2893−2906.
(46) Glover, F. Tabu Search - Part I. *ORSA J. Comput.* **1989**, *1*, 190−206.
(47) Laio, A.; Parrinello, M. Escaping Free-Energy Minima. *Proc. Natl. Acad. Sci. U. S. A.* **2002**, *99*, 12562−12566.
(48) Laio, A.; Gervasio, F. L. Metadynamics: a Method to Simulate Rare Events and Reconstruct the Free Energy in Biophysics, Chemistry and Material Science. *Rep. Prog. Phys.* **2008**, *71*, 126601.
(49) Guengerich, F. P. Common and Uncommon Cytochrome P450 Reactions Related to Metabolism and Chemical Toxicity. *Chem. Res. Toxicol.* **2001**, *14*, 611−650.
(50) Anzenbacher, P.; Anzenbacherová, E. Cytochromes P450 and Metabolism of Xenobiotics. *Cell. Mol. Life Sci.* **2001**, *58*, 737−747.
(51) Evans, W. E.; Relling, M. V. Pharmacogenomics: Translating Functional Genomics into Rational Therapeutics. *Science* **1999**, *286*, 487−491.
(52) Guengerich, F. P. Role of Cytochrome P450 Enzymes in Drug-Drug Interactions. *Adv. Pharmacol.* **1997**, *43*, 7−35.
(53) Otyepka, M.; Skopalík, J.; Anzenbacherová, E.; Anzenbacher, P. What Common Structural Features and Variations of Mammalian P450s Are Known to Date? *Biochim. Biophys. Acta, Gen. Subj.* **2007**, *1770*, 376−389.
(54) Johnson, E. F.; Stout, C. D. Structural Diversity of Human Xenobiotic-Metabolizing Cytochrome P450 Monooxygenases. *Biochem. Biophys. Res. Commun.* **2005**, *338*, 331−6.
(55) Otyepka, M.; Berka, K.; Anzenbacher, P. Is There a Relationship Between the Substrate Preferences and Structural Flexibility of Cytochromes P450? *Curr. Drug Metab.* **2012**, *13*, 130−142.
(56) Cojocaru, V.; Winn, P. J.; Wade, R. C. The Ins and Outs of Cytochrome P450s. *Biochim. Biophys. Acta, Gen. Subj.* **2007**, *1770*, 390−401.
(57) Rendic, S. Summary of Information on Human CYP Enzymes: Human P450 Metabolism Data. *Drug Metab. Rev.* **2002**, *34*, 83−448.
(58) Denisov, I. G.; Makris, T. M.; Sligar, S. G.; Schlichting, I. Structure and Chemistry of Cytochrome P450. *Chem. Rev.* **2005**, *105*, 2253−77.
(59) Baylon, J. L.; Lenov, I. L.; Sligar, S. G.; Tajkhorshid, E. Characterizing the Membrane-Bound State of Cytochrome P450 3A4: Structure, Depth of Insertion and Orientation. *J. Am. Chem. Soc.* **2013**, *135*, 8542−8551.
(60) Berka, K.; Paloncýová, M.; Anzenbacher, P.; Otyepka, M. Behavior of Human Cytochromes P450 on Lipid Membranes. *J. Phys. Chem. B* **2013**, *117*, 11556−11564.
(61) Pronk, S.; Páll, S.; Schulz, R.; Larsson, P.; Bjelkmar, P.; Apostolov, R.; Shirts, M. R.; Smith, J. C.; Kasson, P. M.; van der Spoel, D.; et al. GROMACS 4.5: A High-Throughput and Highly Parallel Open Source Molecular Simulation Toolkit. *Bioinformatics* **2013**, *29*, 845−854.

DOI: 10.1021/acs.jctc.6b00075
J. Chem. Theory Comput. 2016, 12, 2101−2109

(62) Piana, S.; Laio, A. A Bias-Exchange Approach to Protein Folding. *J. Phys. Chem. B* **2007**, *111*, 4553−4559.
(63) Granata, D.; Camilloni, C.; Vendruscolo, M.; Laio, A. Characterization of the Free-Energy Landscapes of Proteins by NMR-Guided Metadynamics. *Proc. Natl. Acad. Sci. U. S. A.* **2013**, *110*, 6817−6822.
(64) Bisha, I.; Rodriguez, A.; Laio, A.; Magistrato, A. Metadynamics Simulations Reveal a Na+ Independent Exiting Path of Galactose for the Inward-Facing Conformation of vSGLT. *PLoS Comput. Biol.* **2014**, *10*, e1004017.
(65) Branduardi, D.; Gervasio, F. L.; Parrinello, M. From A to B in Free Energy Space. *J. Chem. Phys.* **2007**, *126*, 054103.
(66) Trott, O.; Olson, A. J. AutoDock Vina: Improving the Speed and Accuracy of Docking with a New Scoring Function, EfficientOptimization, and Multithreading. *J. Comput. Chem.* **2010**, *31*, 455−461.
(67) Doudou, S.; Burton, N. A.; Henchman, R. H. Standard Free Energy of Binding from a One-Dimensional Potential of Mean Force. *J. Chem. Theory Comput.* **2009**, *5*, 909−918.
(68) Klamt, A.; Huniar, U.; Spycher, S.; Keldenich, J. COSMOmic: A Mechanistic Approach to the Calculation of Membrane−Water Partition Coefficients and Internal Distributions within Membranes and Micelles. *J. Phys. Chem. B* **2008**, *112*, 12148−12157.
(69) Skopalík, J.; Anzenbacher, P.; Otyepka, M. Flexibility of Human Cytochromes P450: Molecular Dynamics Reveals Differences between CYPs 3A4, 2C9, and 2A6, which Correlate with Their Substrate Preferences. *J. Phys. Chem. B* **2008**, *112*, 8165−8173.
(70) Poulos, T. L. Cytochrome P450 Flexibility. *Proc. Natl. Acad. Sci. U. S. A.* **2003**, *100*, 13121−13122.
(71) Hammes-Schiffer, S.; Benkovic, S. J. Relating Protein Motion to Catalysis. *Annu. Rev. Biochem.* **2006**, *75*, 519−541.
(72) Hendrychová, T.; Anzenbacherová, E.; Hudeček, J.; Skopalík, J.; Lange, R.; Hildebrandt, P.; Otyepka, M.; Anzenbacher, P. Flexibility of Human Cytochrome P450 Enzymes: Molecular Dynamics and Spectroscopy Reveal Important Function-Related Variations. *Biochim. Biophys. Acta, Proteins Proteomics* **2011**, *1814*, 58−68.
(73) Schrödinger Release 2015-1: Maestro Schrödinger Release 2015-1: Maestro 2015.
(74) Moore, C. D.; Shahrokh, K.; Sontum, S. F.; Cheatham, T. E.; Yost, G. S. Improved Cytochrome P450 3A4Molecular Models Accurately Predict the Phe215 Requirement for Raloxifene Dehydrogenation Selectivity. *Biochemistry* **2010**, *49*, 9011−9019.
(75) Domanski, T. L.; He, Y. A.; Harlow, G. R.; Halpert, J. R. Dual Role of Human Cytochrome P450 3A4 Residue Phe-304 in Substrate Specificity and Cooperativity. *J. Pharmacol. Exp. Ther.* **2000**, *293*, 585−591.
(76) Fowler, S. M.; Taylor, J. M.; Friedberg, T.; Roland Wolf, C.; Riley, R. J. CYP3A4 Active Site Volume Modification by Mutagenesis of Leucine 211. *Drug Metab. Dispos.* **2002**, *30*, 452−456.
(77) Hayashi, T.; Harada, K.; Sakurai, K.; Shimada, H.; Hirota, S. A Role of the Heme-7-Propionate Side Chain in Cytochrome P450cam as a Gate for Regulating the Access of Water Molecules to the Substrate-Binding Site. *J. Am. Chem. Soc.* **2009**, *131*, 1398−1400.
(78) Krishnamoorthy, N.; Gajendrarao, P.; Thangapandian, S.; Lee, Y.; Lee, K. W. Probing Possible Egress Channels for Multiple Ligands in Human CYP3A4: A Molecular Modeling Study. *J. Mol. Model.* **2010**, *16*, 607−614.
(79) Jarzynski, C. *A Nonequilibrium Equality for Free Energy Differences* **1996**, 11 arXiv:cond-mat/9610209.
(80) Lüdemann, S. K.; Lounnas, V.; Wade, R. C. How Do Substrates Enter and Products Exit the Buried Active Site of Cytochrome P450cam? 2. Steered Molecular Dynamics and Adiabatic Mapping of Substrate Pathways. *J. Mol. Biol.* **2000**, *303*, 813−830.
(81) Napolitano, L. M. R.; Bisha, I.; De March, M.; Marchesi, A.; Arcangeletti, M.; Demitri, N.; Mazzolini, M.; Rodriguez, A.; Magistrato, A.; Onesti, S.; et al. A Structural, Functional, and Computational Analysis Suggests Pore Flexibility as the Base for the Poor Selectivity of CNG Channels. *Proc. Natl. Acad. Sci. U. S. A.* **2015**, *112*, E3619−E3628.

DOI: 10.1021/acs.jctc.6b00075
J. Chem. Theory Comput. 2016, 12, 2101−2109

BBA - General Subjects xxx (xxxx) xxx–xxx

Contents lists available at ScienceDirect

BBA - General Subjects

journal homepage: www.elsevier.com/locate/bbagen

Molecular insights into the role of a distal F240A mutation that alters CYP1A1 activity towards persistent organic pollutants

Veronika Navrátilová[a], Markéta Paloncýová[a], Karel Berka[a], Shintaro Mise[b], Yuki Haga[c], Chisato Matsumura[c], Toshiyuki Sakaki[d], Hideyuki Inui[b,e,*], Michal Otyepka[a,*]

[a] Regional Centre of Advanced Technologies and Materials, Department of Physical Chemistry, Faculty of Science, Palacký University Olomouc, tř. 17. listopadu 12, 771 46, Olomouc, Czech Republic
[b] Graduate School of Agricultural Science, Kobe University, Kobe, Hyogo 657-8501, Japan
[c] Hyogo Prefectural Institute of Environmental Sciences, Kobe, Hyogo 654-0037, Japan
[d] Biotechnology Research Center, Faculty of Engineering, Toyama Prefectural University, Imizu, Toyama 939-0398, Japan
[e] Biosignal Research Center, Kobe University, Kobe, Hyogo 657-8501, Japan

ARTICLE INFO

Keywords:
Biotransformation
Tunnel
MM-PBSA
Protein engineering
Distal mutation
Rational enzyme design

ABSTRACT

Background: Cytochromes P450 are major drug-metabolizing enzymes involved in the biotransformation of diverse xenobiotics and endogenous chemicals. Persistent organic pollutants (POPs) are toxic hydrophobic compounds that cause serious environmental problems because of their poor degradability. This calls for rational design of enzymes capable of catalyzing their biotransformation. Cytochrome P450 1A1 isoforms catalyze the biotransformation of some POPs, and constitute good starting points for the design of biocatalysts with tailored substrate specificity.

Methods: We rationalized the activities of wild type and mutant forms of rat cytochrome P450 1A1 towards 2,3,7,8-tetrachloro-dibenzo-*p*-dioxin (TCDD) and 3,3′,4,4′-tetrachlorobiphenyl (PCB77) using experiments and molecular dynamics simulations.

Results: We showed that the enhanced activity of the CYP1A1 mutant towards TCDD was due to more efficient binding of the substrate in the active site even though the mutated site was over 2.5 nm away from the catalytic center. Moreover, this mutation reduced activity towards PCB77.

General significance: Amino acids that affect substrate access channels can be viable targets for rational enzyme design even if they are located far from the catalytic site.

1. Introduction

Cytochromes P450 (CYP) monooxygenases are important in the biotransformation of many endogenous substrates and xenobiotics including toxic environmental pollutants such as persistent organic pollutants (POPs) [1]. POPs can be classified into three groups according to their chemical composition: polychlorinated dibenzo-*p*-dioxins (PCDDs), polychlorinated dibenzofurans (PCDFs) and polychlorinated biphenyls (PCBs) [2]. PCDDs and PCDFs are by-products of various industrial chemical processes including chlorination, pesticide manufacture and combustion, while PCBs were industrial compounds used in transformers and condensers. They are considered to be highly toxic [2] and they are also very hydrophobic compounds that readily accumulate in lipid-rich tissues such as the visceral fat and skin of animals [3] and humans [4]. In humans, some POPs undergo slow biotransformation processes catalyzed mainly by CYP1 isoforms [5].

Mammalian CYPs are attached to biomembranes via N-terminal anchors, and their catalytic domains are partially membrane-immersed (Fig. 1) [6–8]. Their active sites are deeply buried in their structures [9,10] and are connected to the external environment via a complex network of access channels [11]. Substrates must travel through these channels to reach the catalytic site [12,13]. The channels differ from each other in terms of factors such as their lengths, widths, and mouth opening locations. Detailed analyses of the biotransformation kinetics of polycyclic substrates with different sizes catalyzed by chimeric CYP1A enzymes have suggested that amino acids located on the protein's surface at the channel entrances may be involved in substrate recognition and could strongly affect the efficiency of biotransformation [13]. Channels whose mouth openings face the hydrophobic membrane core (channels 2af, 2b, 2c, and 4) may serve as ligand access

* Correspondence to: H. Inui, Graduate School of Agricultural Science, Kobe University, Kobe, Hyogo 657-8501, Japan; M. Otyepka, Regional Centre of Advanced Technologies and Materials, Department of Physical Chemistry, Faculty of Science, Palacký University Olomouc, tř. 17. listopadu 12, 771 46, Olomouc, Czech Republic.
E-mail addresses: hinui@kobe-u.ac.jp (H. Inui), michal.otyepka@upol.cz (M. Otyepka).

http://dx.doi.org/10.1016/j.bbagen.2017.08.002
Received 4 April 2017; Received in revised form 30 June 2017; Accepted 1 August 2017
0304-4165/ © 2017 Elsevier B.V. All rights reserved.

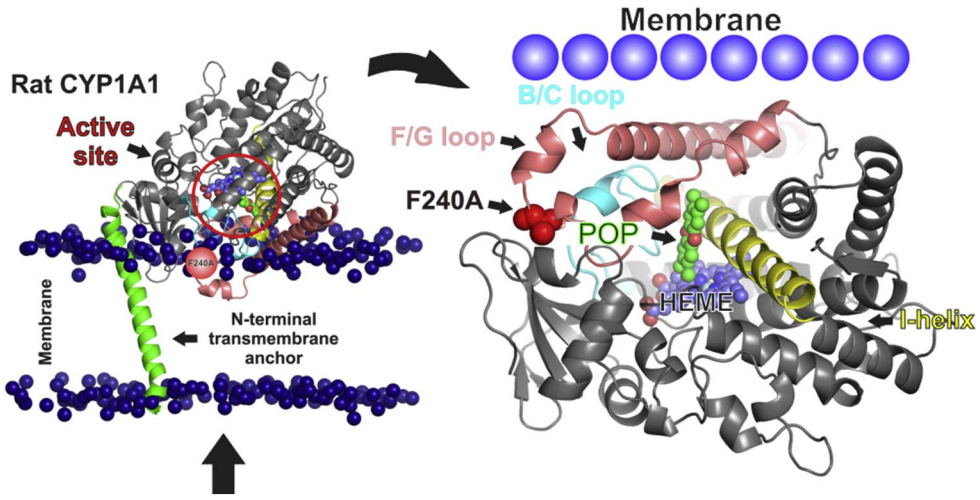

Fig. 1. The structure of rat CYP1A1, showing its major structural features. On the left: the catalytic domain of rat CYP1A1 (for clarity, only secondary structural elements are shown) embedded in a DOPC membrane (for clarity, the phosphate groups are represented as blue spheres and the lipid moieties are not shown). The hollow red circle encloses the active site, and the position of the mutated amino acid F/A240 is indicated by a solid red circle. The N-terminal transmembrane anchor, which is embedded in the hydrophobic interior of the membrane, is represented as a green helix. On the right: a detailed image of the rat CYP1A1 catalytic domain. The mutated amino acid F/A240 is represented by red spheres, the TCDD molecule is shown using green (carbons and chlorines) and red (oxygen) spheres, and the heme cofactor is shown using purple (carbon), blue (nitrogen) and red (oxygen) spheres. The I-helix is represented as a yellow ribbon, the B/C loop is shown in cyan, and the F/G loop is shown in pink.

channels for hydrophobic ligands, which tend to accumulate inside the membrane [14]. Conversely, channels with exits pointing to the solvent (notably the solvent channel, S) are assumed to be metabolite egress channels. Because lipophilic compounds exhibit different patterns of accumulation across membrane regions [3,14], their metabolism may be influenced by the locations of the channel mouths [15].

POPs are usually poorly degradable but most can be metabolized by CYPs [16]. An important exception is the most dangerous dioxin, 2,3,7,8-tetrachloro-dibenzo-*p*-dioxin (TCDD), which cannot be metabolized by any wild-type CYP in a reasonable timeframe and therefore has a strong tendency to persist and accumulate in food chains [17]. While other POPs can be metabolized by a wide range of CYPs (including human CYP1A1, 1A2, 2C9, rat CYP1A1, and porcine CYP1A1), TCDD remains untouched by these enzymes [18–21]. Because of its toxicity and resistance to degradation, it is used as a reference compound when computing toxic equivalency factor (TEF) values for other POPs [17]. The hydroxylation reactions catalyzed by CYPs preferentially target unsubstituted positions on the skeleton of POPs. Therefore, monochloro-, dichloro-, and trichlorodibenzo-*p*-dioxins can be metabolized by rat CYP1A1 but TCDD, which has four chlorine-substituted positions, cannot. An enzyme capable of degrading TCDD was previously created by using site-directed mutagenesis to replace the large phenylalanine residue at position 240 of rat CYP1A1 with alanine [18]. The mutated residue is located around 24 Å from the heme iron atom (i.e. at the protein surface), and it is not yet clear how such a distant mutation can so strongly affect the enzyme's activity.

The mechanistic reason for the enhanced activity of the rat F240A-CYP1A1 mutant enzyme towards TCDD remains unknown. In principle, many factors could affect the mutated enzyme's activity and substrate specificity, including the accessibility of the active site through access channels [13,22], the enzyme's orientation in the membrane [23,24], the alignment of the access channels openings with the substrate's location in the membrane [7], and the enzyme's binding affinity for the substrate. Because rational enzyme design depends on a robust understanding of the roles played by activity-changing mutations (as beautifully demonstrated by the engineering of haloalkane dehalogenase [25,26] and cytochrome *c* peroxidase [27]) and there is a need for designed CYP enzymes capable of metabolizing POPs, we analyzed the mechanistic effect of the F240A mutation on CYP1A1 activity. To decipher the mechanism responsible for the increased TCDD-degrading activity of the F240A mutant of rat CYP1A1 [18], we performed molecular dynamics (MD) simulations of the wild type (WT) and mutant enzymes attached to a lipid bilayer. We also compared the activity of both enzymes towards a member of another class of POPs, 3,3′,4,4′-tetrachlorobiphenyl (PCB77), using both simulations and experiments. To rationalize the differences between the two compounds, we performed MD simulations of the WT enzyme and the F240A mutant in ligand-free form as well as their complexes with PCB77 and TCDD. The results obtained shed new light on the enzyme's dynamics and the catalytic changes resulting from the F240A mutation, demonstrating that mutations far from the active site can profoundly affect the uptake, binding and release of the studied POPs.

2. Materials and methods

2.1. Experimental studies

PCB77 and ^{13}C-labeled hydroxylated (OH)-PCBs as internal standards were purchased from AccuStandard (New Haven, CT) and Wellington Laboratories (Guelph, Canada), respectively. The genes for the wild type (WT) rat CYP1A1 enzyme and the F240A mutant were expressed in *Saccharomyces cerevisiae* strain AH22 cells using the plasmid pGYR, which contains the gene for yeast NADPH-P450 oxidoreductase. Microsomal fractions were purified from recombinant *S. cerevisiae* cells as reported previously [28]. The expression of the CYPs was determined by the method of Omura and Sato using reduced CO difference spectra [29].

The metabolism of PCB77 by WT rat CYP1A1 and the F240A mutant was evaluated as reported previously, using 40 pmol of the appropriate CYP [30]. PCB77 was added to the reaction mixture at 250, 500, 1000, or 2000 ppb with 0.1% dimethyl sulfoxide, and an NADPH regeneration system comprising 0.5 mM NADPH, 5 mM glucose-6-phosphate (G6P), and 1 unit G6P dehydrogenase) was used. The reaction mixture was shaken continuously for 2 h at 37 °C. The reaction was then halted by incubation on ice, and 100 ppb of the appropriate ^{13}C-labeled OH-PCB was added. Metabolites were extracted twice with 2 mL hexane, and their methylated derivatives were determined and quantified by high-resolution gas chromatography and high-resolution mass spectrometry (HRGC/HRMS) as reported previously [31,32]. The hydroxylated metabolite of PCB77 was determined by comparison to the retention time of 4-OH-3,3′,4′,5-tetrachlorobiphenyl.

2.2. Computational studies

2.2.1. Structure preparation

The structure of the complete rat WT CYP1A1 (UNIPROT ID: P00185), i.e. the catalytic domain and the N-terminal transmembrane anchor, was obtained by homology modelling with Modeller 9.10 [33]. The template structure was obtained by taking the X-ray structure of human CYP1A1 (PDB ID: 4I8V) and removing its α-naphthoflavone ligand [34]. The structure of the F240A mutant was obtained by deleting the phenyl ring of F420 using the Pymol 1.7 software package [35].

AMBER ff99SB [36] was used for both enzymes. Parameters for the heme cofactor were adopted from literature [37]. The initial membrane model consisted of 121 molecules of 1,2-dioleoyl-sn-glycero-3-phosphocholine (DOPC) in each leaflet; the lipids were modeled using the Slipids force field [38]. The pure DOPC bilayer was equilibrated at 310 K by MD simulation in TIP3P water [39] for 200 ns. The WT and mutant F240A enzymes were then embedded into the equilibrated DOPC lipid bilayer using g_membed tool [40]. The complex of WT/F240A attached to the DOPC membrane was then placed in a rectangular box and solvated using the TIP3P water model [39]. Forty-seven Na^+ and 47 Cl^- ions were added to simulate the physiological ionic strength of 0.1 mol/L.

2.2.2. Parametrization of PCB77 and TCDD molecules

Structures of PCB77 and TCDD molecules were drawn using Marvin 14.7.7.0 software; ChemAxon (http://www.chemaxon.com). Same tool was used for clogP prediction. Molecules were parameterized for MD simulations according to a tested protocol [41] compatible with the Slipids [38] and AMBER ff99SB [36] force fields. Electrostatic potential (ESP) values were calculated using Gaussian 09 [42] at the HF/6-31G* level of theory. Partial charges were then calculated by the RESP method using AMBER 11 [43]. Bonded parameters and atom types were taken from GAFF [44]. Finally, the amb2gmx tool [45] was used to convert data in the Amber file format to the Gromacs format. Structures were then positioned in active site by alignment to the position occupied by α-naphthoflavone position in the template protein structure.

2.2.3. Molecular dynamics

MD simulations were performed using GROMACS 4.5.5 [46]. The same protocol was used for both systems: after minimization by the steepest descent method with a threshold (maximum force) of 10 kJ mol^{-1} nm^{-1}, we performed a 1-ns-long pre-equilibration with the semi-isotropic Berendsen barostat [47] set to 1.013 bar and the V-rescale thermostat [48] set to 310 K, an isothermal compressibility of 4.5×10^{-5} bar^{-1}, and positional constraints applied to backbone Cα atoms. Then we performed a 200-ns-long MD simulation with the Nosé-Hoover thermostat [49,50] at 310 K, the Parinello-Rahman barostat [51] at 1.013 bar with semi-isotropic conditions, an isothermal compressibility of 4.5×10^{-5} bar^{-1}, 2-fs-long time steps, constraints applied to hydrogen bonds, periodic boundary conditions in all directions, the Particle Mesh Ewald method [52] (with 0.1 nm cutoff), van der Waals interactions switched off from 0.8 to 0.9 nm, and pair-lists generated with the group cut-off scheme.

After the ligand-free simulations we inserted the ligands (PCB77 and TCDD) into the active sites of both structures at the same position, which is occupied by α-naphthoflavone (aNF) in the X-ray structure of the human WT enzyme [34]. We then followed the same simulation protocol as for the ligand-free forms. We thus performed 200-ns-long MD simulations of the WT and F240A enzymes with PCB77 or TCDD molecule bound in the position occupied by the ligand in the template X-ray structure (see Supporting Information Fig. S1) in order to estimate the effect of ligand binding on the access channel network.

All analyses were performed using the GROMACS 4.5.5 tools [46]. Heme tilt angle (HTA) analyses were performed using the g_sgangle tool. The HTA was defined as the angle between the heme porphyrin plane and the membrane plane in the z-axis [7].

2.2.4. Channel analysis

Channels were identified using MOLE 2.0 [53] with the following parameters: Interior Threshold 1.0, Origin Radius 5, Bottleneck Radius 1.0, Probe Radius 5, Surface CoverRadius 10. The starting point was located ~3 Å above the iron atom of the heme cofactor. Channel identification was performed on 101 structural snapshots taken every 500 ps over the last 100 ns of the MD simulation. Channels were classified into channel families according to the nomenclature introduced by Wade and co-workers [11], with the exception of two channels belonging to subfamily 2 (2a and 2f), which were united into one channel called 2af due to their high structural similarity. We also analyzed the fraction of frames from the MD simulations in which the channels of various families were open; a channel was considered open when its bottleneck radius was above ~0.1 nm. Water molecules, ions and hydrogen atoms, and membrane atoms were not considered in channel analyses.

2.2.5. MM-PBSA analysis

Ligand binding energies were computed using molecular mechanics – specifically, the Poisson-Boltzmann surface area (MM-PBSA) method [54] as implemented in the g_mmpbsa tool [55] from the Gromacs package (http://rashmikumari.github.io/g_mmpbsa/), based on the last 100 ns of each MD simulation. MM-PBSA enables the estimation of the free energy change for the binding of a ligand to a protein in solvent, $\Delta G_{binding}$, according to Eq. (1):

$$\Delta G_{binding} = G_{complex} - (G_{protein} + G_{ligand}), \quad (1)$$

where $G_{complex}$ is the total free energy of the protein-ligand complex and $G_{protein}$ and G_{ligand} are the total free energies of the isolated protein and ligand in solvent, respectively. The free energy for each individual entity x (i.e., protein, ligand and protein-ligand complex) is given by Eq. (2):

$$G_x = \langle E_{MM} \rangle_x - TS_x + \langle G_{solvation} \rangle_x, \quad (2)$$

where $\langle E_{MM} \rangle$ is the average molecular mechanics potential energy in vacuum, T and S denote the temperature and entropy, respectively, and the last term $\langle G_{solvation} \rangle$ is the free energy of solvation.

If we are interested in differences between the binding energies of a given ligand for the WT and mutated enzymes, we can assume that the binding entropies and solvation entropies for the two proteins are essentially identical, giving Eq. (3):

$$\begin{aligned} \Delta\Delta G_{binding} &= \Delta G_{binding}(F240A) - \Delta G_{binding}(WT) \cong \\ &\cong \langle E_{MM} \rangle_{complex}(F240A) - (\langle E_{MM} \rangle_{protein}(F240A) + \langle E_{MM} \rangle_{ligand}(F240A)) \\ &\quad - \langle E_{MM} \rangle_{complex}(WT) + (\langle E_{MM} \rangle_{protein}(WT) + \langle E_{MM} \rangle_{ligand}(WT)) \end{aligned} \quad (3)$$

2.2.6. COSMOmic free energy profiles calculation

Neutral structures of compounds were generated from SMILES with the LigPrep module from the Small-Molecule Drug Discovery Suite 2015-4 [56]. Next, individual conformers of each compound were generated within MacroModel [56] using the OPLS_2005 force field in vacuum. Mixed MCMM/LMC2 conformational searches were performed to enable low-mode conformation searching with Monte Carlo structure selection. Conformers were selected for further analysis if they were within 5 kcal/mol of the lowest energy conformer and (to reduce the number of very similar conformers) had an atom-positional RMSD of at least 2 Å relative to all other selected conformers. Each selected conformer was subjected to a series of DFT/B-P/cc-TZVP vacuum and COSMO optimizations using Turbomole 6.3 [57] within the cuby4 framework [58]. After each optimization step, single point energy calculations at the DFT/B-P/cc-TZVPD level with a fine grid were performed to obtain COSMO files for each conformer. The structures of 15 lipid conformers of each lipid (DOPC, ceramide NS, lignoceric acid, cholesterol) were extracted from a 200 ns free MD simulation. COSMO files were then obtained in the same way as for the other compounds using Tubomole 6.3. The atomic distribution in DOPC, CER or SCmix bilayers was calculated using the g_density tool from the Gromacs package [46], by averaging the last 50 ns of the appropriate MD simulation and slicing one membrane layer into 50 sections. We prepared conformer sets for both studied compounds, calculated 15 free energy profiles for each of them and each lipid conformer using COSMOmic X15 [59], and then averaged these profiles to obtain final profiles.

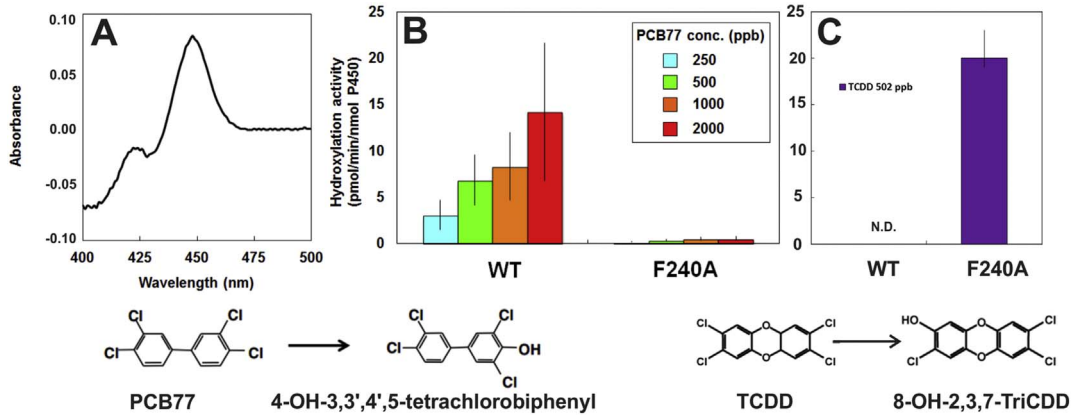

Fig. 2. Experimental activities of rat CYP1A1 enzymes. Panel A shows CO difference spectrum for rat CYP1A1 F240A mutant extracted from recombinant yeast cells. Panels B and C show the hydroxylation activity of the WT and F240A mutant of rat CYP1A1 towards PCB77 (panel B) and TCDD (panel C). The error bars in panels B and C represent one standard deviation based on three replicate analyses. Data for TCDD taken from Shinkyo et al. [18] Structures of PCB77 and TCDD are shown in the bottom together with metabolites.

3. Results and discussion

3.1. Hydroxylation activity of WT and mutant F240A

To investigate the effect of the F240A mutation on the metabolism of POPs other than TCDD, [18] we analyzed its hydroxylation activity towards PCB77. The F240A mutation was shown to make rat CYP1A1 capable of hydroxylating TCDD, a capability not previously observed in any other CYP [16,18]. Whereas the WT enzyme binds TCDD but exhibits no detectable hydroxylation activity towards it, the F240A mutant has an activity of 20 pmol/min/nmol P450 [18,60] towards this substrate (Fig. 2). Surprisingly, the F240A mutant exhibited weaker hydroxylation activity towards PCB77 than did the WT (Fig. 2), the WT enzyme's activity was 3–14 pmol/min/nmol P450, while the mutant's was around an order of magnitude lower as F240A was biologically active (Fig. 2). This stands in sharp contrast to the trends reported for TCDD by Shinkyo and coworkers [18]. These experimental results strongly suggest that the hydroxylation activity of rat CYP1A1 can be significantly altered by distal mutation at the F240 position despite its considerable distance from the active site, and that such mutations can even enable the degradation of highly metabolism-resistant molecules such as TCDD. To explain these observations, the strikingly different activities of the WT and the F240A mutant were investigated computationally using MD simulations.

We identified several potential causes of the differences in the efficiencies of the WT and the F240A mutant towards TCDD and PCB77: i) differences in the membrane positions of the two molecules and the active CYP access channels, ii) differences in access channel size, i.e. active site accessibility, and iii) differences in the affinities of TCDD and PCB77 for the two CYPs. The following paragraphs discuss these potential causes in more detail.

3.2. Membrane position of PCB77 and TCDD

We analyzed the membrane affinities of PCB77 and TCDD and their preferred positions in DOPC membranes in terms of free energies along the membrane normal. Both compounds exhibited high affinities for the membrane (− 8.8 and − 9.9 kcal/mol for PCB77 and TCDD, respectively, Fig. 3), which was expected because of their strongly lipophilic character (clogP of PCB77 is 6.04 and of TCDD is 5.42.). The free energy profiles suggested that PCB77 and TCDD tend to accumulate in the membrane core. However, because the minima are shallow and broad, both compounds are widely distributed in the lipophilic membrane core, i.e. the region within 1.1 nm of the membrane's center line (Fig. 3). The profiles of both molecules suggest that they should accumulate in the membrane, leading to their pre-concentration and enhancing enzyme activity.

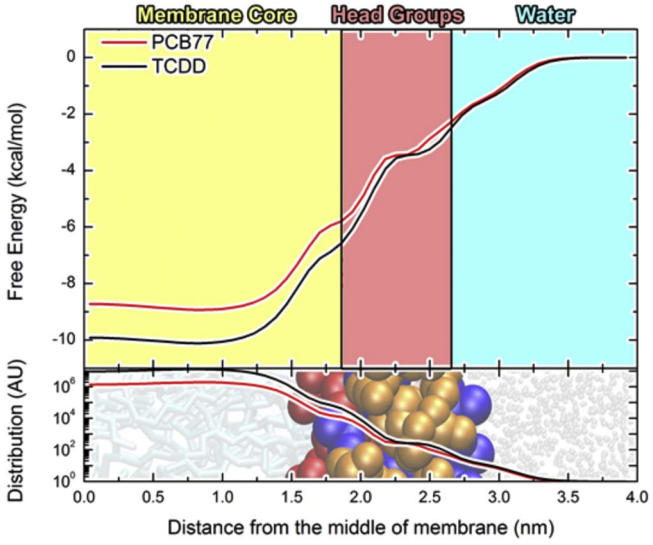

Fig. 3. Free energy profiles of PCB77 and TCDD in membranes surrounded by water (top panel). Both compounds have deep free energy minima inside the membrane (yellow) and much higher free energies in water (blue). The free energy profile and the abundance of PCB77 and TCDD as a function of distance from the membrane's center line (bottom panel) indicate a strong tendency for both compounds to accumulate in the hydrophobic core of the DOPC membrane. The lower panel's background shows the structure of a DOPC membrane – oxygens of waters are represented as grey dots, lipid tails are shown as cyan sticks, and the atoms of the head groups are shown as spheres (red for carbonyl oxygens, orange for phosphates, and blue for nitrogens).

3.3. Position and orientation of rat CYP 1A1/F240A on the membrane

We performed 200 ns long MD simulations of the WT and F240A mutant with empty active site cavities to analyze the structure and orientation of the CYPs on the DOPC membrane. Both enzymes adopted essentially identical membrane positions and orientations, and the centers of mass of their catalytic domains both converged to a similar distance (~3.8 ± 0.2 nm) from the membrane center (Supporting Information: Fig. S2). The HTA, i.e. the angle between the plane of the heme porphyrin nitrogen atoms and the membrane plane in the z-axis, which reflects the inclination of the CYP catalytic domain to the membrane [7,15,61], stabilized after approximately 150 ns at values of 54.7° ± 4.2° and 53.6° ± 6.3° for the WT and F240A, respectively (Fig. 4). These computed HTAs agree well with the value determined experimentally for CYP3A4 on a POPC nanodisc (59.1° ± 4.1) [62]. The global fold of CYP was preserved during the MD simulations; we observed only small rearrangements. However, rotational movements

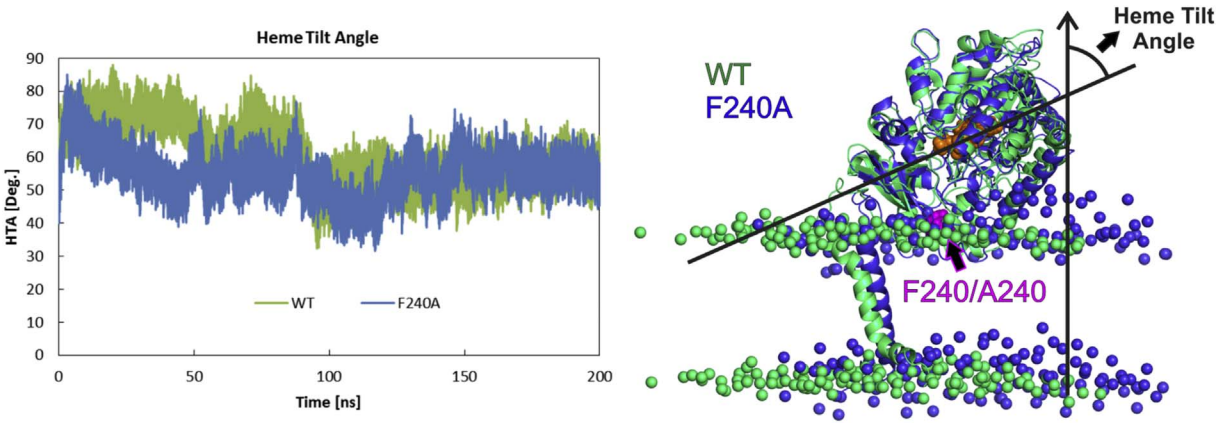

Fig. 4. Left: time evolution of the heme tilt angle of the WT and F240A mutant during MD simulations. There are no significant differences between the two proteins after 150 ns of simulated time, indicating that the catalytic domains of both enzymes adopt similar membrane orientations (as shown in the right-hand panel). Right: the structures of the WT (green) and F240A mutant (blue) on DOPC membranes at the end of the MD simulations. Secondary structural elements are shown in cartoon form, while membrane phosphates are represented as spheres and the heme cofactor is shown in orange. For clarity, water molecules are not shown. The mutated amino acid F240A is depicted as a collection of magenta spheres located close to the membrane head groups.

of certain amino acid residues (R81, I82, T85, Y114, Y236, D239 and R245) in close proximity to the mutated F240 in the F/G loop region (Supporting Information: Figs. S3 and S4) caused changes in the shapes of some internal cavities and active site access channels, as discussed below.

3.4. Analysis of active site access channels

The PCB77 and TCDD molecules enter (and their metabolites leave) the active site cavity via the enzymes' networks of access channels. While the global characteristics of the WT access channel network were shared with the F240A mutant, structural changes in the vicinity of the mutated site caused changes in channel opening and closing. In the MD simulations of the substrate-free WT enzyme, the preferred channels (i.e. those that were open most of the time and had bottlenecks wider than ~0.1 nm) were S and 2b. These channels were less frequently open in the simulations of the F240A mutant (see Figs. 5 and 6, and Supporting Information: Figs. S5–S7). However, the 2af and 2c channels were open more frequently in the mutant. The distal side of the CYP enzymes is known to be very malleable, and may control their overall substrate specificity [63]. The F240A mutation is localized in the flexible F/G loop and lies between two flexible regions, FR6 and FR2 [63]. The large phenylalanine side chain of the native residue at position 240 may serve as the “lid” of the 2af and 2b channels, and may also induce the closure of surrounding access tunnels. The simulations of the two proteins revealed significant differences in their channel openings (Supporting Information Figs. S6 and S7).

The presence of a ligand in the active site also significantly affects the opening of the access and egress channels (Fig. 6, Supporting Information Figs. S5–S7). In the WT enzyme, the binding of either PCB77 or TCDD in the active site closed most of the channels. While many active site access channels are closed in the WT-PCB77 complex, the active site could be still reached through some channels, such as 2d or 2b. However, the WT-TCDD complex is very closed, and almost no channels were accessible during the simulation. This is consistent with an earlier study on channel opening in WT porcine CYP1A1, where TCDD induced complete channel closure but other dioxins did not [21].

The F240A mutant behaved differently upon ligand binding. PCB77 caused some channels to open and others to close, whereas TCDD binding only caused channels to open. While the numbers of open channels in the WT and F240A complexes with PCB77 are quite similar (Fig. 6), the 2e and 2d channels in the mutant are less frequently open than in the WT. Channel 2b remained similarly open in both cases. As noted before, the WT-TCDD structure is closed, but the F240A-TCDD complex exhibited substantial opening of several access/egress channels including 2af, 2b, 2c and 2d. The different effects of TCDD and PCB77 may relate to the rigidity of TCDD molecule, which “locks” the WT active site in the closed state. This can be experimentally verified by performing pressure-jump experiments, as demonstrated for CYP2B by Zhang et al. [64]. The F240A mutation appears to prevent the active site closure after binding to TCDD. The smaller and more flexible PCB77 ligand does not cause such extensive closure of the WT enzyme, and its binding to the F240A mutant induced only conformational changes that modified the enzyme’s pattern of channel openings.

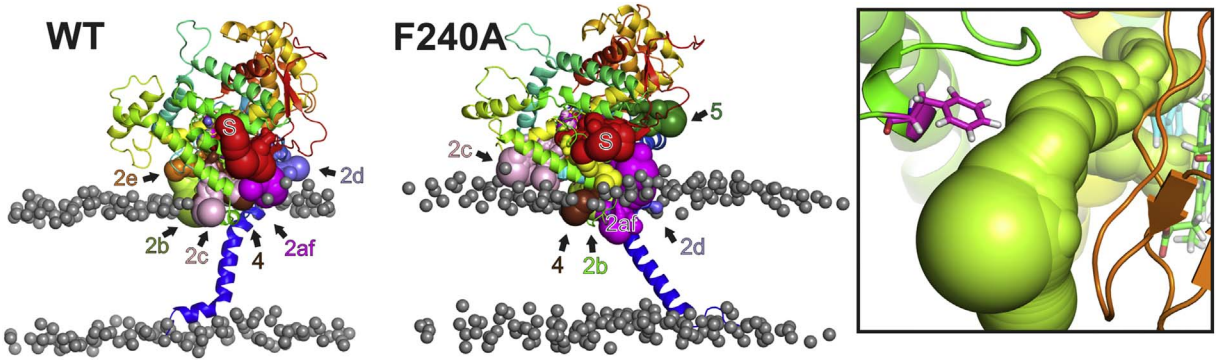

Fig. 5. Left: active site access channels of the WT and the F240A mutant. For clarity, only channels that are wide and mostly open are shown. Right: the potential function of the F240 residue (magenta sticks) as the gatekeeper of channel 2b/2af (green spheres).

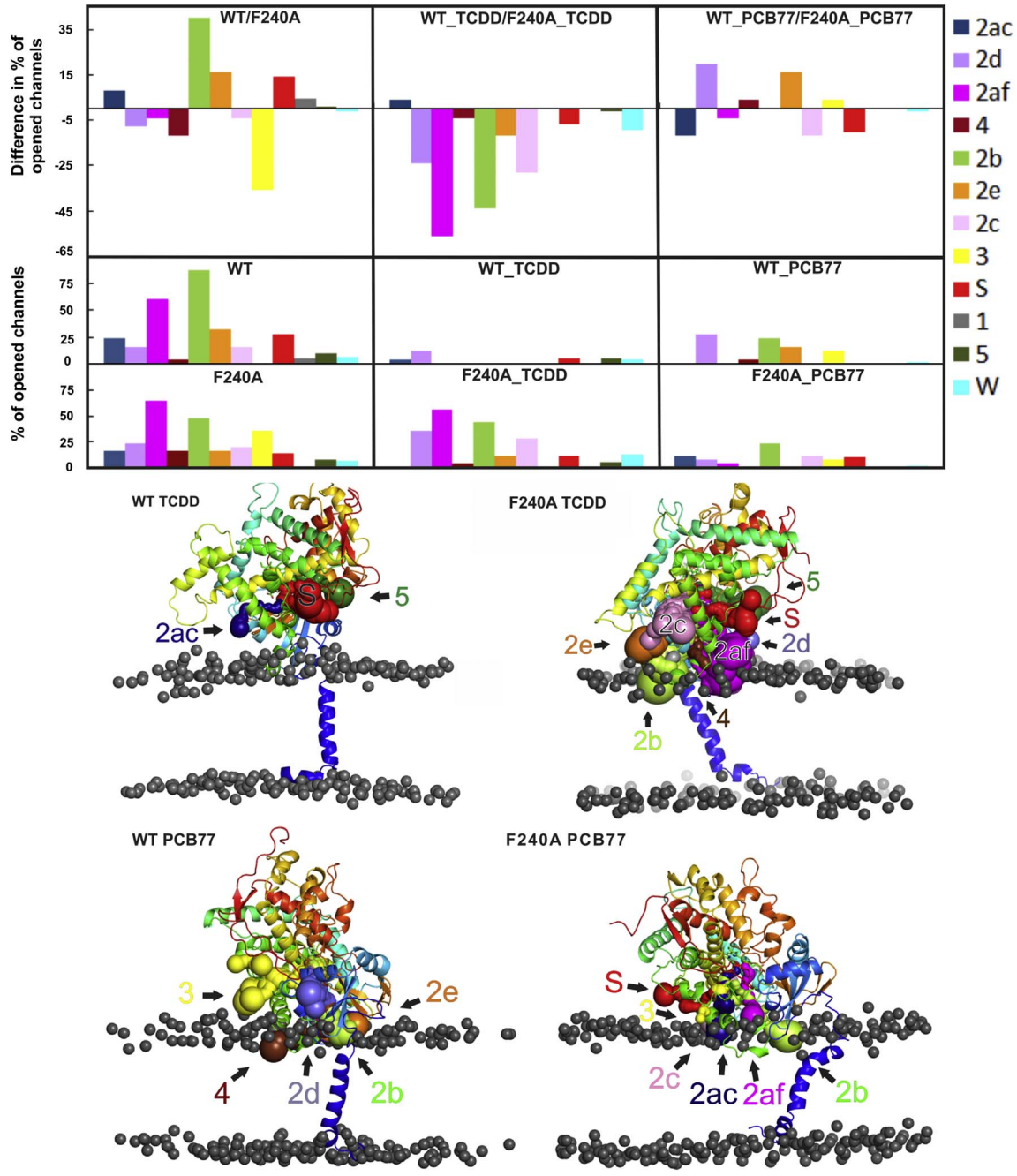

Fig. 6. Top panel: Differences in channel openings between the WT enzyme and the F240A mutant, and structural overview of the channels' locations. The middle and bottom rows show the proportion of simulated time during which each channel was open in the two enzymes and their complexes with TCDD and PCB77; the top row shows the channel-by-channel differences between the WT and the mutant in terms of these proportions. The channels are abbreviated as follows: subfamily 2 channels are labeled 2a, 2af, 2b, 2c, 2d, and 2e; channels 1, 3, 4, and 5 are labeled as they are numbered; and the water and solvent channels are labeled W and S, respectively. Bottom panel: structures of the WT and F240A mutant bound to TCDD and PCB77, showing the positions of key channel entrances. Channel entrances are indicated by spheres colored as follows: S – red, channel 3 – yellow, channel 4 – brown, 2af – magenta, 2ac – deep blue, 2b – green, 2c – pink, 2e – orange, 2d – light purple. For clarity, water channels are not shown. Rat CYP1A1 is shown in cartoon form, and membrane phosphates are shown as gray spheres. The TCDD-bound F240A complex has more open channels than the corresponding PCB77-bound complex. Moreover, significantly more open channels were observed in the F240A complexes than in the corresponding WT complexes. The major access channels in the former case seem to be 2b and 2af. The most frequently open egress pathway was the solvent channel.

3.5. POPs binding energies to WT and F240A rat CYP1A1

Finally, we assessed the differences in the binding free energies of PCB77 and TCDD to the active sites of the WT and F240A mutant using the MM-PBSA method (Supporting Information Scheme S1), revealing that they correlated with the experimentally determined hydroxylation activities of WT/F240A towards PCB77 (as reported above) and TCDD (Shinkyo et al. [18]). A relationship between enzyme activity and the binding free energy was derived using the quasi steady-state approximation (see Supporting Information for details). We observed that the binding of PCB77 to the WT enzyme was more favorable than that to the F240A mutant ($\Delta\Delta G_{F240-WT}^{PCB77} = +3.2$ kcal/mol). The comparatively weak affinity of PCB77 for F240A is consistent with the experimental observation that the WT is significantly more proficient at hydroxylating PCB77 (Fig. 2 and Supporting Information Fig. S8). Conversely, the mutant bound TCDD more strongly than did the WT

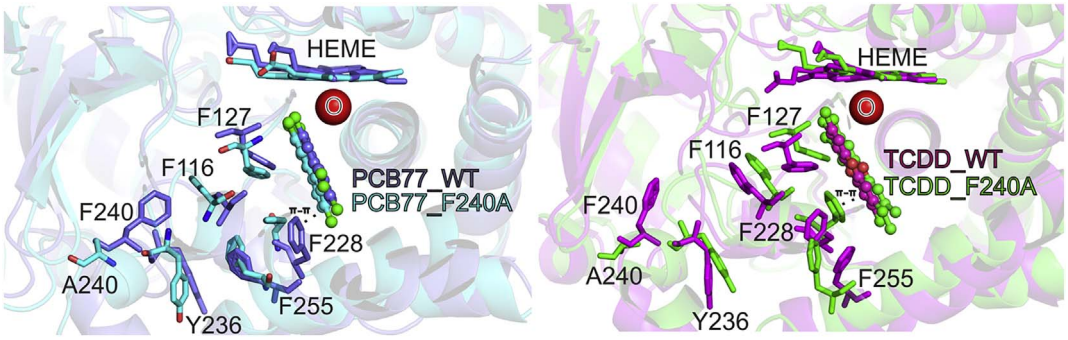

Fig. 7. Average positions of PCB77 and TCDD (represented by ball and stick models) in the active sites of WT CYP1A1 and the F240A mutant obtained from the last 50 ns of the MD simulations. The heme is represented as a stick model, and helices are shown as curls. The predicted position of oxygen in the Compound I state of CYP is indicated by a red sphere.

($\Delta\Delta G_{F240-WT}^{TCDD} = -1.4$ kcal/mol). This is consistent with the experimental results of Shinkyo et al., who found that the F240A mutant catalyzed TCDD hydroxylation but the WT did not [18] (Supporting Information Scheme S1).

These differences in binding energies and hydroxylation activity presumably stem from the interactions of amino acid 240 with its surroundings. In all cases, PCB77 and TCDD are bound at least 1 nm from the mutated amino acid (Supporting Information: Table S1). However, aromatic amino acids localized in the BC- and FG-loops (F116, F127, F228, F255, Y236, F240) form a hydrophobic cluster connected by π-π stacking interactions (Fig. 7). In the ligand-free WT protein, these loops and their clustered amino acids move to occupy the active site, and F228 occupies the binding site of POPs. When PCB77 binds to the WT, F228 forms a π-π stacking interaction with one of the PCB77 phenyl rings. To enable this, the G-helix bearing F255 moves forward. Conversely, in the TCDD_WT complex, F255 remains in the location it occupies in the ligand-free structure, forcing F228 to unstack from TCDD. The F240A mutation seems to affect the rearrangement of the aromatic clusters, allowing F228 to leave the binding site in the ligand-free structure. This occurs in parallel with larger movements along the broken F-helix, which Urban et al. found to have important effects on CYP1A substrate specificity [13]. When PCB77 binds to the mutant enzyme, F228 remains unstacked because it is attracted to F255 in the shifted G-helix. Finally, because the position of F255 in the ligand-free F240A mutant is similar to that in the TCDD_F240A complex, F228 has enough space to form a stable π-π stacking interaction with the bound TCDD (Fig. 7).

The closest atoms to the heme iron are chlorine atoms in both cases. The oxygen of compound I can reach the closest carbon atoms (*cf*. Fig. 7 and Supporting Information: Fig. S8), which are within the 0.5 nm distance suggested as the requirement for the hydroxylation reaction to proceed [65]. These sites of metabolism are consistent with the proposed mechanisms of TCDD oxidation to 8-hydroxy-2,3,7-TriCDD [66], and the oxidation of PCB77 to 3,3′,4′,5-tetrachloro-4-biphenylol or 3,3′,4′,4-tetrachloro-5-biphenylol [67,68]. They are also consistent with the experiments reported in this work (Fig. 2).

In contrast to TCDD and PCB77, Molcan et al. showed that dioxins with no lateral chlorine atoms (e.g. TriCDD) bind more closely to the heme in porcine CYP1A1 [22]. Consequently, such dioxins have i) a higher catalytic rate, k_{cat}, leading to more rapid metabolism; and ii) K_M and k_{cat} values that are both sensitive to mutations (as shown by Shinkyo et al. [18]). In our case, we can expect k_{cat} to be almost constant because the two POPs bind in almost identical positions relative to the heme. In addition, the reaction rates with TCDD and PCB77 are slow enough that we can safely assume $k_{cat} \ll k_r$, so K_M is directly coupled to the compound's binding affinity. As a result, any increase in the reaction rate is directly attributable to an increase in the ligand's binding affinity towards CYP1A1.

The key findings of these studies were that: i) the position of PCB77 and TCDD with respect to the heme moiety is virtually unchanged in the F240A mutant which in effect should not change activation energy of the reaction; ii) π-π stacking with F228 facilitates binding to POPs and may enhance catalytic efficiency; ii) the F240A mutation primarily affects the movement of the F-helix; and iii) binding of PCB77 to the F240A mutant causes a shift of the G-helix that counteracts the otherwise positive effect of the F240A mutation on PCB77 binding.

4. Conclusions

We analyzed the behavior of the WT microsomal rat CYP1A1 and its F240A mutant with and without bound TCDD and PCB77 to rationalize the experimentally observed differences in their activity towards these compounds. The WT enzyme shows almost no detectable hydroxylation activity towards TCDD [16,18], whereas the F240A mutant shows appreciable activity. However, the mutant is less active than the WT towards PCB77. A rationalization of this finding was deemed important for the rational design of efficient enzymes capable of catalyzing the biotransformation of POPs and the development of environmentally friendly technologies for degrading these toxic and very persistent compounds.

Molecular dynamics simulations showed that both hydrophobic compounds accumulated in the membrane and were pre-concentrated there. They could enter the CYP1A1 active site via a network of access channels whose mouth openings are inside the membrane bilayer. The F240A mutation caused some channels to open more widely, and may facilitate substrate access to the active site. However, this alone cannot explain the different activities of the two enzymes towards PCB77 and TCDD.

An analysis of active site binding energies revealed differences between the two substrates and the two enzyme forms that agreed with the experimental observations. The different binding free energies stem from structural rearrangements in the vicinity of the bound PCB77 and TCDD caused by the distal F240A mutation, which enabled more efficient binding of TCDD. However, the retention of F240 in the WT enzyme helped to position PCB77 for efficient catalysis, while the F240A mutation reduced the strength of PCB77 binding.

Our results show that a rather distal mutation (the C_α of F/A240 is 2.5 nm from the heme Fe center) can significantly affect enzyme activity by modifying access channel behavior and causing structural changes that affect the residues around the ligand binding site. These findings will be useful in modulating the activity of designed CYP1A1 mutants with tailored substrate preferences and the rational design of catalysts for biotransformation of POPs. Specifically, these results show that amino acids that control substrate access can be good targets for rational enzyme design and protein engineering even if they are distant from the active site.

Abbreviations

CYP	cytochrome P450
POP	persistent organic pollutants
WT	rat CYP1A1 wild type
F240A	rat CYP1A1 F240A mutant
MD	molecular dynamics
PCB77	3,3′,4,4′-tetrachlorobiphenyl
TCDD	2,3,7,8-tetrachloro-dibenzo-*p*-dioxin
MM-PBSA	molecular mechanics – Poisson-Boltzmann surface area

Transparency Document

The Transparency document associated with this article can be found, in the online version.

Acknowledgement

This work was supported by the Czech Grant Agency [project P208/12/G016]. V.N. and M.P. acknowledge support from a student project of Palacký University Olomouc IGA_PrF_2017_028. The authors gratefully acknowledge support from the Ministry of Education, Youth and Sports of the Czech Republic [project LO1305]. This work was in part supported by a Grant-in-Aid for Challenging Exploratory Research [grant number 25550064] from the Japan Society for the Promotion of Science for H. I.

Appendix A. Supplementary data

Fig. S1 shows the starting positions of TCDD and PCB77 in the active site relative to the template crystal structure; Fig. S2 shows the distances between the centers of CYP1A1 and membrane; Fig. S3 shows changes in the inner cavities of the WT enzyme and the F240A mutant; Fig. S4 shows RMSF values for the WT and F240A; Fig. S5 shows patterns of channels opening in ligand-free and ligand-bound structures; Fig. S6 shows the evolution of distance between amino acid 240 F/A and the nearest rigid amino acid P391; Fig. S7 shows Frequency of opening of channels 2af and 2b; Scheme S1 presents further details of the MM-PBSA analysis and explanation of the kinetic model; Fig. S8 shows predicted sites-of-metabolism of TCDD and PCB77; Table S1 depicts the average minimal distance between the PCB77/TCDD and amino acid 240. Supplementary data associated with this article can be found in the online version, at doi:http://dx.doi.org/10.1016/j.bbagen.2017.08.002.

References

[1] F.P. Guengerich, Intersection of the roles of cytochrome P450 enzymes with xenobiotic and endogenous substrates: relevance to toxicity and drug interactions, Chem. Res. Toxicol. 30 (2017) 2–12.
[2] M. de S. Pereira, Polychlorinated dibenzo-*p*-dioxins (PCDD), dibenzofurans (PCDF) and polychlorinated biphenyls (PCB): main sources, environmental behaviour and risk to man and biota, Quim Nova 27 (2004) 934–943.
[3] S. Endo, I.B. Escher, K.-U. Goss, Capacities of membrane lipids to accumulate neutral organic chemicals, Environ. Sci. Technol. 45 (2011) 5912–5921.
[4] S. Watanabe, K. Kitamura, M. Nagahashi, Effects of dioxins on human health: a review, J. Epidemiol. 9 (1999) 1–13.
[5] H. Inui, T. Itoh, K. Yamamoto, S. Ikushiro, T. Sakaki, Mammalian Cytochrome P450-dependent Metabolism of Polychlorinated Dibenzo-*p*-dioxins and Coplanar Polychlorinated Biphenyls, (2014), pp. 14044–14057.
[6] S.D. Black, Membrane topology of the mammalian P450 cytochromes, FASEB J. 6 (1992) 680–685.
[7] K. Berka, M. Paloncýová, P. Anzenbacher, M. Otyepka, Behavior of human cytochromes P450 on lipid membranes, J. Phys. Chem. B 117 (2013) 11556–11564.
[8] E.E. Scott, C.R. Wolf, M. Otyepka, S.C. Humphreys, J.R. Reed, C.J. Henderson, L.A. McLaughlin, M. Paloncýová, V. Navrátilová, K. Berka, P. Anzenbacher, U.P. Dahal, C. Barnaba, J.A. Brozik, J.P. Jones, D.F. Estrada, J.S. Laurence, J.W. Park, W.L. Backes, M. Paloncyova, et al., The role of protein-protein and protein-membrane interactions on P450 function, Drug Metab. Dispos. 44 (2016) 576–590.
[9] M. Otyepka, J. Skopalík, E. Anzenbacherová, P. Anzenbacher, What common structural features and variations of mammalian P450s are known to date? Biochim. Biophys. Acta Gen. Subj. 1770 (2007) 376–389.
[10] E.F. Johnson, C.D. Stout, Structural diversity of eukaryotic membrane cytochrome P450s, J. Biol. Chem. 288 (2013) 17082–17092.
[11] V. Cojocaru, P.J. Winn, R.C. Wade, The ins and outs of cytochrome P450s, Biochim. Biophys. Acta Gen. Subj. 1770 (2007) 390–401.
[12] M. Paloncýová, V. Navrátilová, K. Berka, A. Laio, M. Otyepka, Role of enzyme flexibility in ligand access and egress to active site: bias-exchange metadynamics study of 1,3,7-trimethyluric acid in cytochrome P450 3A4, J. Chem. Theory Comput. 12 (2016) 2101–2109.
[13] P. Urban, G. Truan, D. Pompon, Access channels to the buried active site control substrate specificity in CYP1A P450 enzymes, Biochim. Biophys. Acta Gen. Subj. 1850 (2015) 696–707.
[14] M. Paloncýová, R. DeVane, B. Murch, K. Berka, M. Otyepka, Amphiphilic drug-like molecules accumulate in a membrane below the head group region, J. Phys. Chem. B 118 (2014) 1030–1039.
[15] K. Berka, T. Hendrychová, P. Anzenbacher, M. Otyepka, Membrane position of ibuprofen agrees with suggested access path entrance to cytochrome P450 2C9 active site, J. Phys. Chem. A 115 (2011) 11248–11255.
[16] T. Sakaki, K. Yamamoto, S. Ikushiro, Possibility of application of cytochrome P450 to bioremediation of dioxins, Biotechnol. Appl. Biochem. 60 (2013) 65–70.
[17] M. Van den Berg, The 2005 World Health Organization reevaluation of human and mammalian toxic equivalency factors for dioxins and dioxin-like compounds, Toxicol. Sci. 93 (2006) 223–241.
[18] R. Shinkyo, T. Sakaki, T. Takita, M. Ohta, K. Inouye, Generation of 2,3,7,8-TCDD-metabolizing enzyme by modifying rat CYP1A1 through site-directed mutagenesis, Biochem. Biophys. Res. Commun. 308 (2003) 511–517.
[19] T. Shimada, Xenobiotic-metabolizing enzymes involved in activation and detoxification of carcinogenic polycyclic aromatic hydrocarbons, Drug Metab. Pharmacokinet. 21 (2006) 257–276.
[20] P. Urban, G. Truan, D. Pompon, High-throughput enzymology and combinatorial mutagenesis for mining cytochrome P450 functions, Expert Opin. Drug Metab. Toxicol. 4 (2008) 733–747.
[21] T. Molcan, S. Swigonska, K. Orlowska, K. Myszczynski, A. Nynca, A. Sadowska, M. Ruszkowska, J.P. Jastrzebski, R.E. Ciereszko, Structural-functional adaptations of porcine CYP1A1 to metabolize polychlorinated dibenzo-*p*-dioxins, Chemosphere 168 (2017) 205–216.
[22] M. Otyepka, K. Berka, P. Anzenbacher, Is there a relationship between the substrate preferences and structural flexibility of cytochromes P450? Curr. Drug Metab. 13 (2012) 130–142.
[23] M. Paloncýová, K. Berka, M. Otyepka, Molecular insight into affinities of drugs and their metabolites to lipid bilayers, J. Phys. Chem. B 117 (2013) 2403–2410.
[24] A. Luthra, M. Gregory, Y.V. Grinkova, I.G. Denisov, S.G. Sligar, Nanodiscs in the studies of membrane-bound cytochrome P450 enzymes, in: I.R. Phillips, E.A. Shephard, P.R. Ortiz de Montellano (Eds.), Methods Mol. Biol, Humana Press, Totowa, NJ, 2013, pp. 115–127.
[25] P. Banáš, M. Otyepka, P. Jeřábek, M. Petřek, J. Damborský, Mechanism of enhanced conversion of 1,2,3-trichloropropane by mutant haloalkane dehalogenase revealed by molecular modeling, J. Comput. Aided Mol. Des. 20 (2006) 375–383.
[26] M. Pavlova, M. Klvana, Z. Prokop, R. Chaloupkova, P. Banas, M. Otyepka, R.C. Wade, M. Tsuda, Y. Nagata, J. Damborsky, Redesigning dehalogenase access tunnels as a strategy for degrading an anthropogenic substrate, Nat. Chem. Biol. 5 (2009) 727–733.
[27] A. Iffland, S. Gendreizig, P. Tafelmeyer, K. Johnsson, Changing the substrate specificity of cytochrome C peroxidase using directed evolution, Biochem. Biophys. Res. Commun. 286 (2001) 126–132.
[28] K. Oeda, T. Sakaki, H. Ohkawa, Expression of rat liver cytochrome P-450MC cDNA in *Saccharomyces cerevisiae*, DNA 4 (1985) 203–210.
[29] T. Omura, R. Sato, The carbon monoxide-biding pigment of liver microsomes I. Evidence for its hemoprotein nature, J. Biol. Chem. 239 (1964) 2379–2385.
[30] K. Yamazaki, M. Suzuki, T. Itoh, K. Yamamoto, M. Kanemitsu, C. Matsumura, T. Nakano, T. Sakaki, Y. Fukami, H. Imaishi, H. Inui, Structural basis of species differences between human and experimental animal CYP1A1s in metabolism of 3,3′,4,4′,5-pentachlorobiphenyl, J. Biochem. 149 (2011) 487–494.
[31] T. Sakiyama, A. Yamamoto, N. Kakutani, J. Fukuyama, T. Okumura, Hydroxylated polychlorinated biphenyls (OH-PCBs) in the aquatic environment: levels and congener profiles in sediments from Osaka, Japan, Organohalogen Compd. 69 (2007) 1380–1383.
[32] S. Mise, Y. Haga, T. Itoh, A. Kato, I. Fukuda, E. Goto, K. Yamamoto, M. Yabu, C. Matsumura, T. Nakano, T. Sakaki, H. Inui, Structural determinants of the position of 2,3′,4,4′,5-pentachlorobiphenyl (CB118) hydroxylation by mammalian cytochrome P450 Monooxygenases, Toxicol. Sci. 152 (2016) 340–348.
[33] A. Šali, T.L. Blundell, Comparative protein modelling by satisfaction of spatial restraints, J. Mol. Biol. 234 (1993) 779–815.
[34] A.A. Walsh, G.D. Szklarz, E.E. Scott, Human cytochrome P450 1A1 structure and utility in understanding drug and xenobiotic metabolism, J. Biol. Chem. 288 (2013) 12932–12943.
[35] Schrodinger LLC, The PyMOL Molecular Graphics System, (2010).
[36] V. Hornak, R. Abel, A. Okur, B. Strockbine, A. Roitberg, C. Simmerling, Comparison of multiple amber force fields and development of improved protein backbone parameters, Proteins Struct. Funct. Bioinforma. 65 (2006) 712–725.
[37] K. Shahrokh, A. Orendt, G.S. Yost, T.E. Cheatham III, Quantum mechanically derived AMBER-compatible heme parameters for various states of the cytochrome P450 catalytic cycle, J. Comput. Chem. 33 (2012) 119–133.
[38] J.P.M. Jämbeck, A.P. Lyubartsev, Another piece of the membrane puzzle: extending slipids further, J. Chem. Theory Comput. 9 (2013) 774–784.

[39] M.W. Mahoney, W.L. Jorgensen, A five-site model for liquid water and the reproduction of the density anomaly by rigid, nonpolarizable potential functions, J. Chem. Phys. 112 (2000) 8910.
[40] M.G. Wolf, M. Hoefling, C. Aponte-Santamaría, H. Grubmüller, G. Groenhof, g_membed: efficient insertion of a membrane protein into an equilibrated lipid bilayer with minimal perturbation, J. Comput. Chem. 31 (2010) 2169–2174.
[41] M. Paloncýová, G. Fabre, R.H. DeVane, P. Trouillas, K. Berka, M. Otyepka, Benchmarking of force fields for molecule–membrane interactions, J. Chem. Theory Comput. 10 (2014) 4143–4151.
[42] M.J. Frisch, G.W. Trucks, H.B. Schlegel, G.E. Scuseria, M.A. Robb, J.R. Cheeseman, J.A. Montgomery Jr., T. Vreven, K.N. Kudin, J.C. Burant, J.M. Millam, S.S. Iyengar, J. Tomasi, V. Barone, B. Mennucci, M. Cossi, G. Scalmani, N. Rega, G.A. Petersson, H. Nakatsuji, et al., Gaussian 09, Revision A02, Gaussian, Inc, Wallingford CT, 2016.
[43] D.A. Case, T.A. Darden III., T.E. Cheatham, C.L. Simmerling, J. Wang, R.E. Duke, R. Luo, R.C. Walker, W. Zhang, K.M. Merz, B. Roberts, B. Wang, S. Hayik, A. Roitberg, G. Seabra, I. Kolossváry, K.F. Wong, F. Paesani, J. Vanicek, J. Liu, et al., AMBER 11, University of California, San Francisco, 2010 (2010).
[44] J. Wang, R.M. Wolf, J.W. Caldwell, P.A. Kollman, D.A. Case, Development and testing of a general amber force field, J. Comput. Chem. 25 (2004) 1157–1174.
[45] D.L. Mobley, J.D. Chodera, K.A. Dill, On the use of orientational restraints and symmetry corrections in alchemical free energy calculations, J. Chem. Phys. 125 (2006) 84902.
[46] D. Van Der Spoel, E. Lindahl, B. Hess, G. Groenhof, A.E. Mark, H.J.C. Berendsen, GROMACS: fast, flexible, and free, J. Comput. Chem. 26 (2005) 1701–1718.
[47] H.J.C. Berendsen, J.P.M. Postma, W.F. van Gunsteren, A. DiNola, J.R. Haak, Molecular dynamics with coupling to an external bath, J. Chem. Phys. 81 (1984) 3684–3690.
[48] G. Bussi, D. Donadio, M. Parrinello, Canonical sampling through velocity rescaling, J. Chem. Phys. 126 (2007) 14101.
[49] S. Nosé, a unified formulation of the constant temperature molecular dynamics methods, J. Chem. Phys. 81 (1984) 511.
[50] W.G. Hoover, Canonical dynamics: equilibrium phase-space distributions, Phys. Rev. A 31 (1985) 1695–1697.
[51] M. Parrinello, A. Rahman, Polymorphic transitions in single crystals: a new molecular dynamics method, J. Appl. Phys. 52 (1981) 7182–7190.
[52] T. Darden, D. York, L. Pedersen, Particle mesh Ewald: an N.log(N) method for Ewald sums in large systems, J. Chem. Phys. 98 (1993) 10089.
[53] D. Sehnal, R. Svobodová Vařeková, K. Berka, L. Pravda, V. Navrátilová, P. Banáš, C.-M. Ionescu, M. Otyepka, J. Koča, MOLE 20: advanced approach for analysis of biomacromolecular channels, J. Cheminform. 5 (2013) 39.
[54] I. Massova, P.A. Kollman, Combined molecularmechanical and continuum solvent approach (MM-PBSA/GBSA) to predict ligand binding, Perspect. Drug Discov. Des. 18 (2000) 113–135.
[55] R. Kumari, R. Kumar, A. Lynn, G-mmpbsa - A GROMACS tool for high-throughput MM-PBSA calculations, J. Chem. Inf. Model. 54 (2014) 1951–1962.
[56] Small-Molecule Drug Discovery Suite 2015-4, Schrödinger, LLC, 2016.
[57] TURBOMOLE V6.3, a Development of University of Karlsruhe and Forschungszentrum Karlsruhe GmbH, (2011).
[58] J. Řezáč, Cuby: an integrative framework for computational chemistry, J. Comput. Chem. 37 (2016) 1230–1237.
[59] A. Klamt, U. Huniar, S. Spycher, J. Keldenich, COSMOmic: a mechanistic approach to the calculation of membrane – water partition coefficients and internal distributions within membranes and micelles, J. Phys. Chem. B 112 (2008) 12148–12157.
[60] R. Shinkyo, T. Sakaki, M. Ohta, K. Inouye, Metabolic pathways of dioxin by CYP1A1: species difference between rat and human CYP1A subfamily in the metabolism of dioxins, Arch. Biochem. Biophys. 409 (2003) 180–187.
[61] P.A. Williams, J. Cosme, V. Sridhar, E.F. Johnson, D.E. McRee, Microsomal cytochrome P450 2C5: comparison to microbial P450s and unique features, J. Inorg. Biochem. 81 (2000) 183–190.
[62] J.L. Baylon, I.L. Lenov, S.G. Sligar, E. Tajkhorshid, Characterizing the membrane-bound state of cytochrome P450 3A4: structure, depth of insertion, and orientation, J. Am. Chem. Soc. 135 (2013) 8542–8551.
[63] J. Skopalík, P. Anzenbacher, M. Otyepka, Flexibility of human cytochromes P450: molecular dynamics reveals differences between CYPs 3A4, 2C9, and 2A6, which correlate with their substrate preferences, J. Phys. Chem. B 112 (2008) 8165–8173.
[64] H. Zhang, C. Kenaan, D. Hamdane, G.H.B. Hoa, P.F. Hollenberg, Effect of conformational dynamics on substrate recognition and specificity as probed by the introduction of a de novo disulfide bond into cytochrome P450 2B1, J. Biol. Chem. 284 (2009) 25678–25686.
[65] R. Lonsdale, R.M. Fort, P. Rydberg, J.N. Harvey, A.J. Mulholland, Quantum mechanics/molecular mechanics modeling of drug metabolism: mexiletine *N*-hydroxylation by cytochrome P450 1A2, Chem. Res. Toxicol. 29 (2016) 963–971.
[66] T. Sawahata, J.R. Olson, R.A. Neal, Identification of metabolites 2,3,7,8-tetrachlorodibenzo-p-dioxin (TCDD) formed on incubation with isolated rat hepatocytes, Biochem. Biophys. Res. Commun. 105 (1982) 341–346.
[67] D.C. Morse, E.K. Wehler, M. van de Pas, A.T.H.J. de Bie, P.J. van Bladeren, A. Brouwer, Metabolism and biochemical effects of 3,3′,4,4′-tetrachlorobiphenyl in pregnant and fetal rats, Chem. Biol. Interact. 95 (1995) 41–56.
[68] C. Ishida, N. Koga, N. Hanioka, H.K. Saeki, H. Yoshimura, Metabolism in Vitro of 3,4,3′,4′- and 2,5,2′,5′-tetrachlorobiphenyl by rat liver microsomes and highly purified cytochrome P-450, J. Pharmacobiodyn. 14 (1991) 276–284.